

ESTI FILE COPY

ESD RECORD COPY

RETURN TO
SCIENTIFIC & TECHNICAL INFORMATION DIVISION
(ESTI), BUILDING 3211

ESD ACCESSION LIST

ESTI Call No. AL 54888

Copy No. 1 of 1 cys.

Technical Report

426

R. K. Crane

Microwave Scattering Parameters
for New England Rain

3 October 1966

Prepared under Electronic Systems Division Contract AF 19(628)-5167 by

Lincoln Laboratory

MASSACHUSETTS INSTITUTE OF TECHNOLOGY

Lexington, Massachusetts



ADDWUTAR

MASSACHUSETTS INSTITUTE OF TECHNOLOGY
LINCOLN LABORATORY

MICROWAVE SCATTERING PARAMETERS
FOR NEW ENGLAND RAIN

R. K. CRANE

Group 61

TECHNICAL REPORT 426

3 OCTOBER 1966

LEXINGTON

MASSACHUSETTS

ABSTRACT

Scattergrams of attenuation coefficient, effective reflectivity factor, single-scattering albedo, and radio refractivity vs liquid-water content, rain rate, and reflectivity factor are presented for a raindrop temperature of 0.0°C and frequencies of 1.29, 2.80, 8.0, 9.35, 15.5, 35.0, 70.0, and 94.0 GHz. The scattergrams were computed using Mie theory to compute the scattering parameters for single raindrops, and single-scattering theory to compute the integrated scattering effects of an ensemble of raindrops. Measured drop-size distributions were used to generate the scattergrams.

Accepted for the Air Force
Franklin C. Hudson
Chief, Lincoln Laboratory Office

CONTENTS

| | |
|--|-----|
| Abstract | iii |
| I. Introduction | 1 |
| II. Computation of Scattering Parameters | 1 |
| III. Raindrop Parameters | 5 |
| IV. Measured and Modeled Scattering Parameters | 8 |
| V. Conclusions | 12 |
| References | 15 |

MICROWAVE SCATTERING PARAMETERS FOR NEW ENGLAND RAIN

I. INTRODUCTION

As part of a study of the effects of the troposphere on space communication systems, the scattering effects of measured raindrop distributions were investigated. The scattering parameters, backscattering, extinction, absorption, and total scattering cross sections per-unit volume were computed for measured drop-size distributions for frequencies of interest to both weather radar and satellite communication systems. Results of these computations are depicted below as scattergrams of attenuation coefficient, effective reflectivity factor, and single-scattering albedo vs liquid-water content, rain rate and reflectivity factor. The liquid-water content, rain rate and reflectivity factor are drop-size dependent meteorological parameters normally used to describe rainfall. The scattering parameter attenuation coefficient is related to the extinction cross section per-unit volume, effective reflectivity factor to the backscatter cross section per-unit volume and the single-scattering albedo to the ratio of the total scattering to extinction cross sections. These scattering parameters are useful in estimating the effects of interest to satellite communications, the total attenuation along a path and changes in receiver noise, using available meteorological data. In addition to the scattering parameters listed above, the effective index of refraction of the scattering medium was computed and the results are depicted in scattergrams of radio refractivity vs the meteorological parameters.

II. COMPUTATION OF SCATTERING PARAMETERS

The many reports on rain scattering for model raindrop distributions composed of spherical drops¹⁻³ show that, to first order, the calculations of the scattering parameters can be based on the theory of diffraction of a plane wave by dielectric spheres. Raindrops have diameters of the order of the wavelength of the microwave radiation, and the theory attributed to Mie must be used. The scattering of a plane wave as observed at a point at a distance from a scatterer is given by⁴

$$\tilde{E} = \tilde{E}^i + \tilde{E}^s = \tilde{E}^i + \underline{S}(n, a, \Theta) \tilde{E}^i \frac{e^{-ikR}}{ikR}$$

where

$k = 2\pi/\lambda$ = wave number in free space where λ is the wavelength

R = distance from center of scatterer to observer

$\underline{\underline{E}} = \begin{pmatrix} E_\ell \\ E_r \end{pmatrix}$ = electric field vector with components ℓ in plane of scattering and r perpendicular to plane of scattering with superscripts i (incident field) and s (scattered field)

$$\underline{\underline{S}}(n, a, \Theta) = \begin{pmatrix} S_2 & 0 \\ 0 & S_1 \end{pmatrix} \text{ scattering matrix}$$

$$S_1(n, a, \Theta) = \sum_{\ell=1}^{\infty} \frac{2\ell + 1}{\ell(\ell + 1)} \{ a_\ell(n, a) \pi_\ell(\cos \Theta) + b_\ell(n, a) \xi_\ell(\cos \Theta) \}$$

$$S_2(n, a, \Theta) = \sum_{\ell=1}^{\infty} \frac{2\ell + 1}{\ell(\ell + 1)} \{ b_\ell(n, a) \pi_\ell(\cos \Theta) + a_\ell(n, a) \xi_\ell(\cos \Theta) \}$$

$a_\ell(n, a)$ and $b_\ell(n, a)$ are Mie series coefficients; S_1 and S_2 are called scattering amplitudes

n = complex index of refraction of liquid water

a = radius of sphere

$$\pi_\ell(\cos \Theta) = (\sin \Theta)^{-1} P_k^1(\cos \Theta)$$

$$\xi_\ell(\cos \Theta) = \frac{d}{d\Theta} P_k^1(\cos \Theta)$$

Θ = scattering angle.

The energy balance for scattering is given in terms of the amplitude of the Poynting vector or the specific intensity I as

$$I^s = \frac{I^i \sigma(n, a)}{R^2}$$

where σ is a scattering cross section. In terms of the scattering cross sections, the energy lost to the incident plane wave is given by the extinction cross section; the total energy scattered by the sphere is given by the scattering cross section; and the total energy absorbed by the sphere is given by the absorption cross section.

$$\sigma_{ext}(n, a) = \frac{4\pi}{k^2} \operatorname{Re} \{ S(n, a) \} = \text{extinction cross section}$$

[where $S(n, a) = S_1(n, a, 0) = S_2(n, a, 0)$]

$$\sigma_{scat}(n, a) = \frac{2\pi}{k^2} \sum_{\ell=1}^{\infty} (2\ell + 1) \{ |a_\ell(n, a)|^2 + |b_\ell(n, a)|^2 \} = \text{scattering cross section}$$

$$\sigma_{\text{abs}}(n,a) = \sigma_{\text{ext}}(n,a) - \sigma_{\text{scat}}(n,a) = \text{absorption cross section}$$

The energy scattered backwards along the direction of incidence is given by the backscattering cross section and is derived from the scattering matrix elements as

$$\begin{aligned}\sigma_{\text{back}}(n,a) &= \frac{4\pi}{k^2} [S_1^*(n,a,\pi) S_1(n,a,\pi)] = \frac{4\pi}{k^2} [S_2(n,a,\pi) S_2^*(n,a,\pi)] \\ &= \text{backscatter cross section}\end{aligned}$$

The coherent energy loss and phase shift due to an ensemble of scatterers is described in terms of the imaginary and real parts of an effective index of refraction for the volume of scatterers. If the spheres can be assumed to scatter energy once, the index of refraction is given by (see Ref. 4, Ch. 4)

$$n_s' = n_s'' - i n_s''' = 1 - i \frac{2\pi}{k^3} \int_{a_{\min}}^{a_{\max}} S(n,a) N(a) da$$

where $N(a)$ is the number density of spheres for drop radius a or the drop-size distribution.

If the spheres scatter more than once, a first-order solution for the expected amplitude and phase of the received field can be expressed in terms of a multiple-scattering index of refraction⁵

$$(n_m' - i n_m'') = (n_s' - i n_s''')^2 + \left[\frac{2\pi}{k^3} \int_{a_{\min}}^{a_{\max}} S_1(n,a,\pi) N(a) da \right]^2$$

where $S_1(n,a,\pi) = -S_2(n,a,\pi)$.

Since the scattering amplitude $S_1(n,a,\pi)$ is small, this can be expressed as

$$\begin{aligned}n_m' &\simeq n_s' + \frac{1}{2} \left(\frac{2\pi}{k^3} \right)^2 \left\{ \left[\int_{a_{\min}}^{a_{\max}} N(a) \operatorname{Re} \{S_1(n,a,\pi)\} da \right]^2 \right. \\ &\quad \left. - \left[\int_{a_{\min}}^{a_{\max}} N(a) \operatorname{Im} \{S_1(n,a,\pi)\} da \right]^2 \right\} \\ n_m'' &\simeq n_s'' - \left(\frac{2\pi}{k^3} \right)^2 \left[\int_{a_{\min}}^{a_{\max}} N(a) \operatorname{Re} \{S_1(n,a,\pi)\} da \right] \\ &\quad \times \left[\int_{a_{\min}}^{a_{\max}} N(a) \operatorname{Im} \{S_1(n,a,\pi)\} da \right]\end{aligned}$$

With either index of refraction, the real and imaginary terms can be expressed more easily in terms of the radio refractivity N given by

$$N = (n' - 1) \times 10^6 , \quad "N \text{ units}"$$

and the attenuation coefficient given by

$$A = n'' (2k \log_{10} e) \times 10^6 , \quad \text{db/km for } a, \lambda \text{ in centimeters}$$

TABLE I
COMPARISON OF SINGLE- AND MULTIPLE-SCATTERING INDEX OF REFRACTION
FOR THE LAWS AND PARSONS DROP-SIZE DISTRIBUTION FOR 101.6-mm/hr RAIN RATE

| Frequency (GHz) | Drop Temperature (°C) | N_s | N_m | A_s (db/km) | A_m (db/km) |
|--------------------|--------------------------|----------|----------|------------------|------------------|
| 4.0 | 0.0 | 5.671114 | 5.671101 | 0.1885542 | 0.1885544 |
| 4.0 | 18.0 | 5.703791 | 5.703778 | 0.1027994 | 0.1027995 |
| 8.0 | 0.0 | 5.731942 | 5.731928 | 1.761978 | 1.761983 |
| 8.0 | 18.0 | 6.011033 | 6.011021 | 2.113060 | 2.113068 |
| 15.5 | 0.0 | 5.079693 | 5.079674 | 6.734227 | 6.734224 |
| 15.5 | 18.0 | 4.749067 | 4.749047 | 7.239070 | 7.239074 |
| 34.86 | 0.0 | 2.319696 | 2.319603 | 21.85193 | 21.85190 |
| 34.86 | 18.0 | 2.247630 | 2.247626 | 20.72679 | 20.72676 |

Index of refraction $n = n' + in''$

$$n' = 1.0 + N \times 10^{-6}$$

$$n'' = \frac{A \times 10^{-5}}{2k \log_{10} e}$$

A comparison of the single- and multiple-scattering index of refraction for the Laws and Parsons averaged liquid-water content distribution is given in Table I for selected temperatures and frequencies. The results show that, for coherent scattering, the single scattering is sufficient to describe the multiple-scattering process because the correction to the single-scattering result is extremely small.

The per-unit volume scattering cross section can be derived directly from the single-sphere cross sections since, for incoherent energy transmission, the phase effects are neglected. Integrated scattering cross sections or scattering coefficients are given by

$$\beta(n) = \int_{a_{\min}}^{a_{\max}} N(a) \sigma(n,a) da$$

from which

$$\beta_{\text{ext}} = 2kn'' = A(\log_{10} e)^{-1} \times 10^{-5} \quad , \quad \text{cm}^{-1} \text{ for } \lambda \text{ in centimeters}$$

$$\beta_{\text{scat}} = \int_{a_{\min}}^{a_{\max}} N(a) \sigma_{\text{scat}}(n,a) da$$

$$\beta_{\text{abs}} = \beta_{\text{ext}} - \beta_{\text{scat}}$$

$$\beta_{\text{back}} = \int_{a_{\min}}^{a_{\max}} N(a) \sigma_{\text{back}}(n,a) da \quad .$$

For ease in describing the relationship between β_{ext} , β_{scat} , and β_{abs} , the parameter, the integrated single-scattering albedo, or single-scattering albedo ω is introduced:

$$\omega = \frac{\beta_{\text{scat}}}{\beta_{\text{ext}}} .$$

The parameters, attenuation coefficient, and single-scattering albedo therefore describe the energy balance relationship per-unit volume of scatterers.

The final per-unit volume scattering parameter to be considered is the integrated backscatter cross section. Radiometeorologists prefer the use of an effective reflectivity factor to describe the radar return from a volume of rain. The reflectivity factor Z is derived from the expression for backscattering given in terms of the Rayleigh scattering theory,

$$\beta_{\text{back, Rayleigh}} = \frac{4\pi}{k^2} |K|^2 \int_{a_{\min}}^{a_{\max}} N(a) (ka)^6 da = \frac{\pi^5}{\lambda^4} |K|^2 Z$$

where

$$Z = \int_{a_{\min}}^{a_{\max}} N(a) (2a)^6 da$$

$$K = \frac{n^2 - 1}{n^2 + 2} .$$

Rayleigh scattering theory does not hold for the microwave frequencies where the wavelength is of the order of the drop diameter. The concept of Z can be retained if an effective reflectivity factor Z_{eff} is used as

$$Z_{\text{eff}} = \frac{\beta_{\text{back}} \lambda^4}{\pi^5 |K|^2}$$

where β_{back} is calculated using Mie theory as above.

The scattering parameters described above were computed on an IBM 7094 computer. Estimated accuracies of the scattering coefficients S_1 and S_2 and the scattering cross section σ_{scat} are better than one part in 10^6 . The per-unit volume parameters are generated by a three-point Gaussian quadrature numerical integration of the parameters over each drop-size interval of the drop-size distribution.

III. RAINDROP PARAMETERS

The per-unit volume parameters are generated using the per-unit volume raindrop size distribution. Drop-size distributions are not generally used to characterize rainfall. The parameters used by meteorologists are Z , the liquid-water content, and the rain rate.

$$L = \int_{a_{\min}}^{a_{\max}} N(a) \left(\frac{4\pi}{3} a^3 \right) \rho da$$

where

L = liquid-water content

ρ = density of water (taken as 1.0 gm/cm³).

$$R = \int_{a_{\min}}^{a_{\max}} N(a) \left(\frac{4\pi}{3} a^3 \right) \rho v(a) da$$

where

R = rain rate

$v(a)$ = terminal velocity in a quiet atmosphere.

The raindrop size samples used in this report were all taken at the ground. The terminal velocity of the raindrops was described by an empirically determined equation fitting the data of Gunn and Kinzer⁶ for standard temperature and pressure

$$V(a) = 950.0 \left\{ 1.0 - \exp \left[- \left(\frac{a}{0.0875} \right)^{1.2} \right] \right\}$$

Two types of drop-size distributions were processed: a model distribution using Laws and Parsons⁷ data, and measured drop-size distributions obtained from the M.I.T. Weather Radar Research Laboratory.[†] The drop-size distributions were measured at Cambridge, Massachusetts using the filter-paper technique which consisted of counting and sizing the number of drops collected on a 440-cm² area in a given length of time. These data were converted to the number of drops per cubic meter using the terminal drop velocity relationship given above. In some instances, two simultaneous measurements were taken with two adjacent pieces of filter paper. The data for these adjacent samples were processed as separate drop-size distributions, and typical resultant raindrop parameters as measured on 1 July and 26 August 1964 are listed in Table II. From the data in the table, it is evident that an extreme variation is possible for adjacent samples. This points to the problem of using a very small sample size. The data were processed with the assumption that the measured drop-size distribution is the parent distribution. This assumption is not quite valid, but no data are available to give an estimate of the parent distribution. Raindrop distributions are often characterized by their Z-R relationship. For this set of drop-size distributions, the Z-R relationship is given by Fig. 10(b) which gives Z_{eff} vs R for 1.29 GHz. In this case the frequency is low enough for Z_{eff} to equal Z , as shown in Fig. 11(a).

The Laws and Parsons model was generated from three years of rain data obtained in the Washington, D. C. area. All their data were averaged after division into drop radius and rain-rate intervals. These data were used as a comparison with the New England data because the rainfall types are similar in each area and the Laws and Parsons model may indicate the expected average for the New England data. The model data were used by converting the liquid-water content value for each interval to a number density. This assumption generated the drop-size distribution curves given in Fig. 1. The distribution was scaled to give the listed rain rates. The resultant rain parameters are listed in Table V.

[†]Courtesy of Dr. Pauline Austin.

TABLE II
DESCRIPTION OF SCATTERING DROP-SIZE DISTRIBUTION

| 1 July 1964 | | | | | | | |
|----------------|----------------------|--|--------------------|--|-------------------------|---------------|------------------|
| Time | Rain Rate (mm/hr) | Liquid-Water Content (gm/m ³) | No./m ³ | Z (mm ⁶ /m ³) ($\times 10^3$) | Median Diameter (mm) | No. in Sample | No. of Intervals |
| 1424L | 3.25 | 0.11 | 16.6 | 6.0 | 1.45 | 36 | 14 |
| 1424R | 3.65 | 0.13 | 28.0 | 7.3 | 1.45 | 52 | 17 |
| 1451L | 2.21 | 0.10 | 73.7 | 2.6 | 0.95 | 91 | 11 |
| 1451R | 3.11 | 0.13 | 70.4 | 5.7 | 1.05 | 91 | 14 |
| 1500L | 16.33 | 0.62 | 155.9 | 28.8 | 1.25 | 73 | 16 |
| 1500R | 31.98 | 1.11 | 138.3 | 82.1 | 1.55 | 77 | 19 |
| 1504L | 25.59 | 0.86 | 120.1 | 117.9 | 1.90 | 51 | 19 |
| 1504R | 22.41 | 0.78 | 136.3 | 63.7 | 1.90 | 58 | 18 |
| 1507L | 11.70 | 0.40 | 110.4 | 50.4 | 1.55 | 61 | 18 |
| 1507R | 8.92 | 0.34 | 163.7 | 20.0 | 1.45 | 86 | 15 |
| 1509L | 3.51 | 0.14 | 105.2 | 5.2 | 1.25 | 82 | 13 |
| 1509R | 4.51 | 0.18 | 130.2 | 6.6 | 1.35 | 106 | 15 |
| 1530L | 5.26 | 0.26 | 236.8 | 2.7 | 0.85 | 111 | 10 |
| 1530R | 7.46 | 0.37 | 325.6 | 4.0 | 0.85 | 155 | 10 |
| 1552L | 7.80 | 0.37 | 370.0 | 6.1 | 0.95 | 158 | 12 |
| 1552R | 12.81 | 0.58 | 379.6 | 11.0 | 0.95 | 188 | 13 |
| 1555L | 7.33 | 0.29 | 85.1 | 10.9 | 1.25 | 82 | 16 |
| 1555R | 7.34 | 0.29 | 95.0 | 7.9 | 1.15 | 92 | 14 |
| 26 August 1964 | | | | | | | |
| 1315L | 8.11 | 0.31 | 71.2 | 10.2 | 1.15 | 60 | 14 |
| 1315R | 8.84 | 0.33 | 68.2 | 16.8 | 1.15 | 59 | 14 |
| 1322L | 107.86 | 4.25 | 1959.9 | 212.8 | 1.25 | 111 | 18 |
| 1322R | 111.45 | 4.46 | 2713.3 | 206.5 | 1.25 | 139 | 18 |
| 1331L | 56.18 | 2.88 | 2706.7 | 26.9 | 0.85 | 146 | 10 |
| 1331R | 88.84 | 3.91 | 2158.4 | 74.0 | 1.05 | 128 | 12 |
| 1339L | 4.42 | 0.21 | 216.8 | 5.9 | 0.85 | 138 | 13 |
| 1339R | 3.12 | 0.18 | 252.7 | 1.2 | 0.65 | 159 | 9 |

IV. MEASURED AND MODELED SCATTERING PARAMETERS

Measured drop-size distributions made in New England were processed to investigate the variability of the scattering parameters to be expected in naturally occurring rainfall. The parameters are calculated by integrating the parameter densities over the range of drop sizes observed. The dielectric constants required for the scattering computations were calculated using the Debye formula⁸ with the constants as given in Kerr (Table 82).⁹ A drop temperature of 0.0°C was used for all computations using natural rain data. The index of refraction of liquid water is, using the above assumptions,

$$n = \sqrt{\frac{88.0 - 5.5}{1 + \frac{13.59}{\lambda}}} + 5.5 \quad , \quad \lambda \text{ in centimeters} .$$

More recent measurements of the index of refraction of water have been made by Grant, et al.¹⁰ Their measurements indicate that slight changes in both the form and constants of the above equation are needed to express the index of refraction over a wide range of frequencies. At 0.0°C, the differences between the two formulations are small, by less than 3 percent for the frequencies and distributions considered. A comparison of the scattering parameters for the frequencies used and the Laws and Parsons model is given in Table III. Because the differences

| TABLE III | | | | | | |
|--|--------|---------|-----------|---|-------|-------|
| COMPARISON OF SCATTERING PARAMETERS FOR REFRACTIVE INDEX OF WATER USED AND THAT ATTRIBUTED TO GRANT, <u>et al.</u> | | | | | | |
| (Drop Temperature: 0.0°C; Rain Rate: 12.7 mm/hr) | | | | | | |
| Computed Using Debye Model with Kerr Coefficients | | | | | | |
| Frequency (GHz) | n' | n'' | A (db/km) | Z _{eff} (mm ⁶ /m ³) | ω | N |
| 8.00 | 7.4786 | -2.7721 | 0.139 | 1.55 × 10 ⁺⁴ | 0.051 | 0.855 |
| 9.35 | 7.0969 | -2.9060 | 0.210 | 1.71 × 10 ⁺⁴ | 0.065 | 0.855 |
| 15.50 | 5.7619 | -3.0278 | 0.666 | 2.05 × 10 ⁺⁴ | 0.166 | 0.831 |
| 35.00 | 3.9533 | -2.4301 | 3.29 | 8.19 × 10 ⁺³ | 0.424 | 0.585 |
| 70.00 | 3.0179 | -1.6856 | 5.71 | 5.63 × 10 ⁺² | 0.494 | 0.169 |
| Computed Using Data Attributed to Grant, <u>et al.</u> | | | | | | |
| 8.00 | 7.6474 | -2.7146 | 0.140 | 1.56 × 10 ⁺⁴ | 0.051 | 0.856 |
| 9.35 | 7.2788 | -2.8692 | 0.213 | 1.72 × 10 ⁺⁴ | 0.064 | 0.857 |
| 15.50 | 5.9459 | -3.0694 | 0.675 | 2.08 × 10 ⁺⁴ | 0.165 | 0.829 |
| 35.00 | 4.055 | -2.5465 | 3.28 | 8.30 × 10 ⁺³ | 0.430 | 0.587 |
| 70.00 | 3.0410 | -1.8093 | 5.72 | 5.68 × 10 ⁺² | 0.501 | 0.169 |

are small and the Debye equation with the constants reported by Kerr have been used for most reported model computations, this formulation of the index of refraction was used.

The fluctuations of parameter density with drop size are illustrated in Figs. 2 through 5 which depict the variations in the parameters for two basically different raindrop distributions giving approximately the same rain rate. Both the measured distributions were taken at different times in the same storm. The number density shows that the sample taken at 1552 hours corresponds reasonably well to the Laws and Parsons model; the sample at 1507 hours has considerably fewer small drops and more large drops. The large total number of drops for the model distribution is the result of assuming a fixed liquid-water content for the extremely small drop sizes. Scattering parameters are computed for a frequency of 8.0 GHz. The curves marked 1-drop locus give the value of parameter density that would occur if one drop were collected in a drop-size interval during the exposure of the filter paper. This curve is used to illustrate the coarseness of the filter-paper measurement because, for short sampling times, only a few of the larger drop intervals will be populated. The scattering characteristics of the particular drops sampled are emphasized in the integration to find the per-unit volume parameters. For frequencies at which the scattering parameters vary strongly for the large drops, the sampling process can give wide fluctuations about the value for the parent distribution. Since the parent distribution is unknown, an estimate of this sampling error may be made by considering the simultaneous filter-paper measurements made on 1 July and 26 August 1964 (see Tables II and IV). Roughly, up to a factor of 2 difference may be present in estimating rain rate, reflectivity, and the attenuation coefficient. A more precise consideration of the sampling process requires better measurements of spatial and temporal raindrop distributions. The data also show that up to a factor of 5.4 difference in the attenuation coefficient at 8.0 GHz may be caused by different drop distributions giving the same rain rate. The increase in this

TABLE IV
EFFECT OF DISTRIBUTION DIFFERENCE ON SCATTERING PARAMETERS

| Distribution | Rain Rate (mm/hr) | Frequency (GHz) | Temperature (°C) | Attenuation Coefficient (db/km) | Radio Reference (N) | Albedo (ω) |
|--------------|-------------------|-----------------|------------------|---------------------------------|---------------------|---------------------|
| L and P | 12.7 | 4.0 | 0.0 | 0.017 | 0.82 | 0.024 |
| 1507L | 11.7 | 4.0 | 0.0 | 0.030 | 0.64 | 0.047 |
| 1552R | 12.8 | 4.0 | 0.0 | 0.016 | 0.86 | 0.019 |
| L and P | 12.7 | 8.0 | 0.0 | 0.139 | 0.86 | 0.051 |
| 1507L | 11.7 | 8.0 | 0.0 | 0.278 | 0.60 | 0.103 |
| 1552R | 12.8 | 8.0 | 0.0 | 0.120 | 0.89 | 0.041 |
| L and P | 12.7 | 15.5 | 0.0 | 0.666 | 0.83 | 0.166 |
| 1507L | 11.7 | 15.5 | 0.0 | 0.910 | 0.49 | 0.393 |
| 1552R | 12.8 | 15.5 | 0.0 | 0.638 | 0.88 | 0.129 |
| L and P | 12.7 | 34.86 | 0.0 | 3.27 | 0.59 | 0.423 |
| 1507L | 11.7 | 34.86 | 0.0 | 2.05 | 0.17 | 0.532 |
| 1552R | 12.8 | 34.86 | 0.0 | 3.42 | 0.65 | 0.413 |

number over the factor of 2 due to sampling is apparently due to basic differences in the raindrop distributions. Again, the existence of large volumes of a rainstorm having these basic differences is not certain.

An illustration of possible differences in scattering parameters caused by drop-size distribution changes where the rain rates are the same is given in Figs. 2 through 5 and Table IV. Figure 2 compares two individual measurements of drop-size number density with the Laws and Parsons model. Figures 3 through 5 compare the imaginary and real index of refraction density and the total scattering coefficient density for the two samples and the model shown in Fig. 2. The 1-drop locus gives an idea of the limitation of the filter-paper sampling method. This curve gives the contribution of one drop in each radius interval. No measured points can lie to the right of the 1-drop loci. The effect of the relatively great number of large drops and the slight number of small drops is evident in the comparison of attenuation coefficients for the 4.0-, 8.0-, and 34.86-GHz frequencies. The peak of the extinction cross section vs radius curve coincides with the large drops for 4.0 GHz and the smaller drops at 34.86 GHz. The resultant attenuation coefficient for the 1507R sample is a factor of 2 higher than the attenuation coefficient for 1552L at 4.0 GHz, and a factor of 2 lower at 34.86 GHz.

The scattergram data given in Figs. 6(a-h) through 17(a-h) show the effect of differing drop sizes and sampling error. The data for low rain rates tend to come from general, widespread rain, while the data for the higher rain rates come from the severe thundershowers. However, samples from thundershowers can have rain rates as low as 0.2 mm/hr. The scattergram data are presented in sections depending upon scattering and rain parameters. For each section, the frequencies vary from 1.29 to 94.0 GHz. This variation in frequency shows the transition of the integrated scattering process from that describable by Rayleigh theory to that by Mie theory.

Rayleigh scattering occurs for drops small compared with the wavelength (see Ref. 4, Ch. 6). For Rayleigh scattering, the forward scattering amplitude is given by

$$\begin{aligned} S(n,a) &= ik^3 \alpha \\ &= iK(ka)^3 = i \frac{3}{4\pi} Kk^3 V \end{aligned}$$

where

k , K are as defined previously

α = polarizability of sphere

V = volume of sphere.

This formula holds for the radius smaller than the wavelength as

$$a \ll \frac{\lambda}{2\pi|n|}, \quad n = \text{index of refraction of water} .$$

For larger spheres, the expression for the forward scattering amplitude can be expanded in a series in ka as

$$S(n,a) = iK(ka)^3 + \frac{2}{3} K^2 (ka)^6 + \dots .$$

These small particle size scattering formulas show that the refractivity and attenuation coefficient depend only upon the drop volume or liquid-water content when the scattering process is describable by Rayleigh theory. This is evident in the scattergrams of refractivity vs liquid-water content [Figs. 15(a-h)]. The departure of the refractivity from a linear dependence on liquid-water content is evident only for frequencies above 10.0 GHz. The dependence of the attenuation coefficient on liquid-water content [Figs. 6(a-h)] shows a departure from a straight line for frequencies as low as 1.3 GHz and high values of liquid-water content. The lower frequency departure of the attenuation coefficient from Rayleigh scattering is due to K, which has an imaginary part of the order of 5 percent or less of its real part for frequencies less than 15.5 GHz. This causes the second term of the expansion of the scattering amplitude in powers of ka to be important for calculating the real part of $S(a,n)$ at a lower frequency than for calculating the imaginary part of $S(a,n)$. The scattergrams for Z_{eff} vs Z [Figs. 11(a-h)] show that the frequency marking the departure of the backscatter cross section per-unit volume from that describable by Rayleigh theory coincides with the frequency of departure for refractivity, or about 10 GHz.

A measure of the uncertainty in an estimate of the attenuation coefficient for a given meteorological parameter can be found using the width of the scattergram. Curves drawn on the scattergram parallel to the Laws and Parsons model curve and including all the data points can be used to define the maximum spread of the data points with reference to the Laws and Parsons model. The distance between these curves measured at a constant rain rate gives the ratio of the maximum to minimum possible attenuation coefficient for the drop distributions, frequency and drop temperature used. This ratio, called an attenuation uncertainty factor, is plotted in Fig. 18 for the three meteorological parameters used to estimate attenuation.

The width of the scattergrams of attenuation coefficient A vs rain rate [Figs. 7(a-h)] show, as a function of frequency, a relative peak in the uncertainty at a factor of 5.4 times at 8.0 GHz, a minimum of 1.8 times at 35 GHz, and a rapid increase in uncertainty at the higher frequencies to a value of 7 times at 94.0 GHz. These results are in accord with Medhurst¹¹ who predicts a relative maximum in the spread between the maximum and minimum values of attenuation coefficient at 5.0-cm (6.0-GHz) wavelength, a minimum at 1.0-cm (30.0-GHz) wavelength, and a rapid increase for wavelengths less than 1.0 cm. The width of the A vs Z scattergrams [Figs. 8(a-h)] shows a minimum uncertainty at about 10.0 GHz, with maximum uncertainties at the low- and high-frequency limits. For most of the frequencies encountered, the uncertainty in A with rain rate increases with increasing rain rate. The uncertainty in A with Z value, however, decreases with increasing Z or rain rate at 8.0 and 9.35 GHz. For the 8.0-GHz frequency, for rain rates greater than 5 mm/hr, the peak uncertainty in A vs rain rate is 5.4 times, and in A vs Z it is 2.0 times. In this region, an estimate of attenuation based on a Z value measurement is superior to that based on rain rate. For the other frequencies, and for rain rates below 5 mm/hr, estimates of attenuation based on rain-rate measurements are superior to those based on Z measurements.

The single-scattering albedo parameter ω gives the ratio of the energy scattered by drops to that lost to a wave propagating through the volume of drops. When ω is small compared to 1, the energy is mainly absorbed by the drops. For ω near 1, the energy is largely scattered and is available for multiple scattering. The wide spread of data points depicted in the scattergrams [Figs. 12(a-h) through 14(a-h)] shows over an order of magnitude uncertainty at the lowest

frequency to less than a factor of two at the highest frequency for all rain parameters used. The data show that most of the energy is absorbed by the drops for frequencies less than 8.0 GHz. At the higher frequencies, the amount of energy absorbed continuously decreased to a value of about one-half for the higher rain rates at 94.0 GHz.

V. CONCLUSIONS

The scattergrams of microwave vs rain parameters show the difficulty encountered in using meteorological data to estimate microwave propagation results. The scatter in data points may be due, in part, to the effects of limited sample sizes. However, it is expected that much of the scatter is due to the natural variation of the raindrop distributions. Computations using the Laws and Parsons model, as given in Table V and shown on the curves A vs Z and A vs rain rate, show that the model agrees reasonably well with the center of the natural rain data.

The computed results show that Rayleigh scattering theory may be used to calculate the refractivity and effective reflectivity factor for frequencies up to about 10 GHz. Computations of attenuation coefficient using Rayleigh theory are, however, useful only for frequencies below about 2.0 GHz.

Comparisons of the attenuation coefficient with meteorological parameters show that, for frequencies in the 8.0- to 9.0-GHz range and the higher rain rates, estimates of attenuation are best made using weather radar data. For other frequencies and rain rates, a measurement of rain rate is best. However, this conclusion depends upon the availability of rainfall rate measurements over large volumes of space. Currently, these measurements are not available and weather radar data are the only data available. The scattergrams of A vs Z represent the best estimation of attenuation from measured rainfall data. The uncertainties in attenuation are extremely high for the higher frequencies and reduce to about a factor of 2 for high rain rates and an 8.0-GHz frequency. The data further show that the Laws and Parsons model makes a reasonable basis for converting weather radar data to attenuation estimates.

TABLE V
RAIN AND SCATTERING PARAMETERS FOR LAWS AND PARSONS MODEL DATA
(Drop Temperature: 0.0°C)

| Frequency (GHz) | Rain Parameters | | | Scattering Parameters | | | |
|--------------------|-----------------|---------------------------|---|-----------------------|--|--------|-------|
| | R (mm/hr) | L (gm/m ³) | Z (mm ⁶ /m ³) | A (db/km) | Z _{eff} (mm ⁶ /m ³) | ω | N |
| 1.29 | 0.254 | 0.019 | 5.45×10^1 | 3.19×10^{-5} | 5.43×10^1 | 0.0005 | 0.027 |
| | 1.27 | 0.073 | 5.63×10^2 | 1.28×10^{-4} | 5.64×10^2 | 0.001 | 0.107 |
| | 2.54 | 0.134 | 1.55×10^3 | 2.35×10^{-4} | 1.54×10^3 | 0.002 | 0.194 |
| | 12.7 | 0.555 | 1.47×10^4 | 1.01×10^{-3} | 1.45×10^4 | 0.004 | 0.809 |
| | 25.4 | 1.04 | 3.89×10^4 | 1.94×10^{-3} | 3.85×10^4 | 0.006 | 1.51 |
| | 50.8 | 1.96 | 1.02×10^5 | 3.76×10^{-3} | 1.00×10^5 | 0.008 | 2.86 |
| | 101.6 | 3.74 | 2.65×10^5 | 7.40×10^{-3} | 2.60×10^5 | 0.010 | 5.45 |
| | 152.4 | 5.47 | 4.63×10^5 | 1.11×10^{-2} | 4.54×10^5 | 0.012 | 7.99 |
| 2.80 | 0.254 | 0.019 | 5.45×10^1 | 1.59×10^{-4} | 5.40×10^1 | 0.002 | 0.027 |
| | 1.27 | 0.073 | 5.63×10^2 | 6.73×10^{-4} | 5.55×10^2 | 0.005 | 0.107 |
| | 2.54 | 0.134 | 1.55×10^3 | 1.28×10^{-3} | 1.51×10^3 | 0.008 | 0.196 |
| | 12.7 | 0.555 | 1.47×10^4 | 6.18×10^{-3} | 1.40×10^4 | 0.015 | 0.817 |
| | 25.4 | 1.04 | 3.89×10^4 | 1.26×10^{-2} | 3.68×10^4 | 0.020 | 1.53 |
| | 50.8 | 1.96 | 1.02×10^5 | 2.64×10^{-2} | 9.49×10^4 | 0.025 | 2.91 |
| | 101.6 | 3.74 | 2.65×10^5 | 5.66×10^{-2} | 2.44×10^5 | 0.030 | 5.58 |
| | 152.4 | 5.47 | 4.63×10^5 | 8.95×10^{-2} | 4.21×10^5 | 0.033 | 8.21 |
| 8.0 | 0.254 | 0.019 | 5.45×10^1 | 1.75×10^{-3} | 5.25×10^1 | 0.013 | 0.027 |
| | 1.27 | 0.073 | 5.63×10^2 | 9.45×10^{-3} | 5.35×10^2 | 0.026 | 0.110 |
| | 2.54 | 0.134 | 1.55×10^3 | 2.08×10^{-2} | 1.49×10^3 | 0.034 | 0.202 |
| | 12.7 | 0.555 | 1.47×10^4 | 1.39×10^{-1} | 1.55×10^4 | 0.051 | 0.855 |
| | 25.4 | 1.04 | 3.89×10^4 | 3.24×10^{-1} | 4.45×10^4 | 0.060 | 1.61 |
| | 50.8 | 1.96 | 1.02×10^5 | 7.60×10^{-1} | 1.25×10^5 | 0.069 | 3.05 |
| | 101.6 | 3.74 | 2.65×10^5 | 1.78×10 | 3.48×10^5 | 0.079 | 5.81 |
| | 152.4 | 5.47 | 4.63×10^5 | 2.93×10 | 6.34×10^5 | 0.086 | 8.48 |
| 9.35 | 0.254 | 0.019 | 5.45×10^1 | 2.54×10^{-3} | 5.25×10^1 | 0.017 | 0.028 |
| | 1.27 | 0.073 | 5.63×10^2 | 1.42×10^{-2} | 5.50×10^2 | 0.033 | 0.111 |
| | 2.54 | 0.134 | 1.55×10^3 | 3.15×10^{-2} | 1.57×10^3 | 0.042 | 0.203 |
| | 12.7 | 0.555 | 1.47×10^4 | 2.09×10^{-1} | 1.71×10^4 | 0.065 | 0.855 |
| | 25.4 | 1.04 | 3.89×10^4 | 4.82×10^{-1} | 4.90×10^4 | 0.078 | 1.60 |
| | 50.8 | 1.96 | 1.02×10^5 | 1.11×10 | 1.37×10^5 | 0.091 | 3.02 |
| | 101.6 | 3.74 | 2.65×10^5 | 2.53×10 | 3.81×10^5 | 0.107 | 5.70 |
| | 152.4 | 5.47 | 4.63×10^5 | 4.07×10 | 6.90×10^5 | 0.117 | 8.26 |

TABLE V (Continued)

| Frequency (GHz) | Rain Parameters | | | Scattering Parameters | | | |
|--------------------|-----------------|---------------------------|---|-----------------------|--|-------|-------|
| | R (mm/hr) | L (gm/m ³) | Z (mm ⁶ /m ³) | A (db/km) | Z _{eff} (mm ⁶ /m ³) | ω | N |
| 15.5 | 0.254 | 0.019 | 5.45×10^1 | 8.33×10^{-3} | 5.52×10^1 | 0.041 | 0.028 |
| | 1.27 | 0.073 | 5.63×10^2 | 4.88×10^{-2} | 6.61×10^2 | 0.080 | 0.111 |
| | 2.54 | 0.134 | 1.55×10^3 | 1.07×10^{-1} | 1.94×10^3 | 0.104 | 0.203 |
| | 12.7 | 0.555 | 1.47×10^4 | 6.66×10^{-1} | 2.04×10^4 | 0.166 | 0.832 |
| | 25.4 | 1.04 | 3.89×10^4 | 1.46×10 | 5.51×10^4 | 0.201 | 1.53 |
| | 50.8 | 1.96 | 1.02×10^5 | 3.17×10 | 1.44×10^5 | 0.240 | 2.81 |
| | 101.6 | 3.74 | 2.65×10^5 | 6.83×10 | 3.70×10^5 | 0.283 | 5.15 |
| | 152.4 | 5.47 | 4.63×10^5 | 1.06×10^1 | 6.33×10^5 | 0.311 | 7.34 |
| 35.0 | 0.254 | 0.019 | 5.45×10^1 | 5.44×10^{-2} | 6.45×10^1 | 0.182 | 0.028 |
| | 1.27 | 0.073 | 5.63×10^2 | 3.10×10^{-1} | 5.81×10^2 | 0.291 | 0.103 |
| | 2.54 | 0.134 | 1.55×10^3 | 6.43×10^{-1} | 1.36×10^3 | 0.335 | 0.177 |
| | 12.7 | 0.555 | 1.47×10^4 | 3.29×10 | 8.18×10^3 | 0.423 | 0.587 |
| | 25.4 | 1.04 | 3.89×10^4 | 6.40×10 | 1.62×10^4 | 0.456 | 0.950 |
| | 50.8 | 1.96 | 1.02×10^5 | 1.21×10^1 | 3.03×10^4 | 0.484 | 1.50 |
| | 101.6 | 3.74 | 2.65×10^5 | 2.23×10^1 | 5.24×10^4 | 0.508 | 2.33 |
| | 152.4 | 5.47 | 4.63×10^5 | 3.15×10^1 | 6.95×10^4 | 0.519 | 3.03 |
| 70.0 | 0.254 | 0.019 | 5.45×10^1 | 2.23×10^{-1} | 2.95×10^1 | 0.367 | 0.020 |
| | 1.27 | 0.073 | 5.63×10^2 | 9.18×10^{-1} | 1.19×10^2 | 0.432 | 0.053 |
| | 2.54 | 0.134 | 1.55×10^3 | 1.62×10 | 2.00×10^2 | 0.455 | 0.077 |
| | 12.7 | 0.555 | 1.47×10^4 | 5.71×10 | 5.63×10^2 | 0.494 | 0.169 |
| | 25.4 | 1.04 | 3.89×10^4 | 9.68×10 | 8.43×10^2 | 0.506 | 0.235 |
| | 50.8 | 1.96 | 1.02×10^5 | 1.64×10^1 | 1.29×10^3 | 0.515 | 0.336 |
| | 101.6 | 3.74 | 2.65×10^5 | 2.81×10^1 | 2.11×10^3 | 0.522 | 0.510 |
| | 152.4 | 5.47 | 4.63×10^5 | 3.87×10^1 | 2.86×10^3 | 0.526 | 0.664 |
| 94.0 | 0.254 | 0.019 | 5.45×10^1 | 3.11×10^{-1} | 1.22×10^1 | 0.419 | 0.019 |
| | 1.27 | 0.073 | 5.63×10^2 | 1.10×10 | 3.63×10^1 | 0.459 | 0.030 |
| | 2.54 | 0.134 | 1.55×10^3 | 1.83×10 | 5.38×10^1 | 0.472 | 0.041 |
| | 12.7 | 0.555 | 1.47×10^4 | 5.95×10 | 1.32×10^2 | 0.497 | 0.078 |
| | 25.4 | 1.04 | 3.89×10^4 | 9.88×10 | 2.04×10^2 | 0.506 | 0.102 |
| | 50.8 | 1.96 | 1.02×10^5 | 1.66×10^1 | 3.27×10^2 | 0.513 | 0.139 |
| | 101.6 | 3.74 | 2.65×10^5 | 2.83×10^1 | 5.49×10^2 | 0.520 | 0.205 |
| | 152.5 | 5.47 | 4.63×10^5 | 3.90×10^1 | 7.45×10^2 | 0.523 | 0.267 |

REFERENCES

1. J. W. Ryde and D. Ryde, "Attenuation of Centimetre and Millimetre Waves by Rain, Hail, Fog, and Clouds," Report No. 8670, General Electric Company Research Laboratory, London (1945).
2. T. Oguchi, "Attenuation of Electromagnetic Wave Due to Rain with Distorted Raindrops," J. Radio Res. Lab (Japan) 7, 467 (1960); Part II, J. Radio Res. Lab (Japan) 11, 19 (1964).
3. D. Deirmendjian, "Complete Microwave Scattering and Extinction Properties of Polydispersed Cloud and Rain Elements," Report No. RAND-R-422-PR, RAND Corporation, Santa Monica, California (December 1963), AD-426-139.
4. H.C. Van de Hulst, Light Scattering by Small Particles (Wiley, New York, 1957), Ch.9.
5. V. Twersky, "On Scattering of Waves by Random Distributions. I. Free-Space Scatterer Formalism," J. Math. Phys. 3, No. 4, 700 (1962).
6. K.L.S. Gunn and G.D. Kinzer, "The Terminal Velocity of Fall for Water Droplets in Stagnant Air," J. Meteorol. 6, No. 4, 243 (1949).
7. J.O. Laws and D.A. Parsons, "The Relation of Rain Drop-Size to Intensity," Am. Geophys. Union Trans. 24, 452 (1943).
8. P. Debye, "Polar Molecules," Chemical Catalog Company, New York (1929), Ch.6.
9. D.E. Kerr, Propagation of Short Radio Waves, Radiation Laboratory Series, M.I.T. (McGraw-Hill, New York, 1951), Vol. 13.
10. E.H. Grant, T.J. Buchanan, and H.F. Cook, "Dielectric Behavior of Water at Microwave Frequencies," J. Chem. Phys. 26, No. 1, 156 (1957).
11. R.G. Medhurst, "Rainfall Attenuation of Centimeter Waves: Comparison of Theory and Measurement," IEEE Trans. Antennas Propag. AP-13, No. 4, 550 (1965).

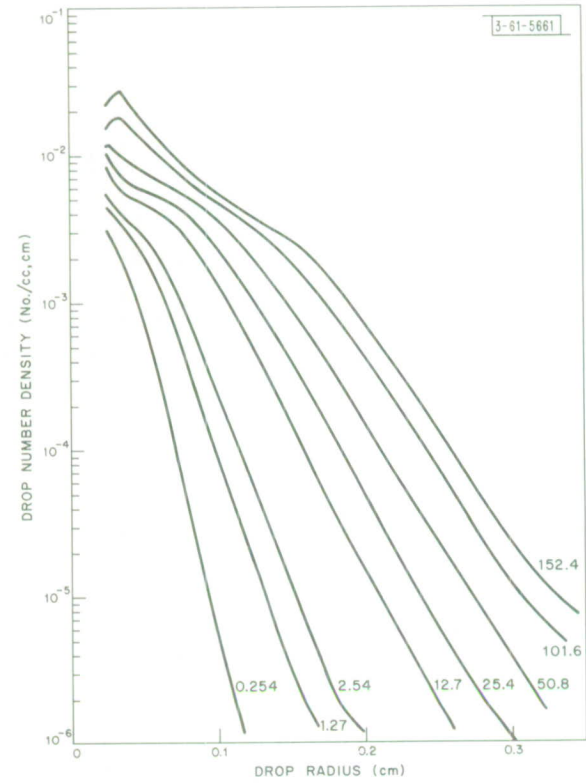


Fig. 1. Drop-size distribution for Laws and Parsons model
(curves labeled with rain rate in mm/hr).

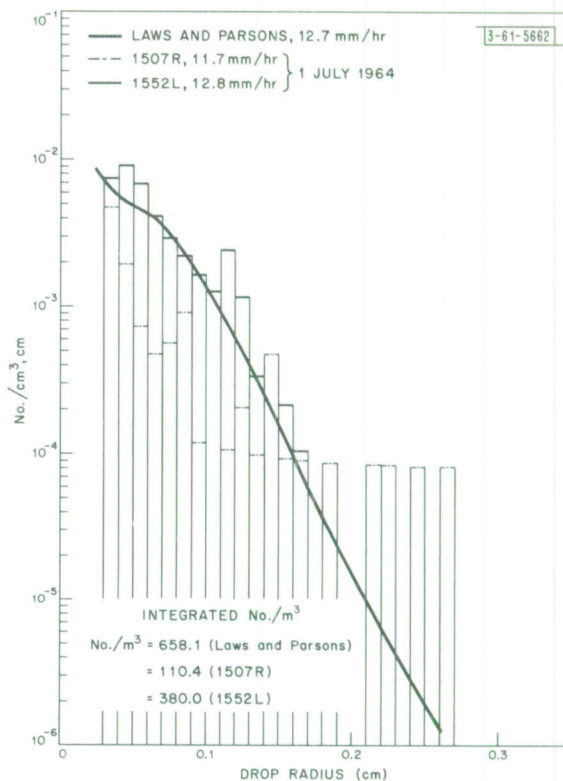


Fig. 2. Comparison of measured and modeled drop distributions, number density ($\text{No.}/\text{cm}^3 \cdot \text{cm}$).

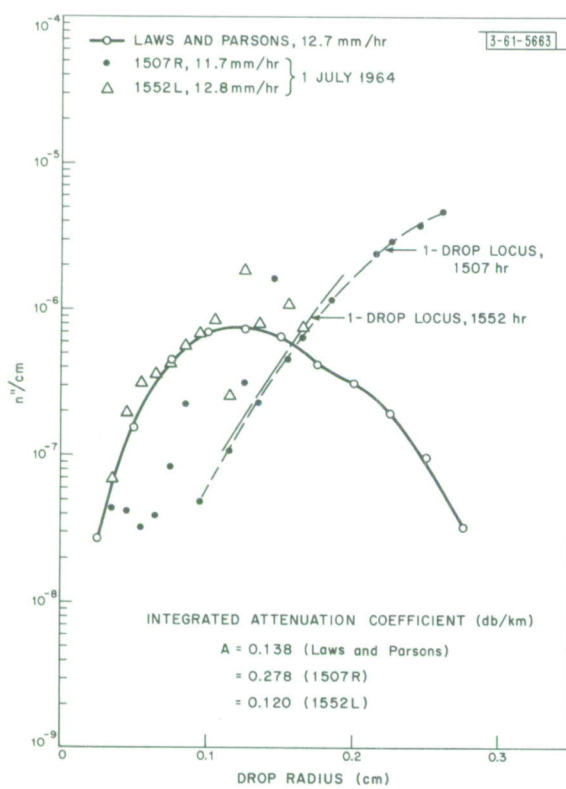


Fig. 3. Comparison of measured and modeled drop distributions, imaginary index of refraction density (n''/cm). Frequency = 8.0 GHz; drop temperature = 0.0°C.

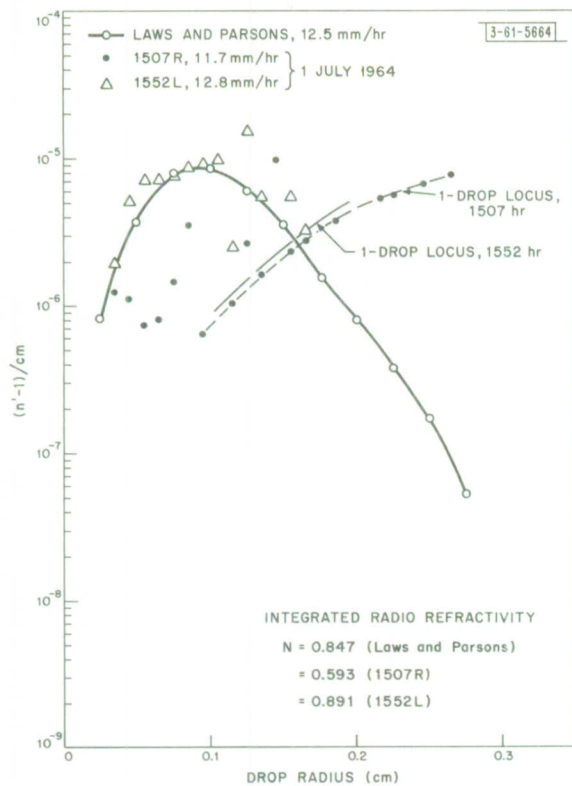


Fig. 4. Comparison of measured and modeled drop distributions, real index of refraction density [$(n' - 1)/\text{cm}$]. Frequency = 8.0 GHz; drop temperature = 0.0°C.

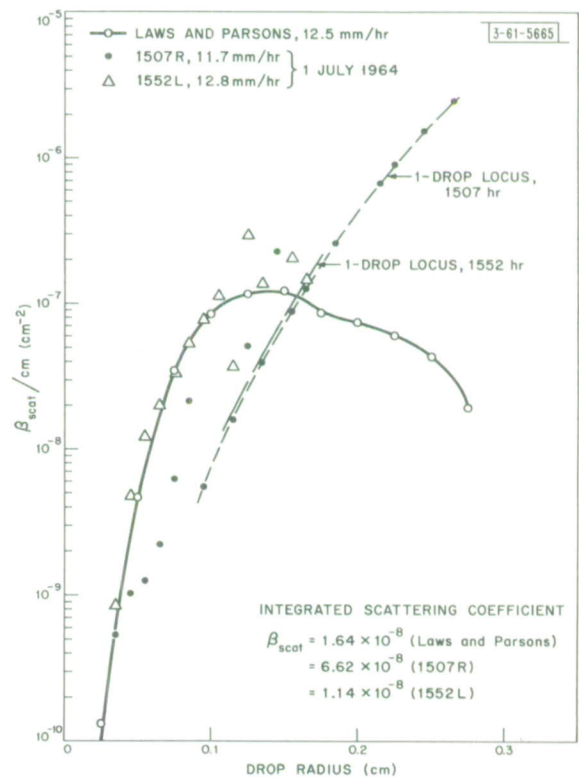
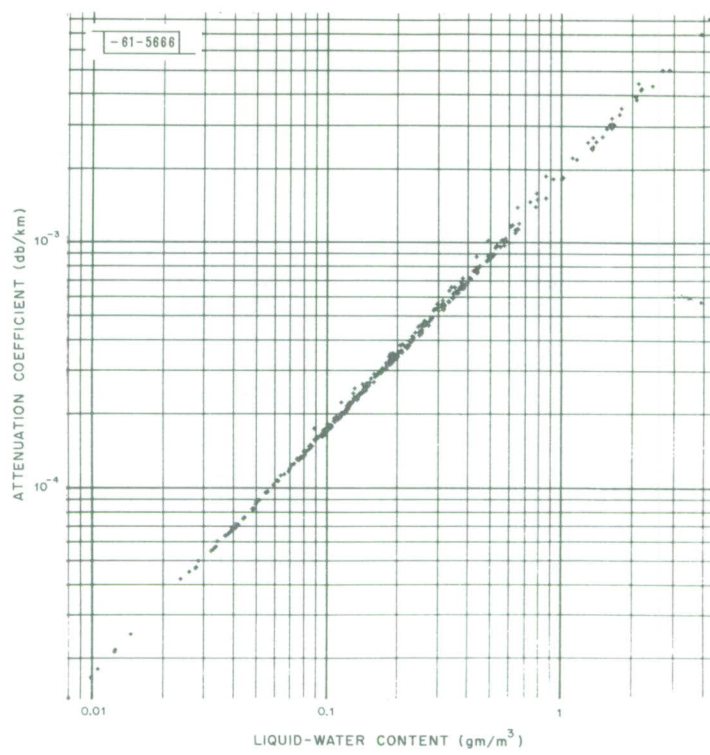
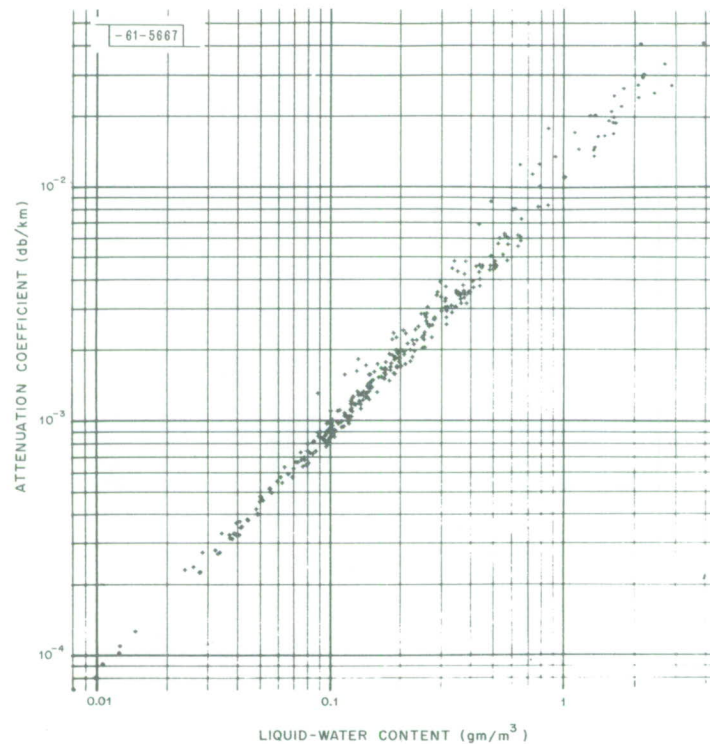


Fig. 5. Comparison of measured and modeled drop distributions, scattering coefficient density ($\beta_{\text{scat}}/\text{cm}$). Frequency = 8.0 GHz; drop temperature = 0.0°C.

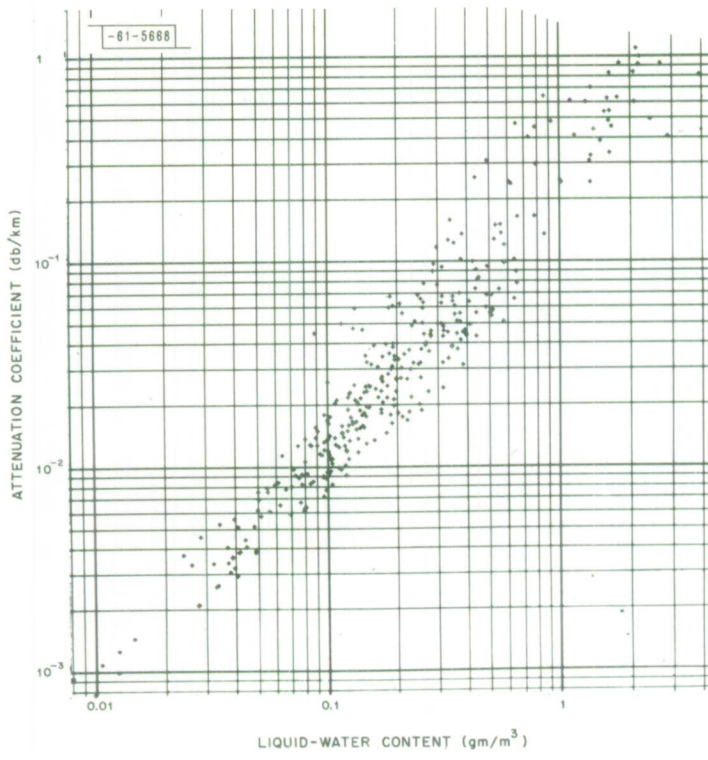


(a) Frequency: 1.29 GHz.

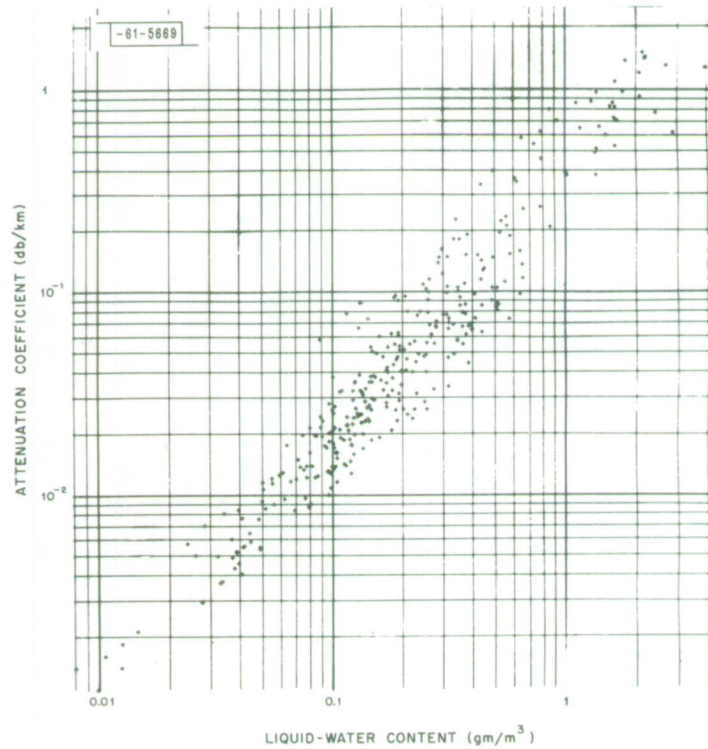


(b) Frequency: 2.80 GHz.

Fig. 6(a-h). Attenuation coefficient A vs liquid-water content L . Drop temperature = 0.0°C.

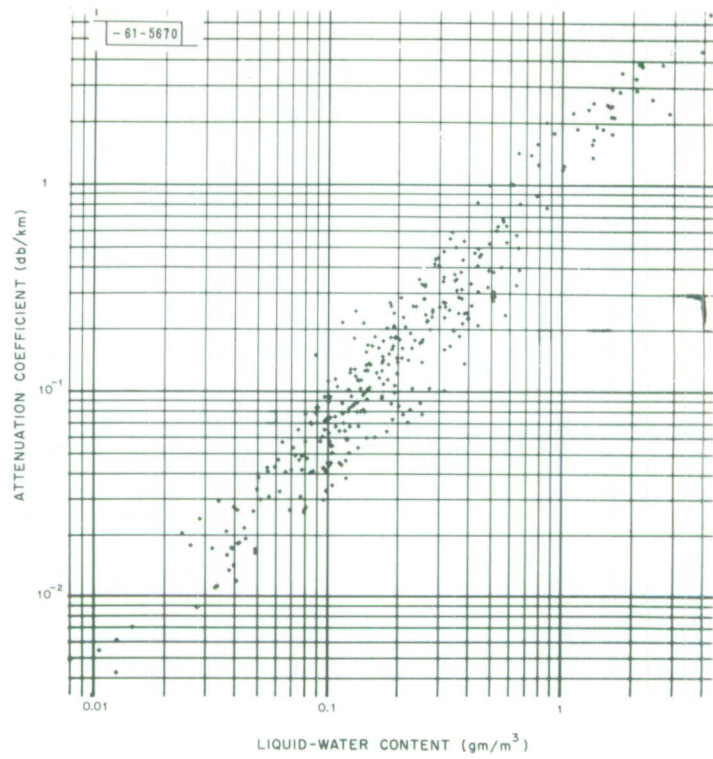


(c) Frequency: 8.0 GHz.

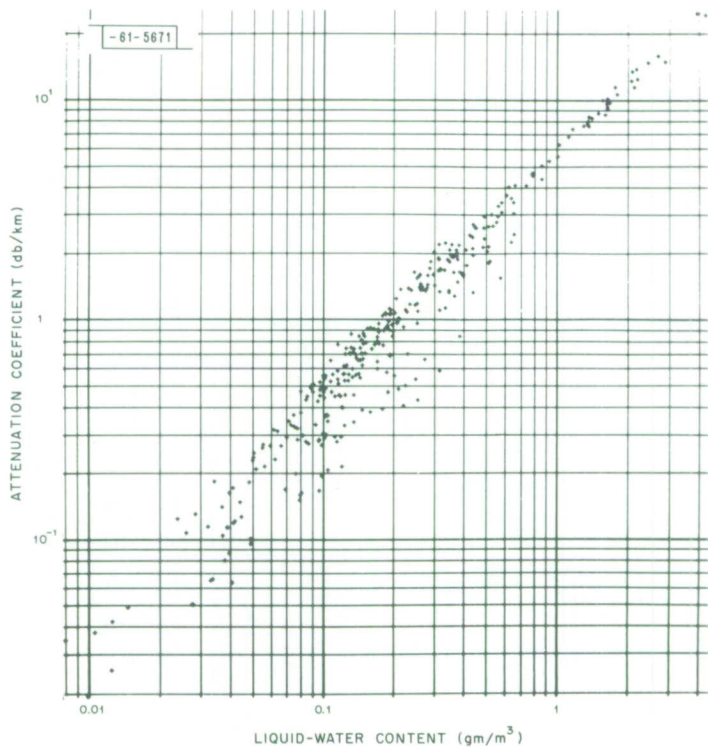


(d) Frequency: 9.35 GHz.

Fig. 6. Continued.

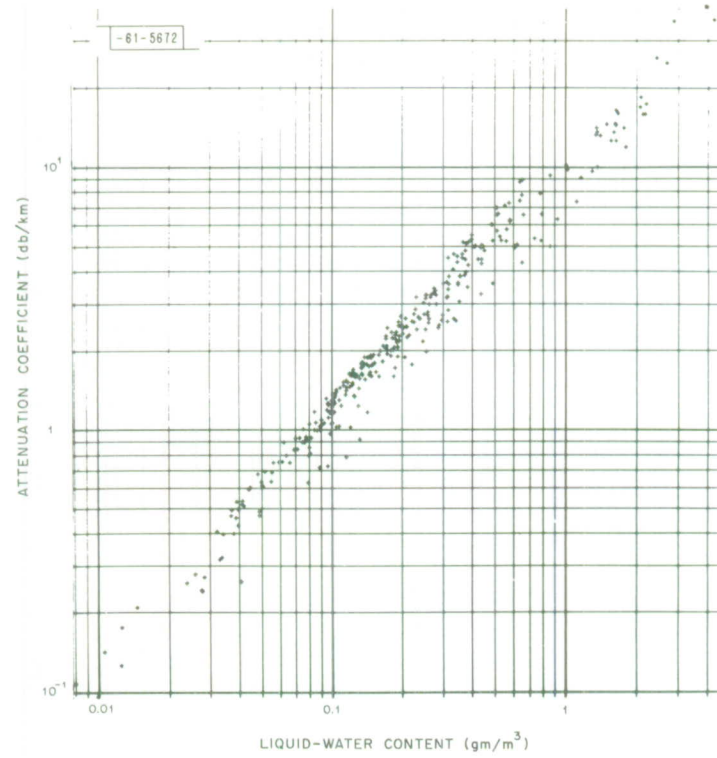


(e) Frequency: 15.5 GHz.

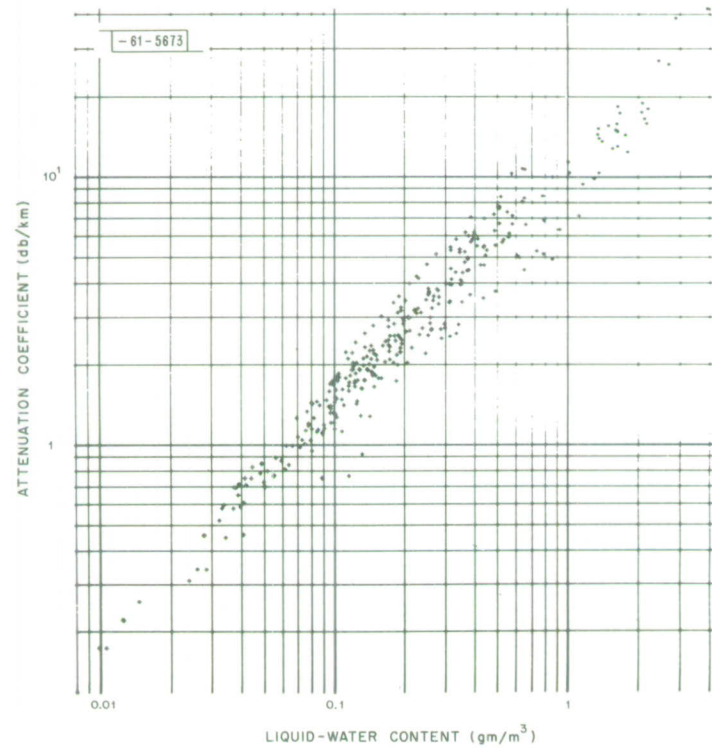


(f) Frequency: 35.0 GHz.

Fig. 6. Continued.

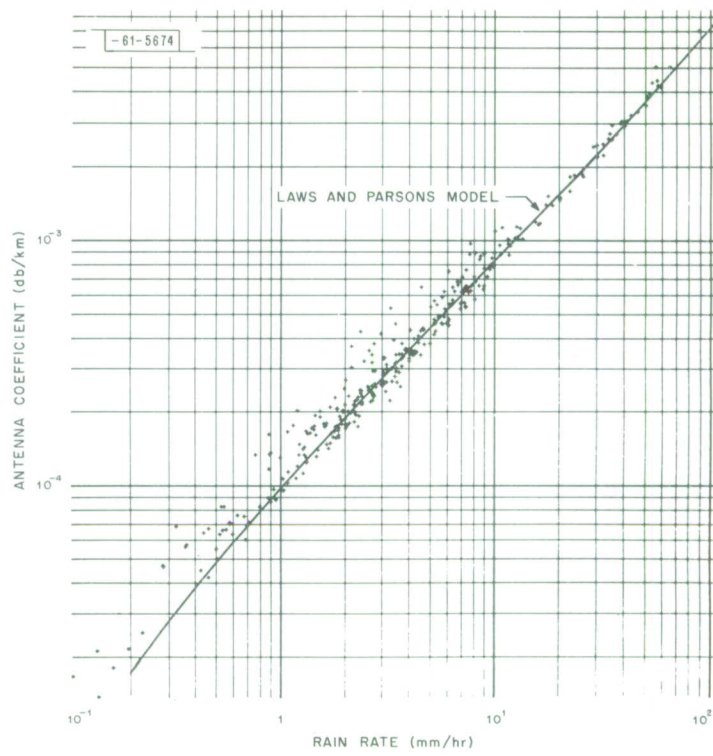


(g) Frequency: 70.0 GHz.

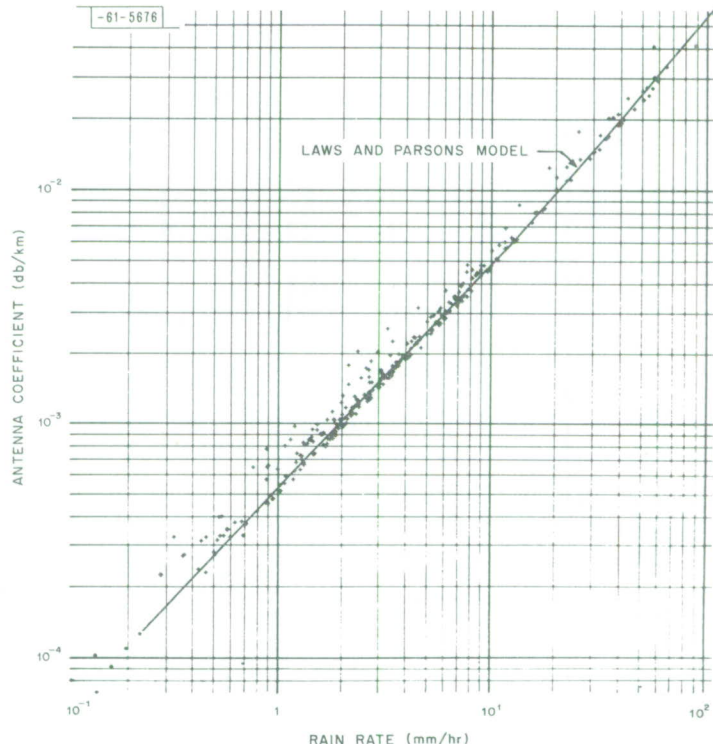


(h) Frequency: 94.0 GHz.

Fig. 6. Continued.

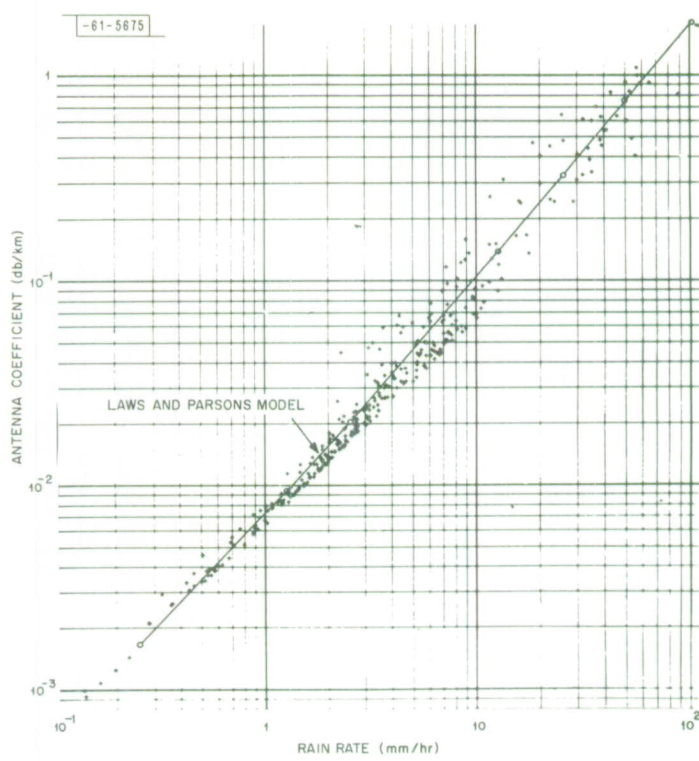


(a) Frequency: 1.29 GHz.

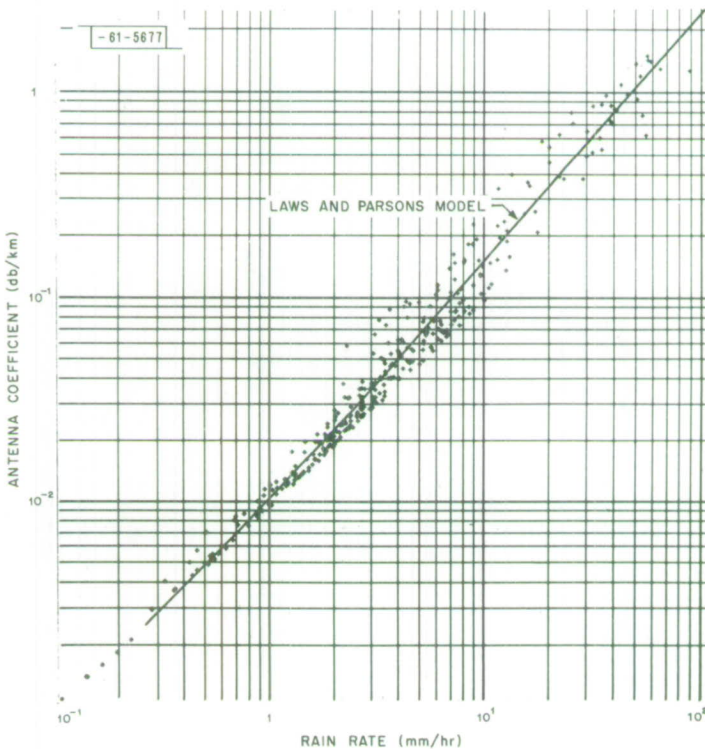


(b) Frequency: 2.80 GHz.

Fig. 7(a-h). Attenuation coefficient A vs rain rate R . Drop temperature = 0.0°C .

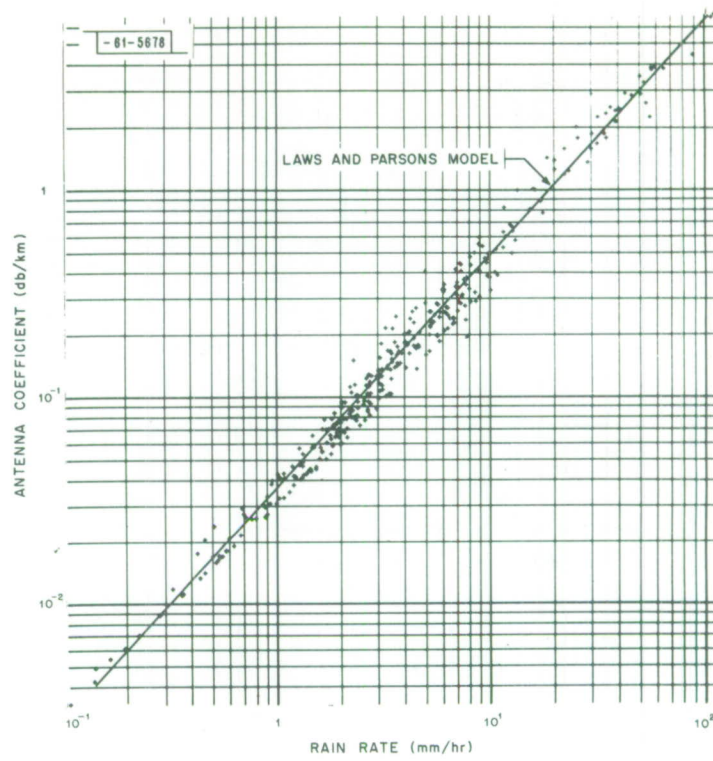


(c) Frequency: 8.0 GHz.

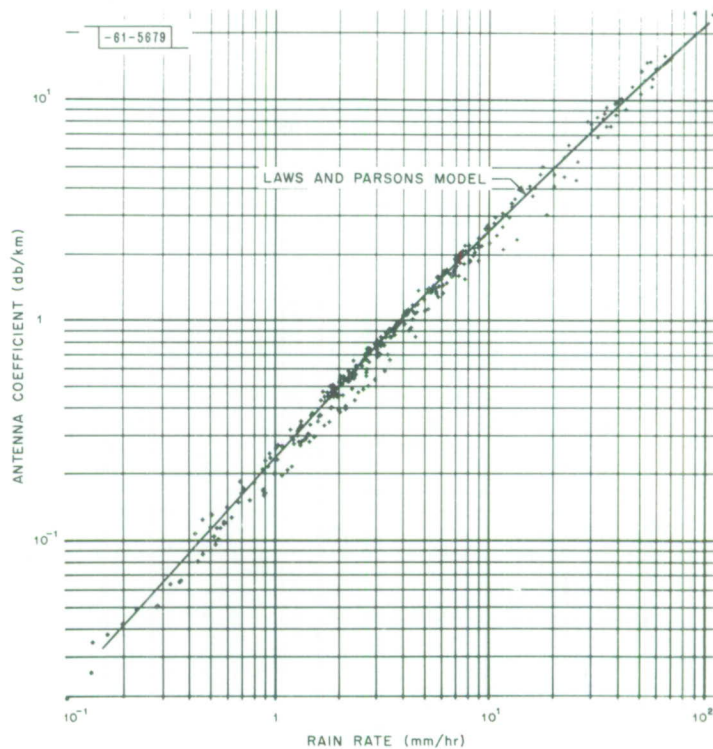


(d) Frequency: 9.35 GHz.

Fig. 7. Continued.

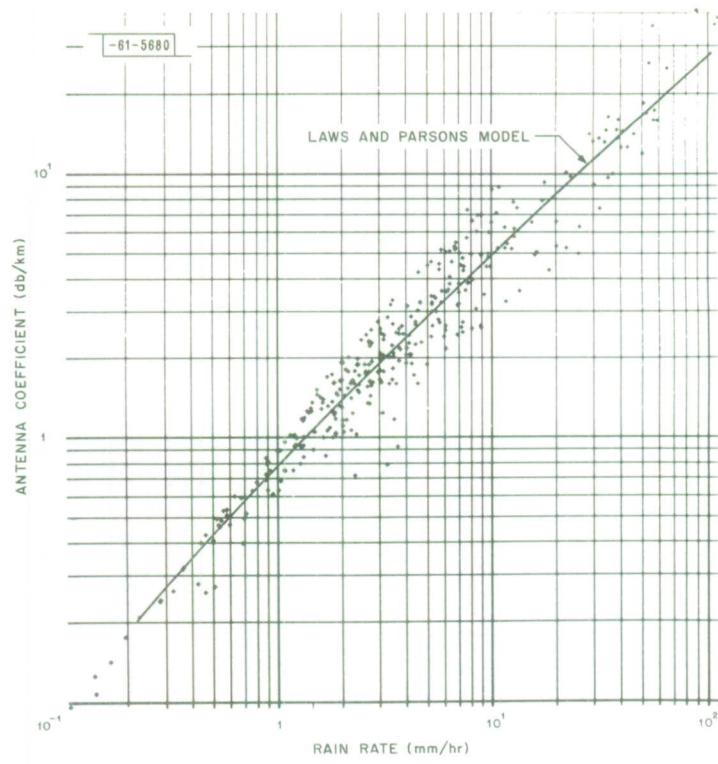


(e) Frequency: 15.5 GHz.

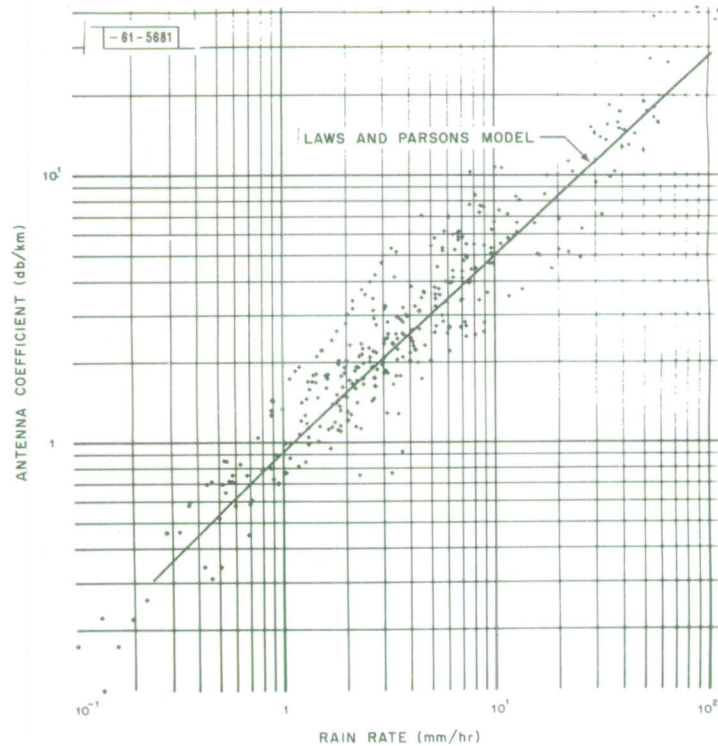


(f) Frequency: 35.0 GHz.

Fig. 7. Continued.

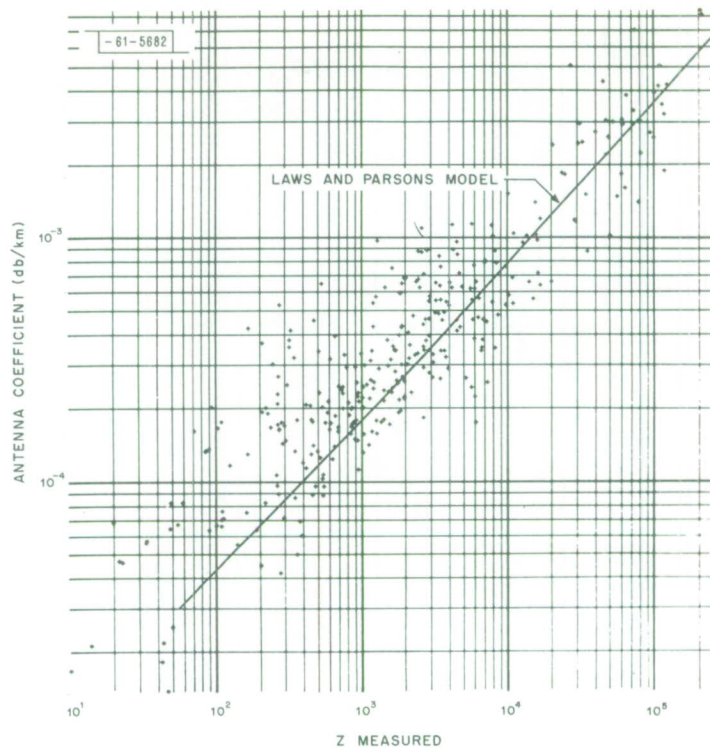


(g) Frequency: 70.0 GHz.

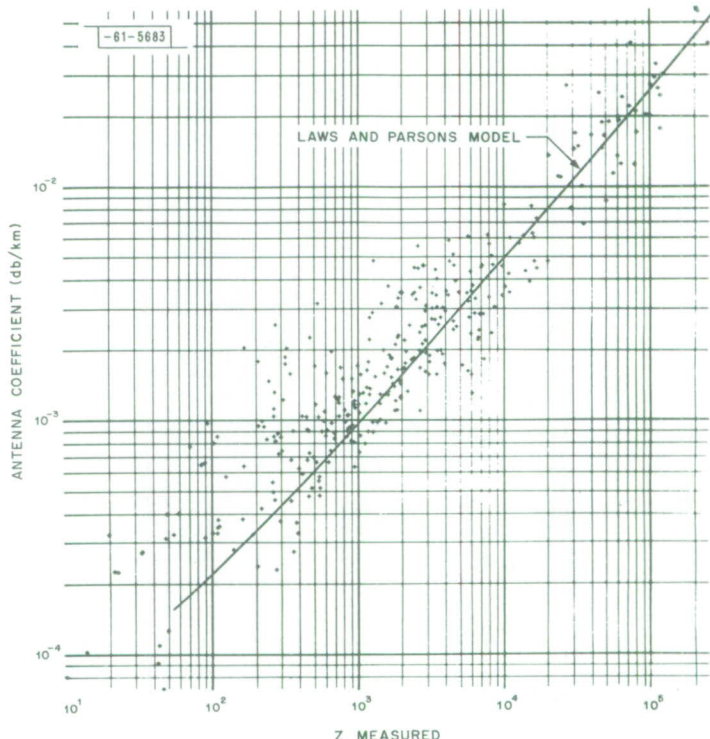


(h) Frequency: 94.0 GHz.

Fig. 7. Continued.

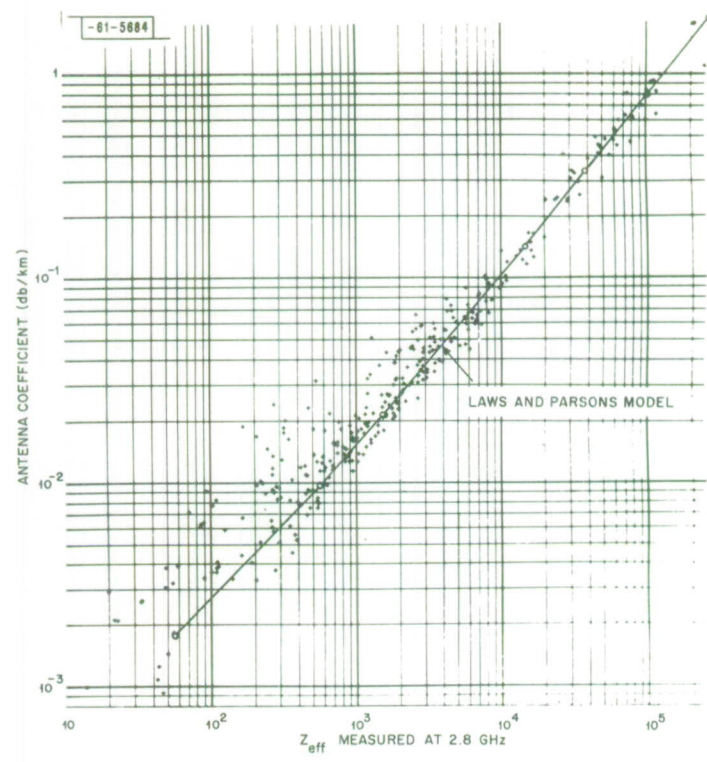


(a) Frequency: 1.29 GHz.

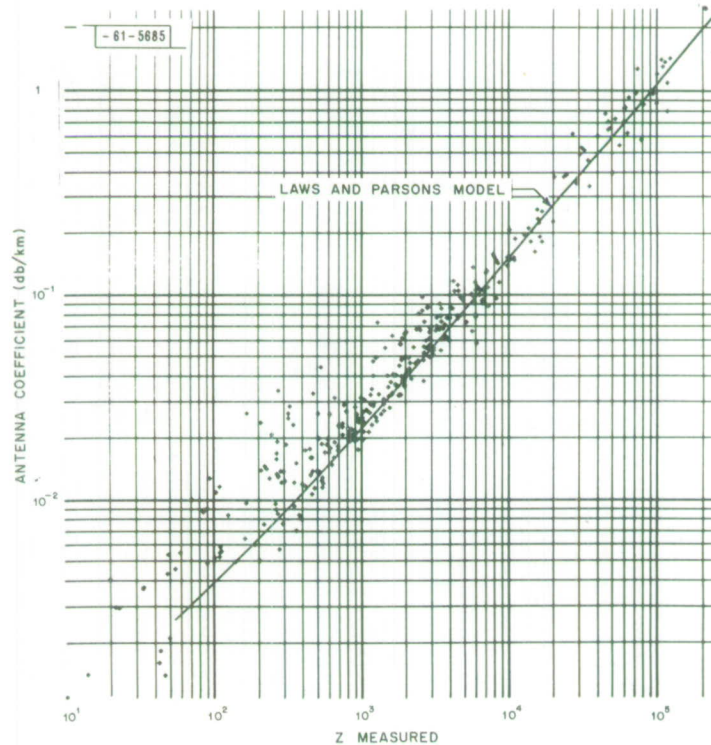


(b) Frequency: 2.80 GHz.

Fig. 8(a-h). Attenuation coefficient A vs reflectivity factor Z . Drop temperature = 0.0°C .



(c) Frequency: 8.0 GHz.



(d) Frequency: 9.35 GHz.

Fig. 8. Continued.

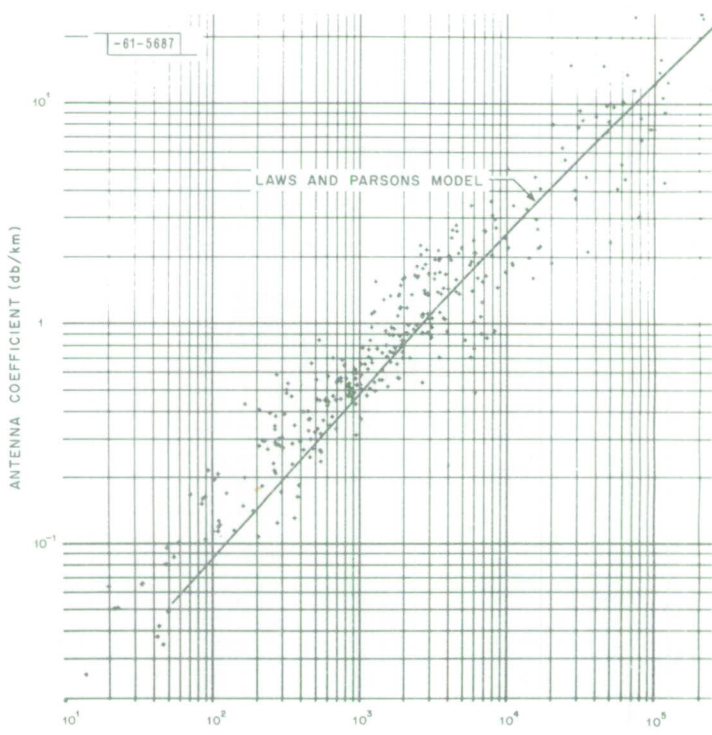
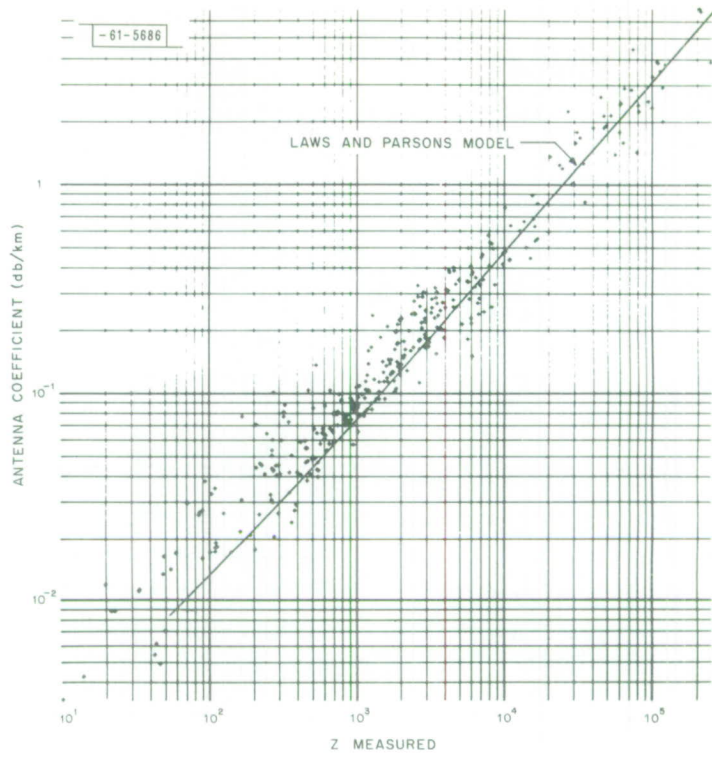
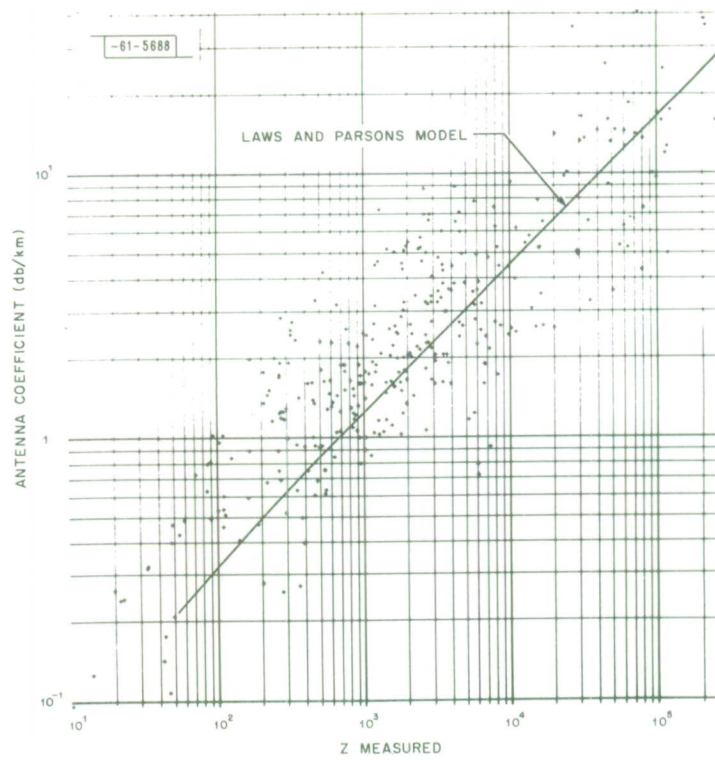
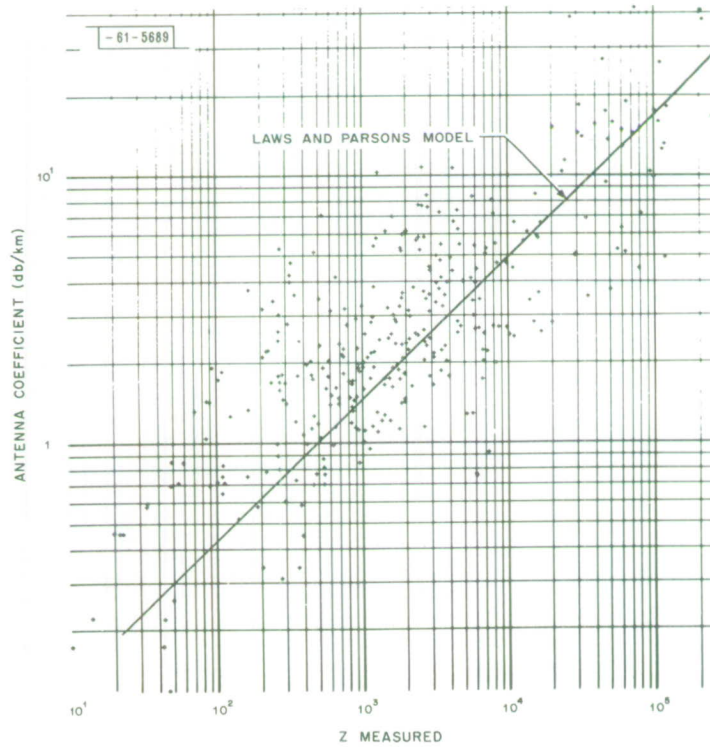


Fig. 8. Continued.

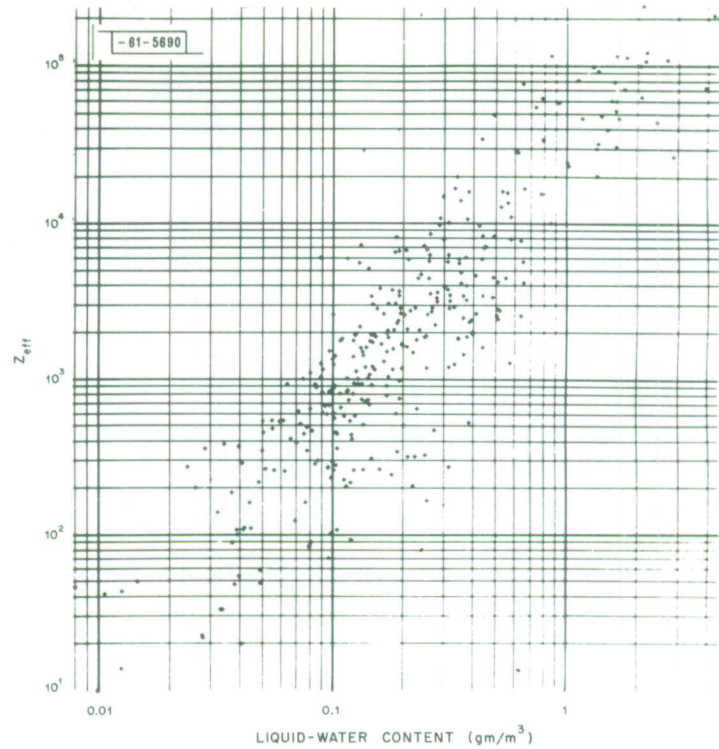


(g) Frequency: 70.0 GHz.

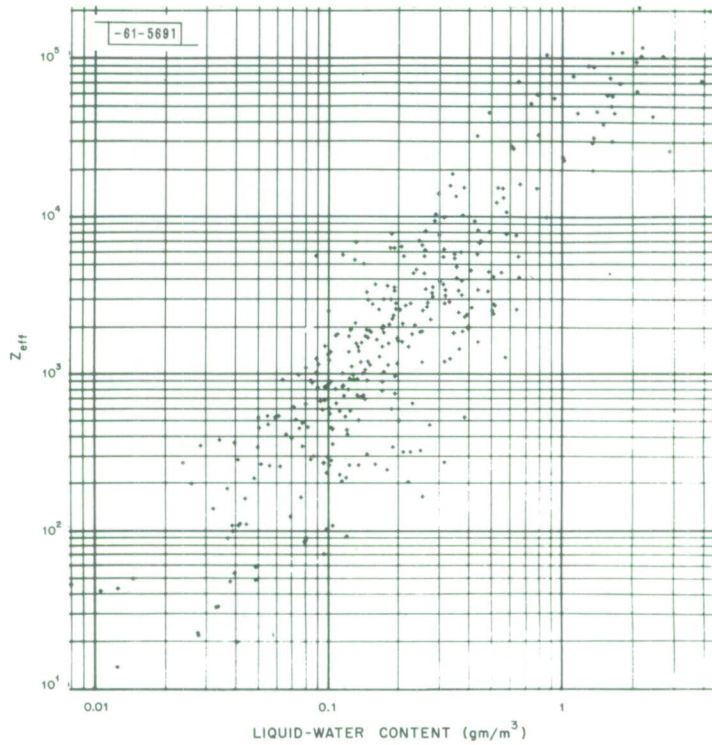


(h) Frequency: 94.0 GHz.

Fig. 8. Continued.

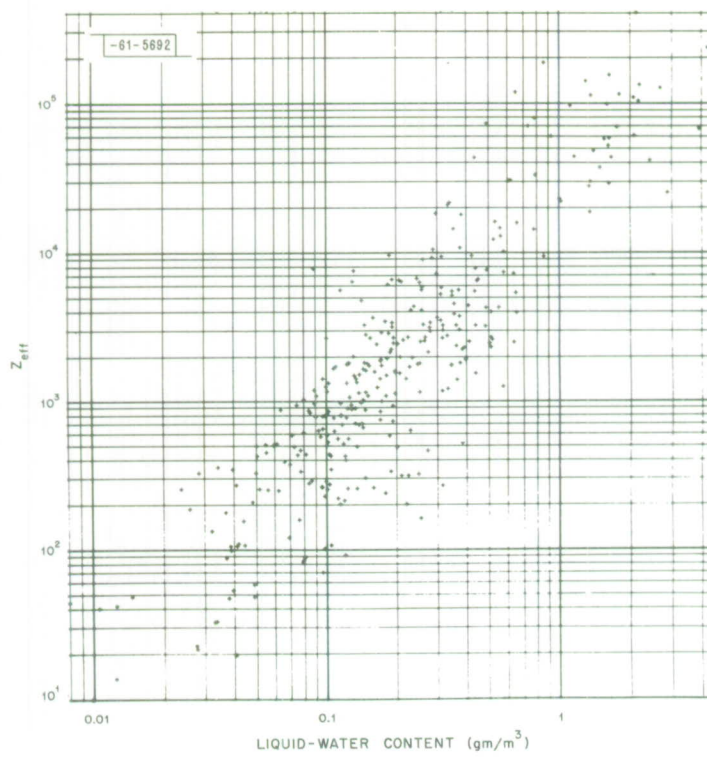


(a) Frequency: 1.29 GHz.

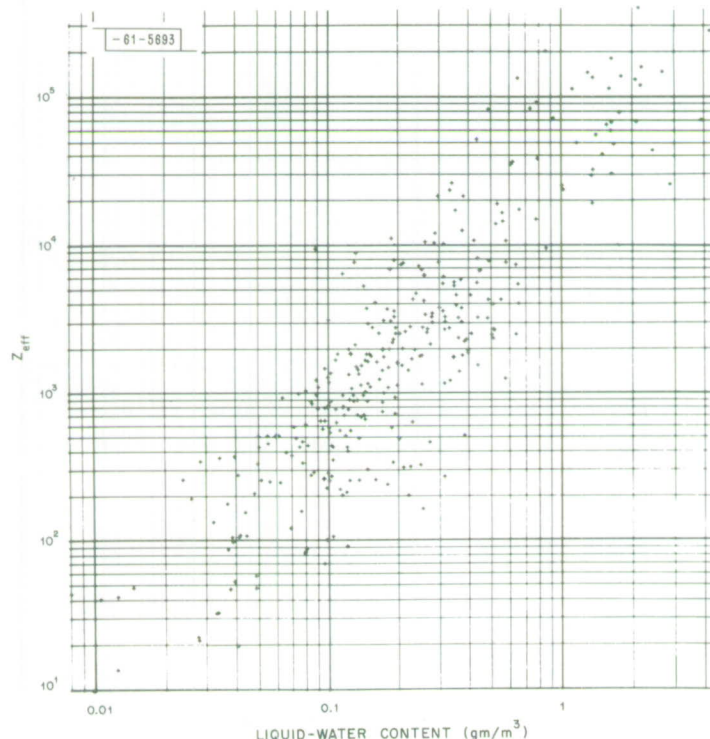


(b) Frequency: 2.80 GHz.

Fig. 9(a-h). Effective reflectivity factor Z_{eff} vs liquid-water content L . Drop temperature = 0.0°C .

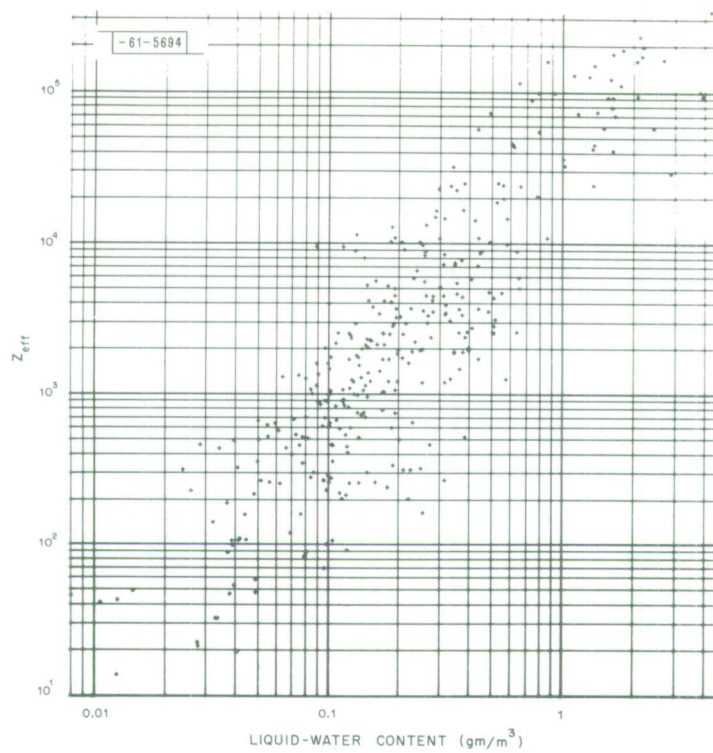


(c) Frequency: 8.0 GHz.

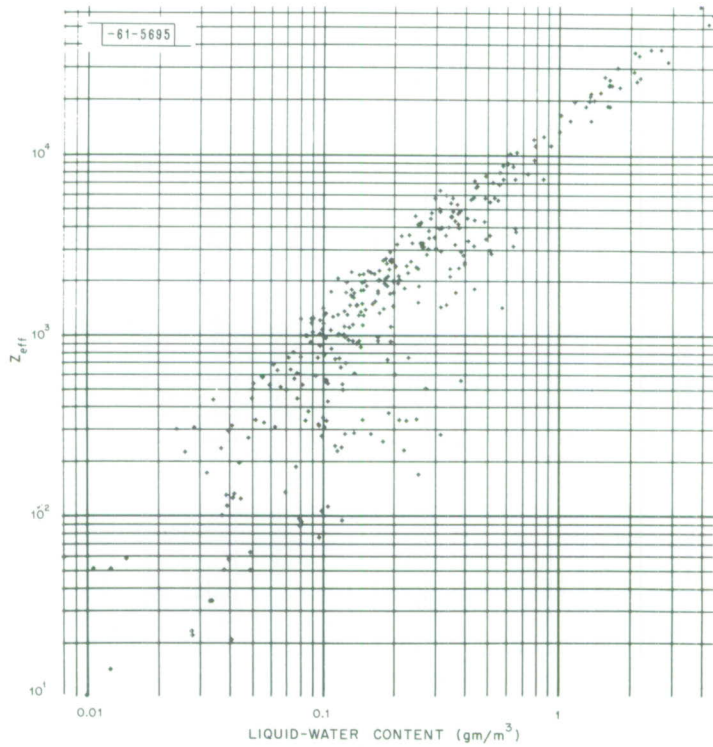


(d) Frequency: 9.35 GHz.

Fig. 9. Continued.

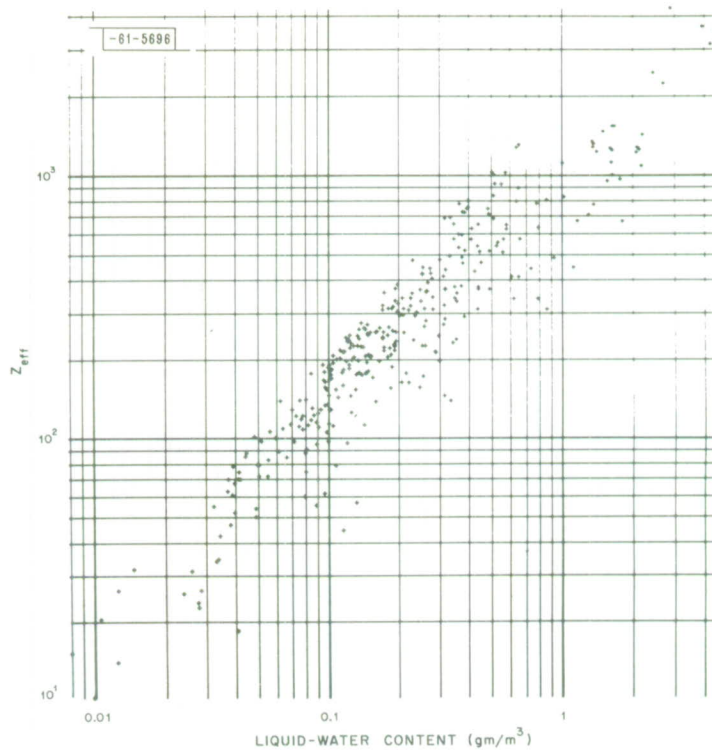


(e) Frequency: 15.5 GHz.

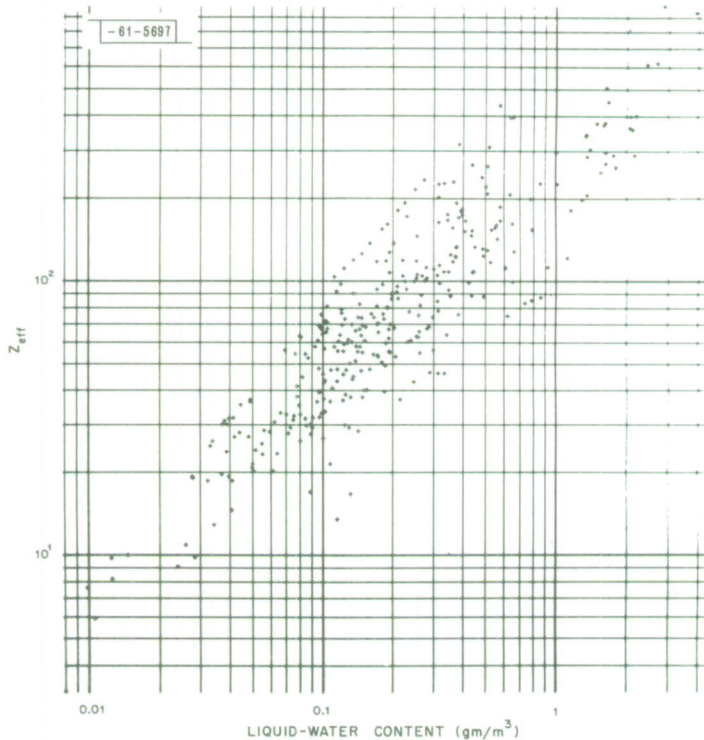


(f) Frequency: 35.0 GHz.

Fig. 9. Continued.

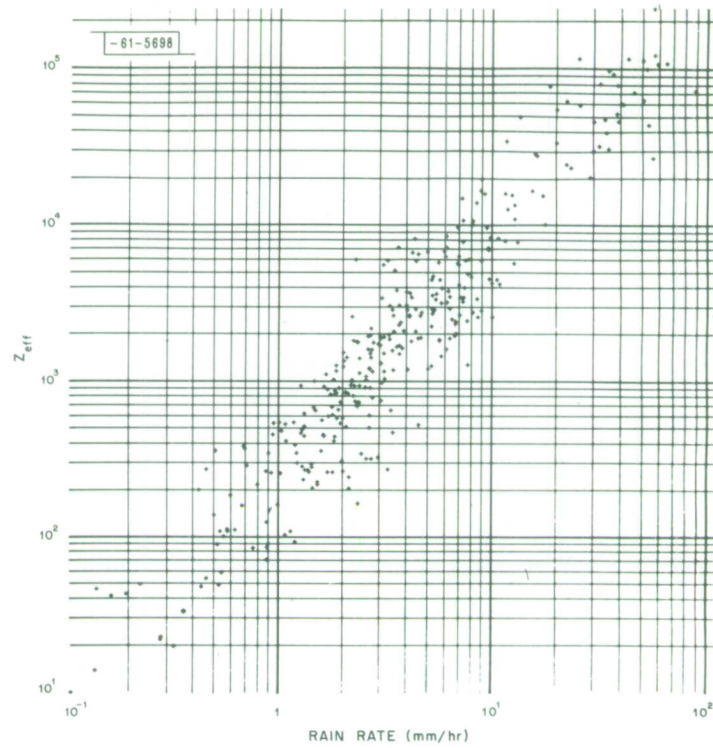


(g) Frequency: 70.0 GHz.

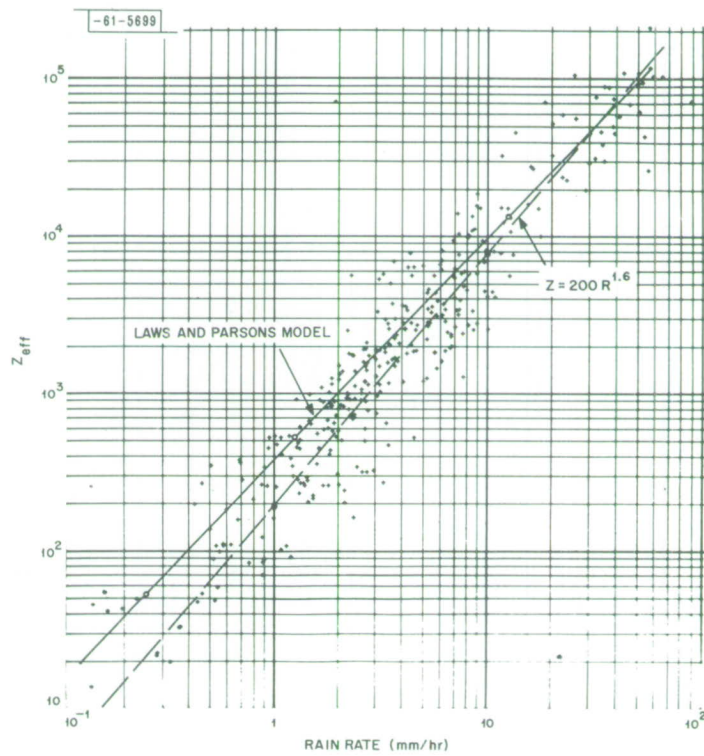


(h) Frequency: 94.0 GHz.

Fig. 9. Continued.

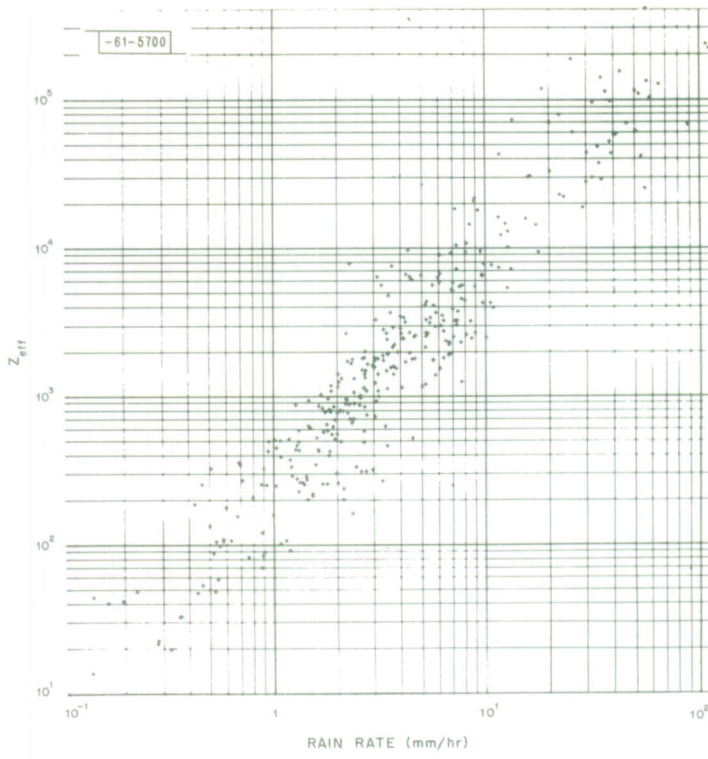


(a) Frequency: 1.29 GHz.

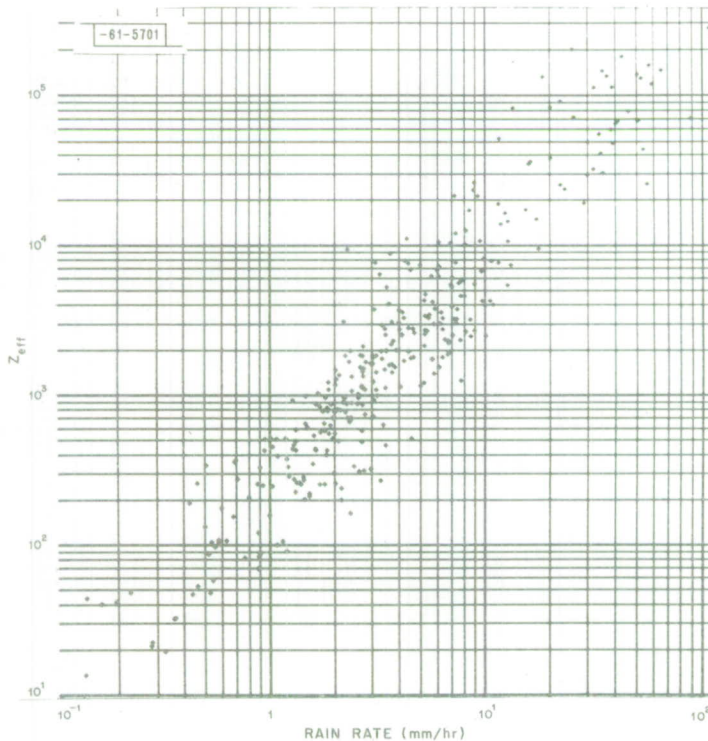


(b) Frequency: 2.80 GHz.

Fig. 10(a-h). Effective reflectivity factor Z_{eff} vs rain rate R . Drop temperature = 0.0°C.

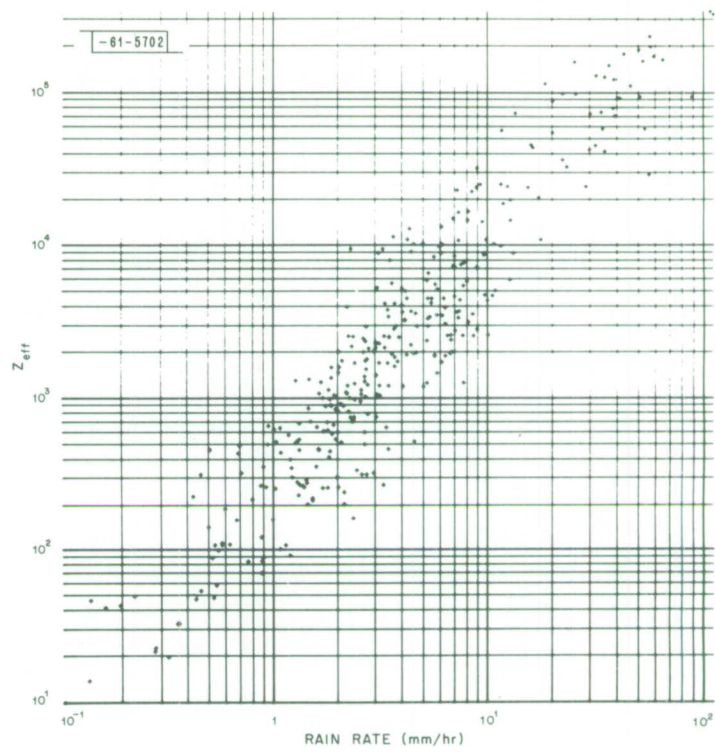


(c) Frequency: 8.0 GHz.

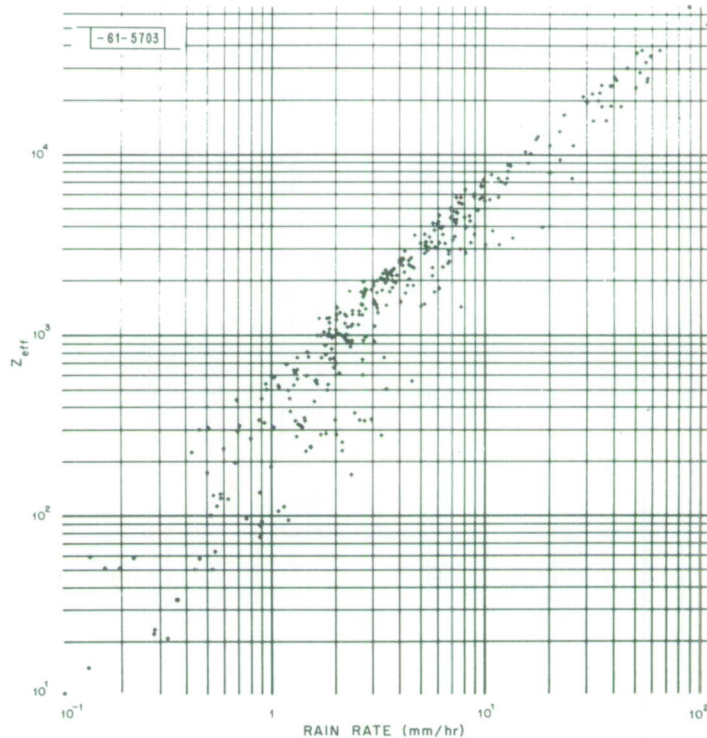


(d) Frequency: 9.35 GHz.

Fig. 10. Continued.

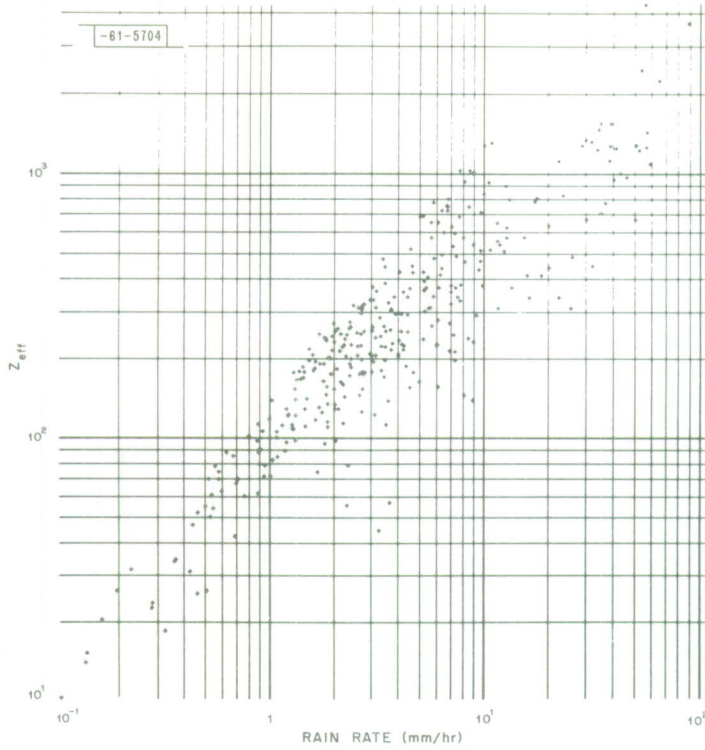


(e) Frequency: 15.5 GHz.

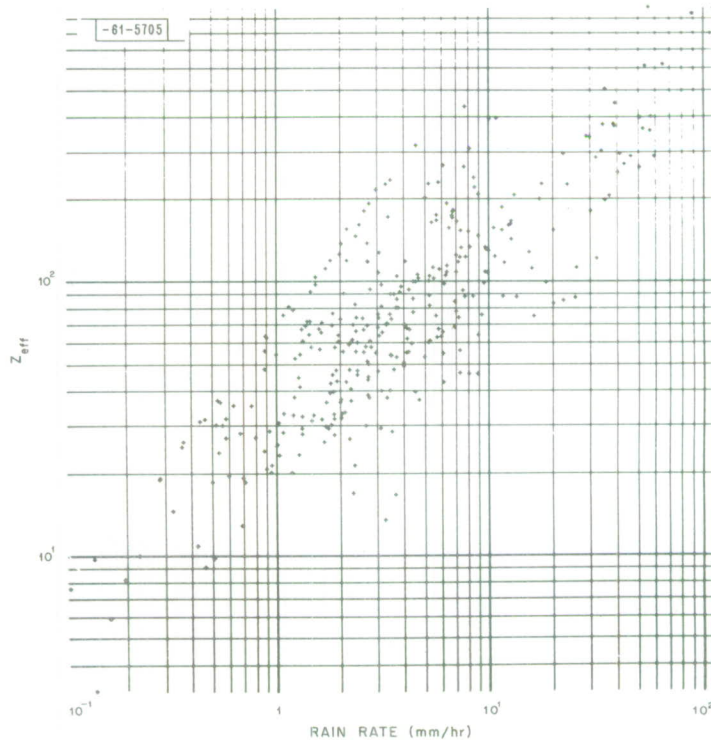


(f) Frequency: 35.0 GHz.

Fig. 10. Continued.

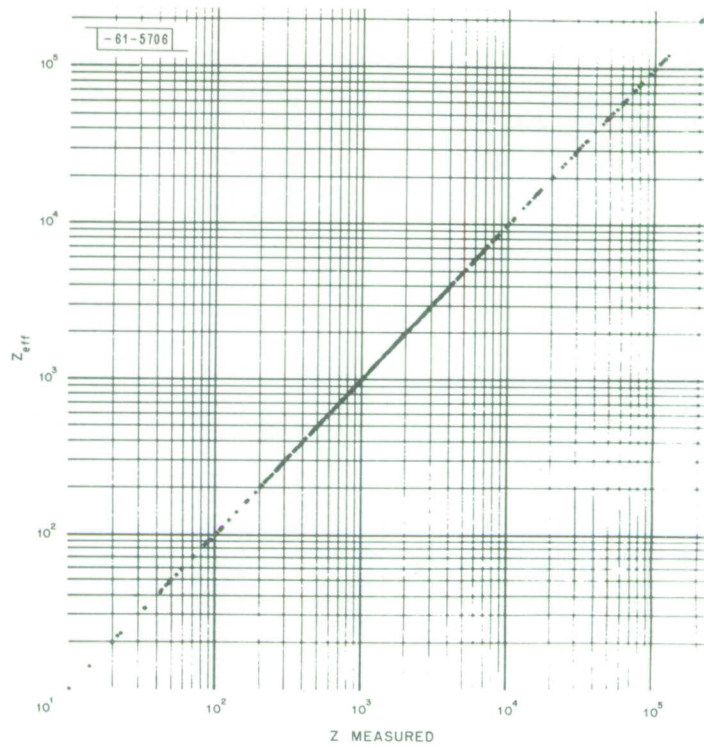


(g) Frequency: 70.0 GHz.

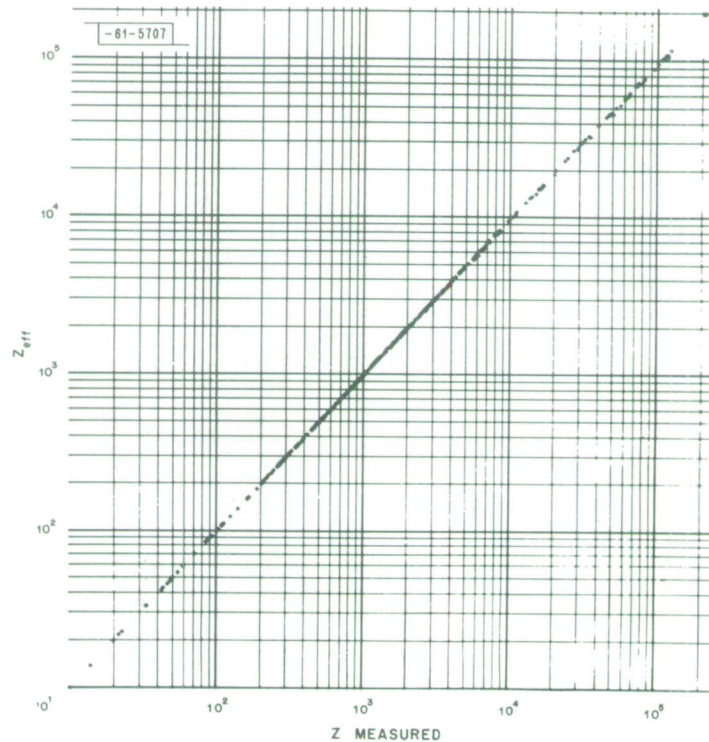


(h) Frequency: 94.0 GHz.

Fig. 10. Continued.

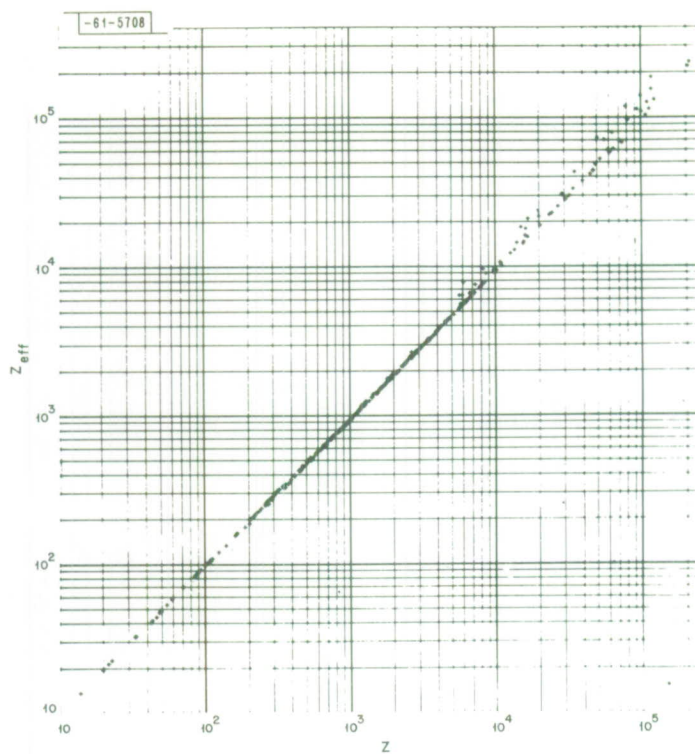


(a) Frequency: 1.29 GHz.

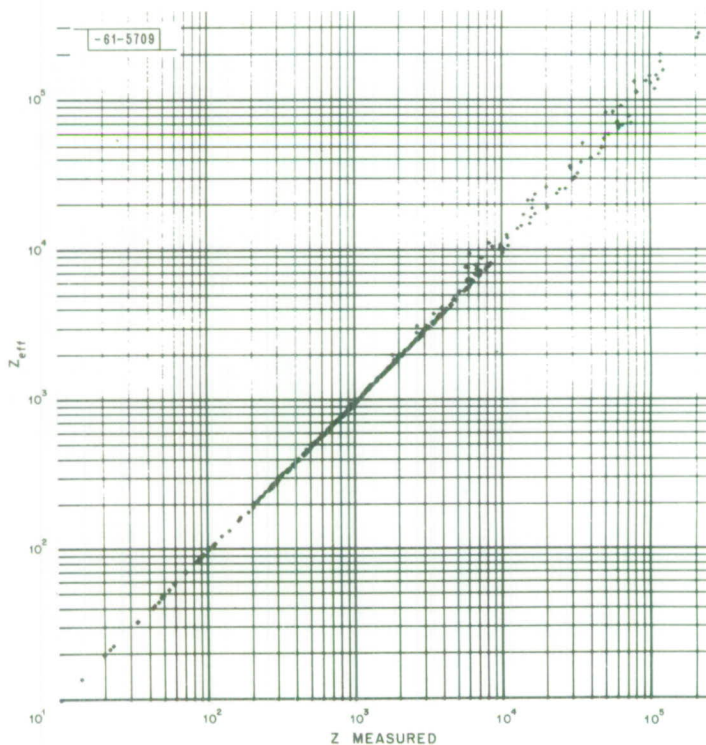


(b) Frequency: 2.80 GHz.

Fig. 11(a-h). Effective reflectivity factor Z_{eff} vs reflectivity factor Z . Drop temperature = 0.0°C.

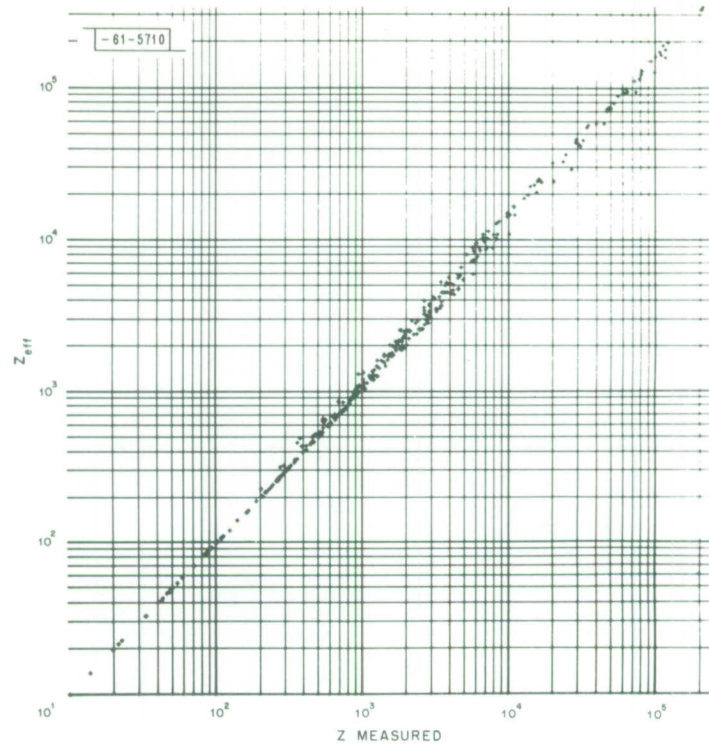


(c) Frequency: 8.0 GHz.

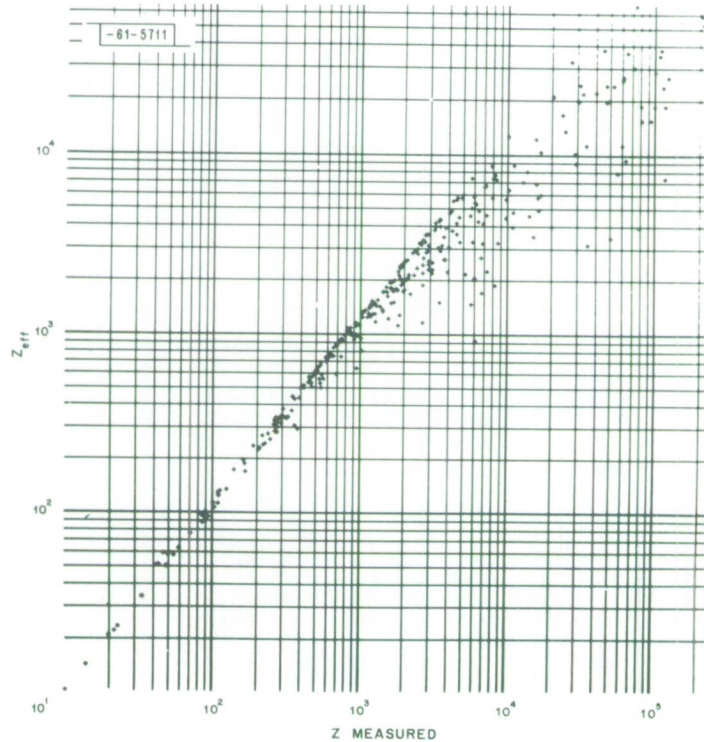


(d) Frequency: 9.35 GHz.

Fig. 11. Continued.

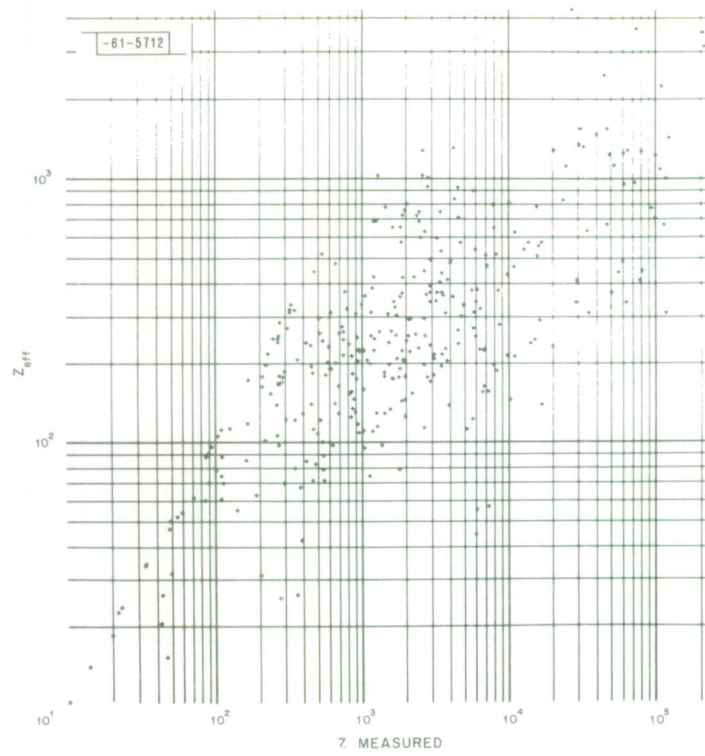


(e) Frequency: 15.5 GHz.

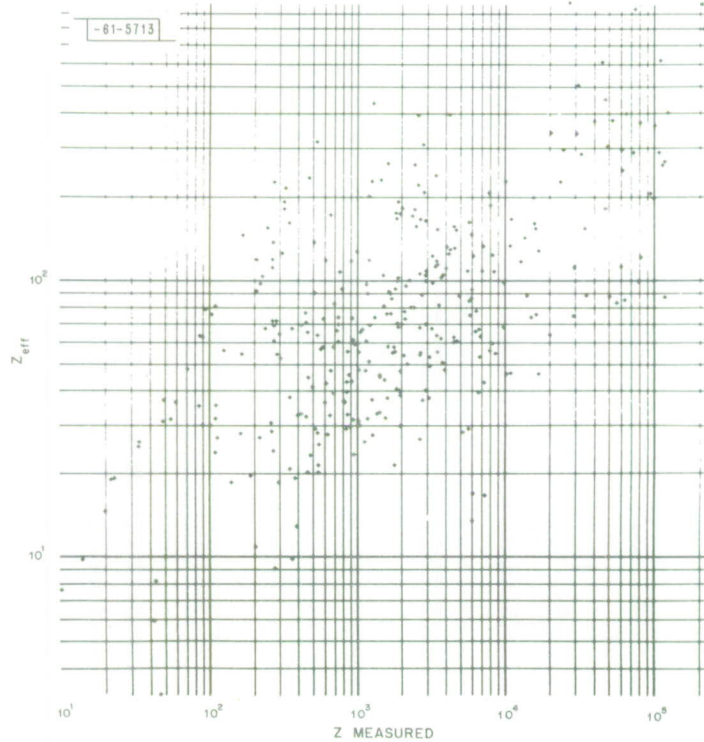


(f) Frequency: 35.0 GHz.

Fig. 11. Continued.

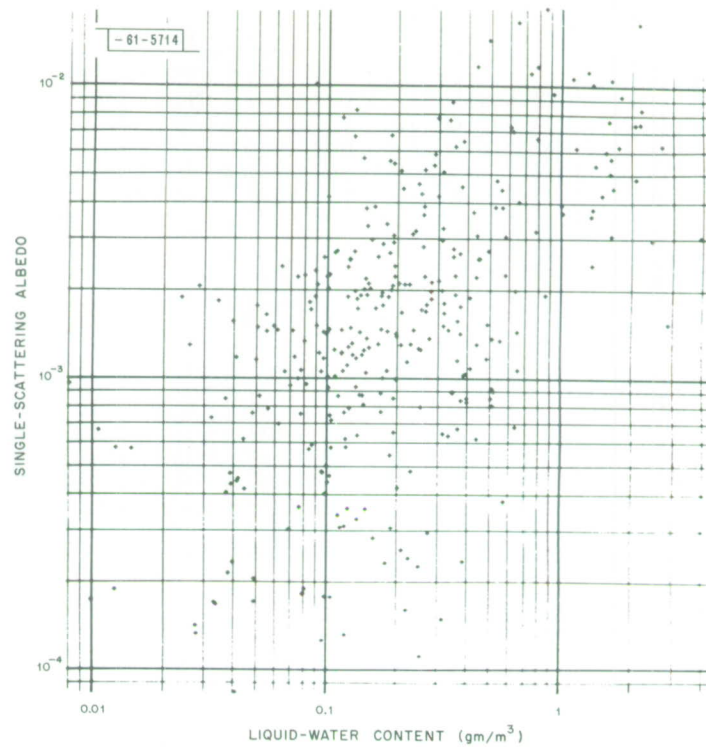


(g) Frequency: 70.0 GHz.

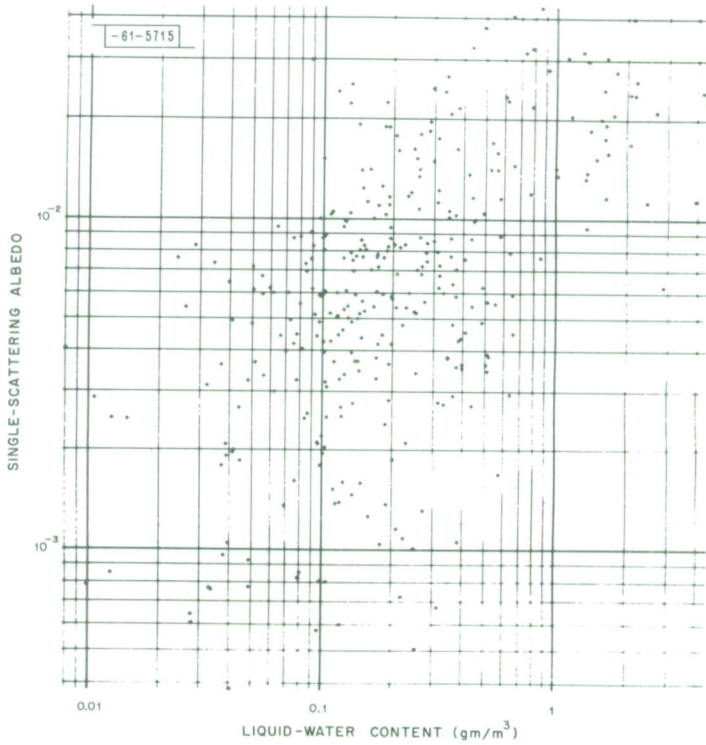


(h) Frequency: 94.0 GHz.

Fig. 11. Continued.

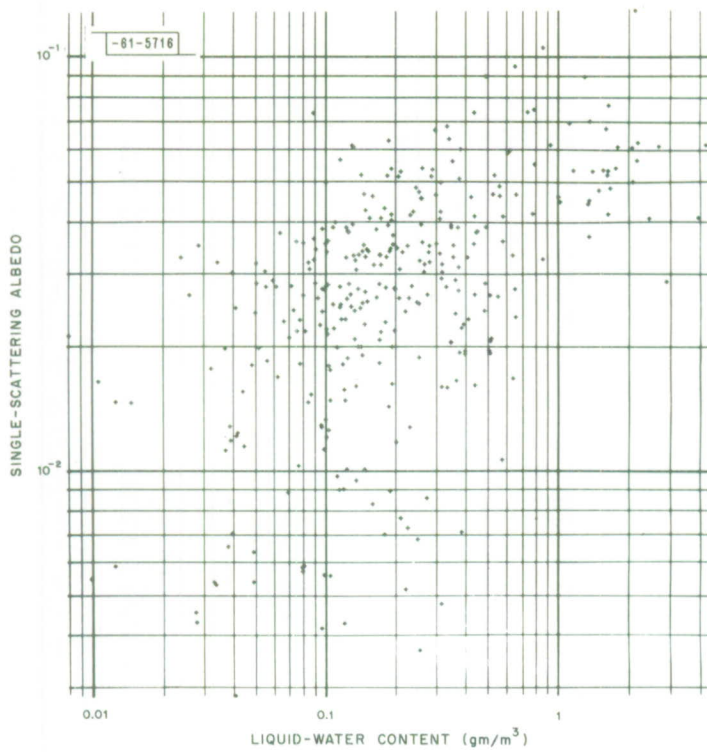


(a) Frequency: 1.29 GHz.

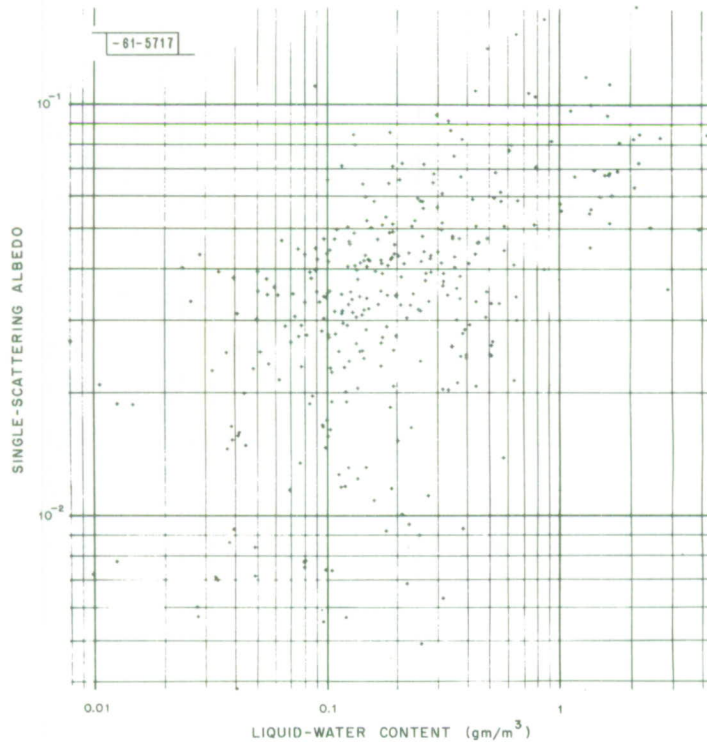


(b) Frequency: 2.80 GHz.

Fig. 12(a-h). Single-scattering albedo ω vs liquid-water content L . Drop temperature = 0.0°C.

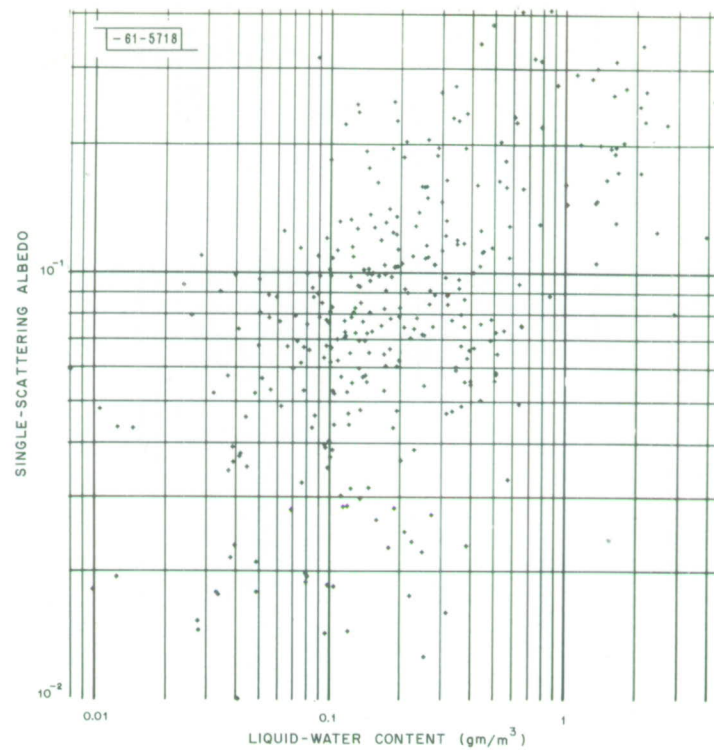


(c) Frequency: 8.0 GHz.

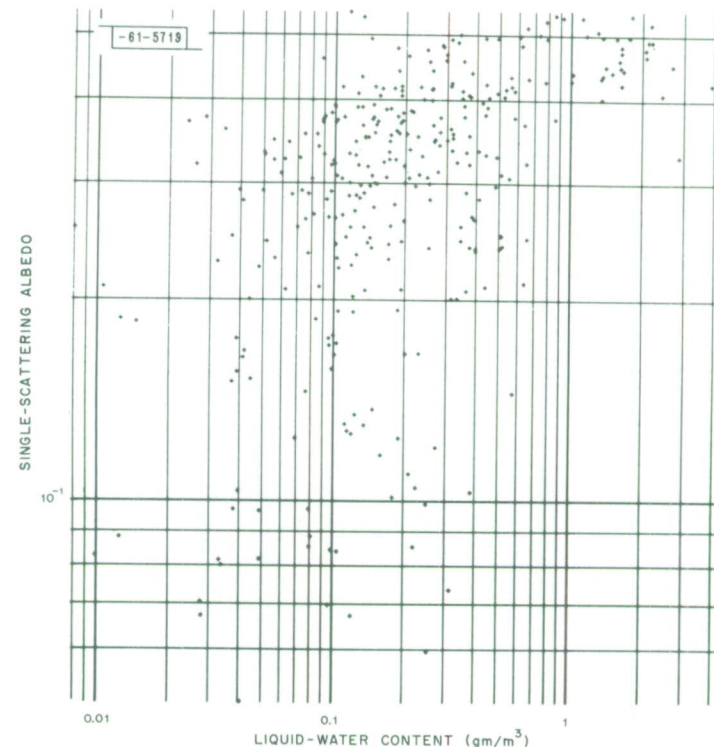


(d) Frequency: 9.35 GHz.

Fig. 12. Continued.

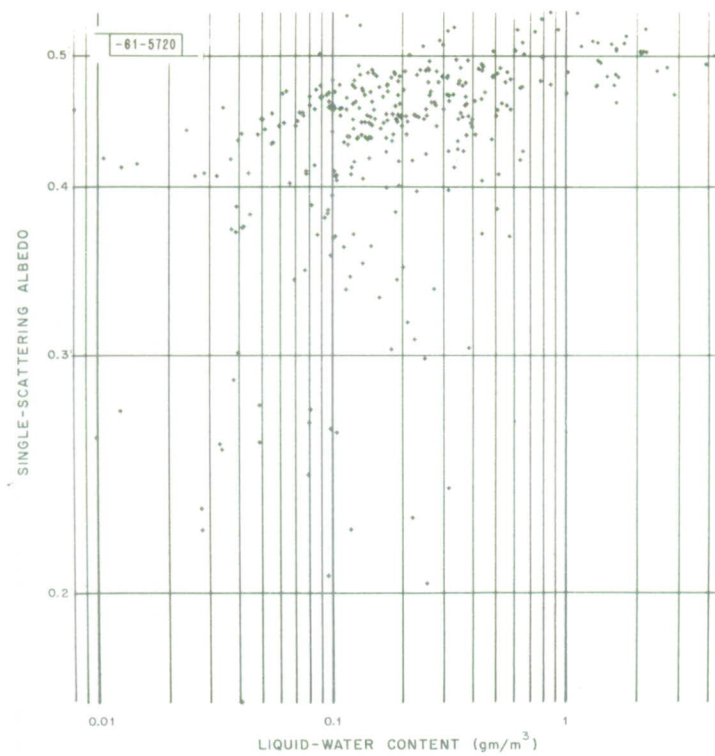


(e) Frequency: 15.5 GHz.

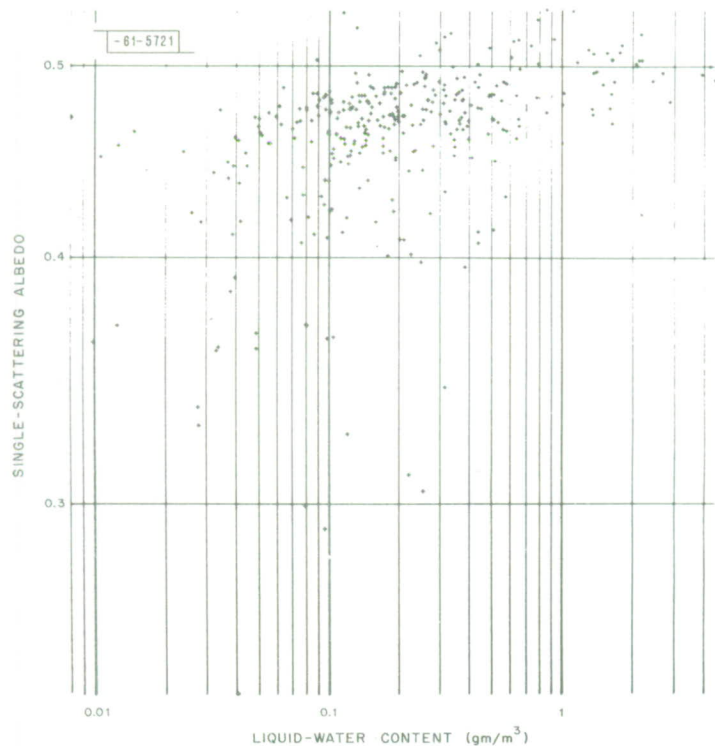


(f) Frequency: 35.0 GHz.

Fig. 12. Continued.

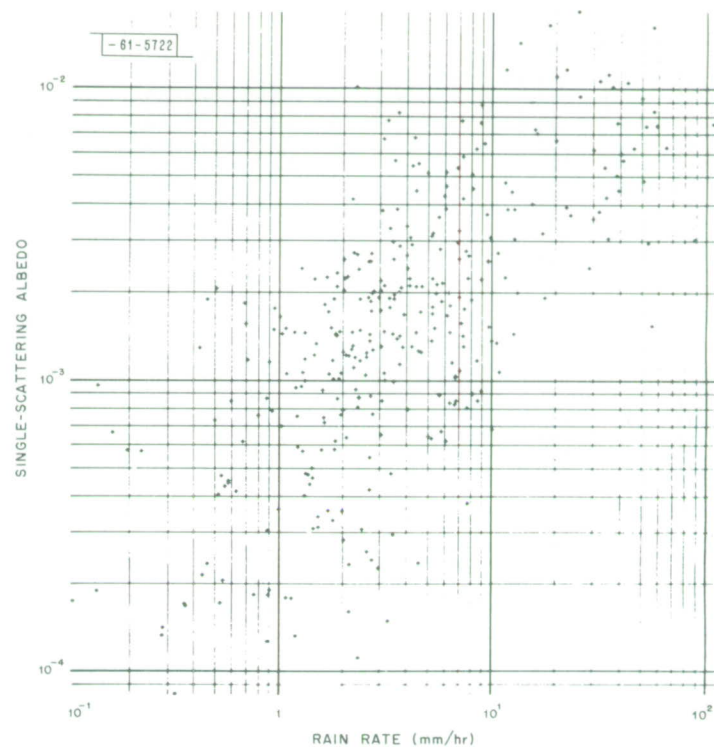


(g) Frequency: 70.0 GHz.

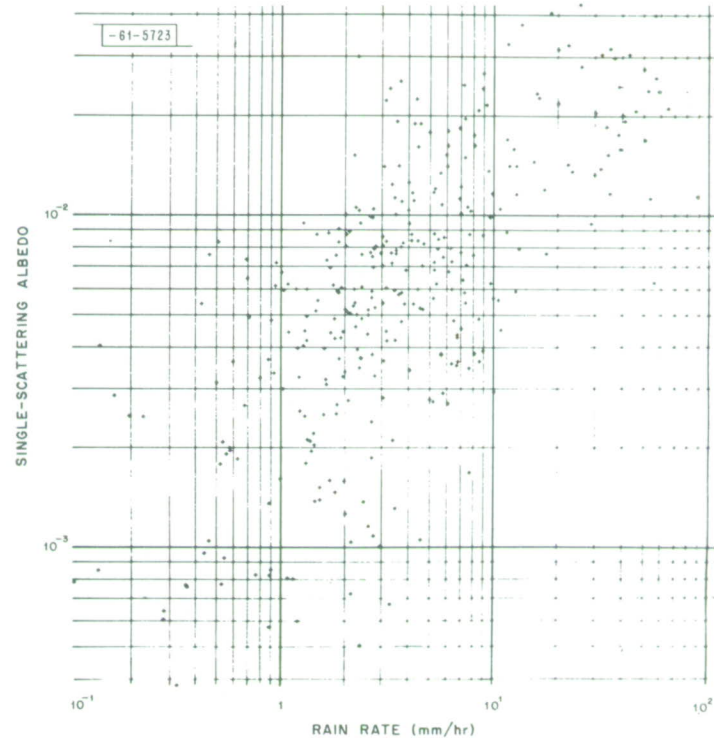


(h) Frequency: 94.0 GHz.

Fig. 12. Continued.

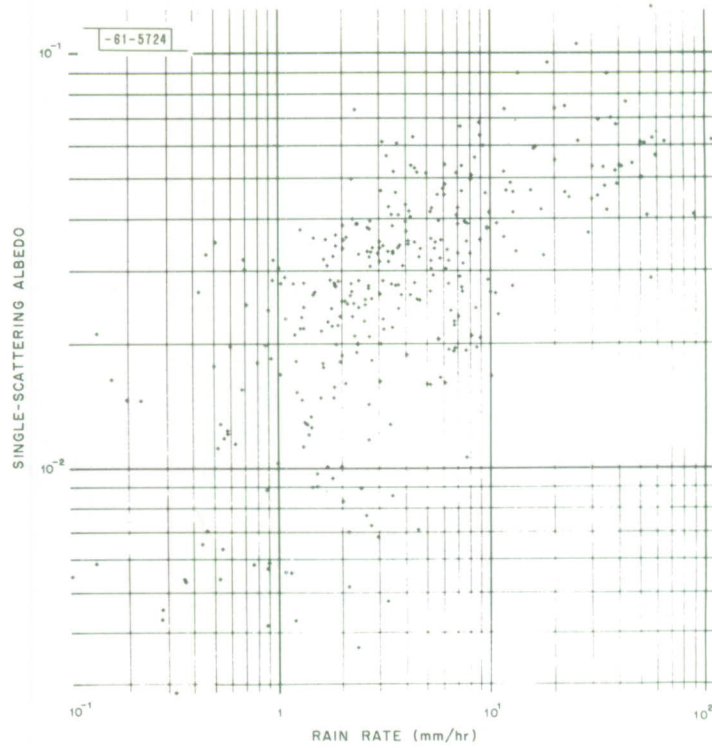


(a) Frequency: 1.29 GHz.

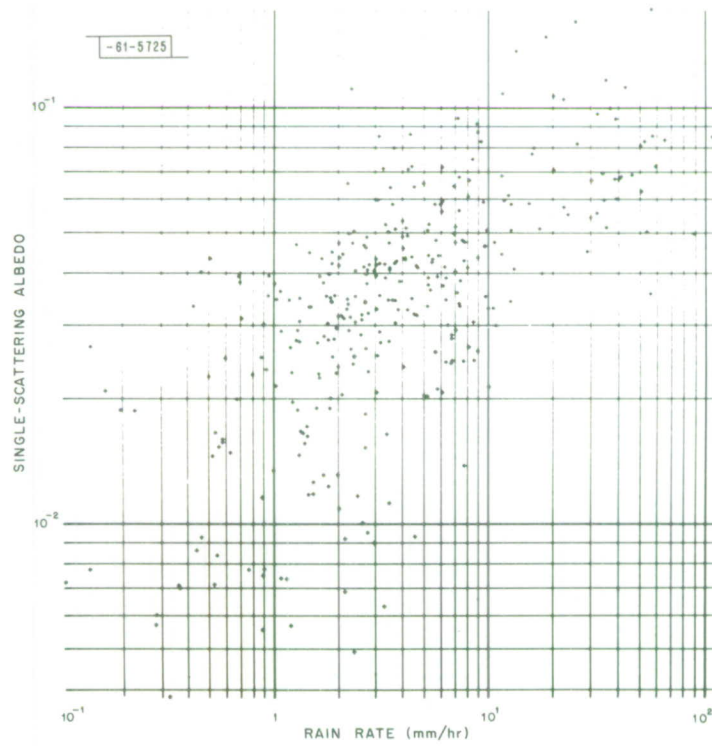


(b) Frequency: 2.80 GHz.

Fig. 13(a-h). Single-scattering albedo ω vs rain rate R . Drop temperature = 0.0°C .

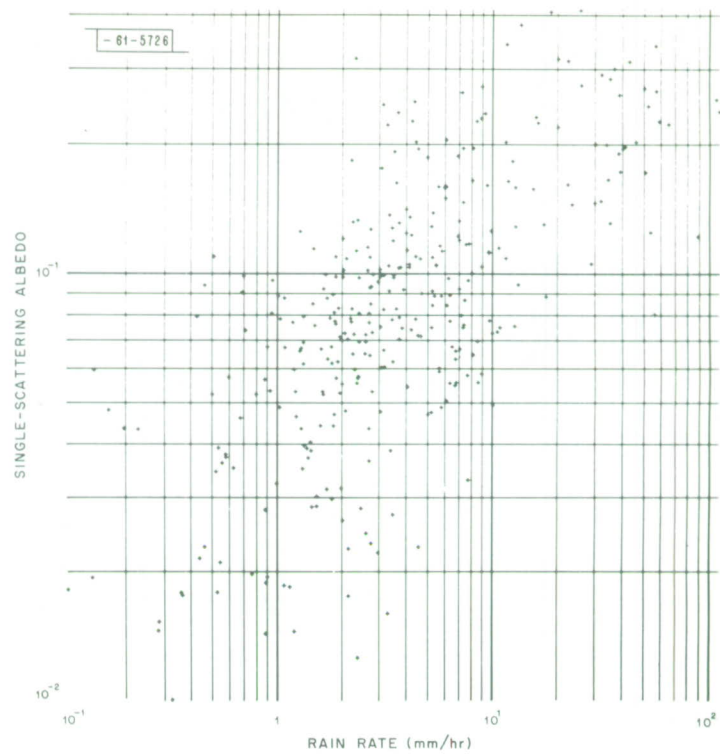


(c) Frequency: 8.0 GHz.

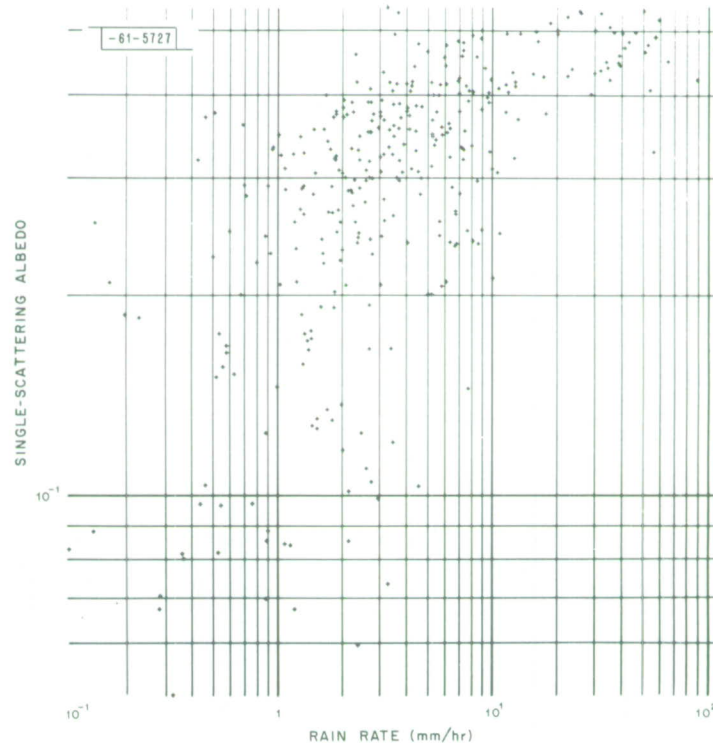


(d) Frequency: 9.35 GHz.

Fig. 13. Continued.

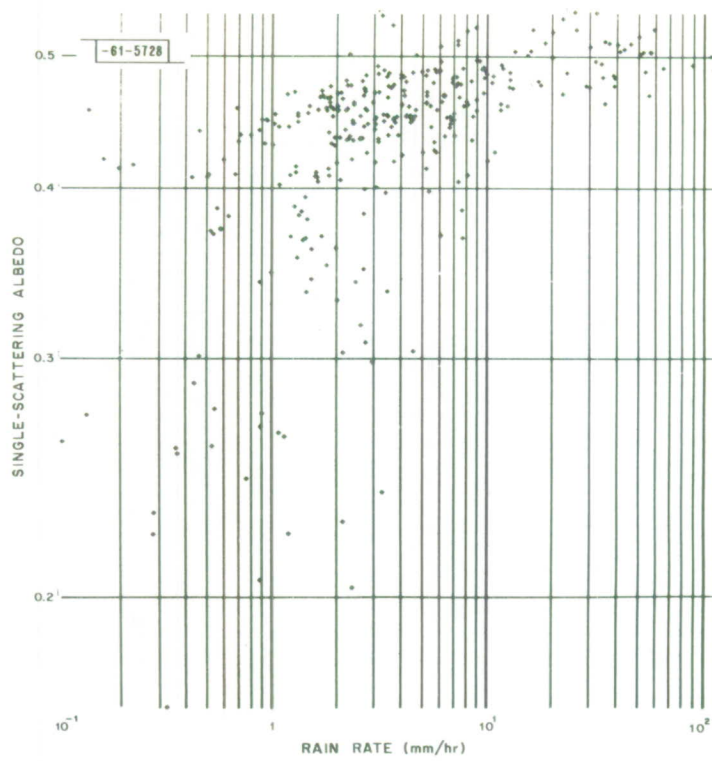


(e) Frequency: 15.5 GHz.

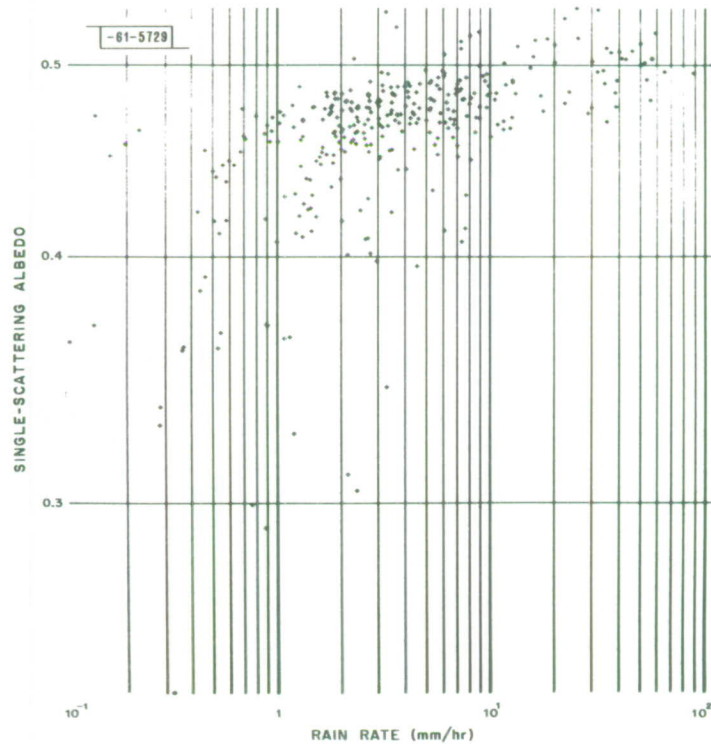


(f) Frequency: 35.0 GHz.

Fig. 13. Continued.

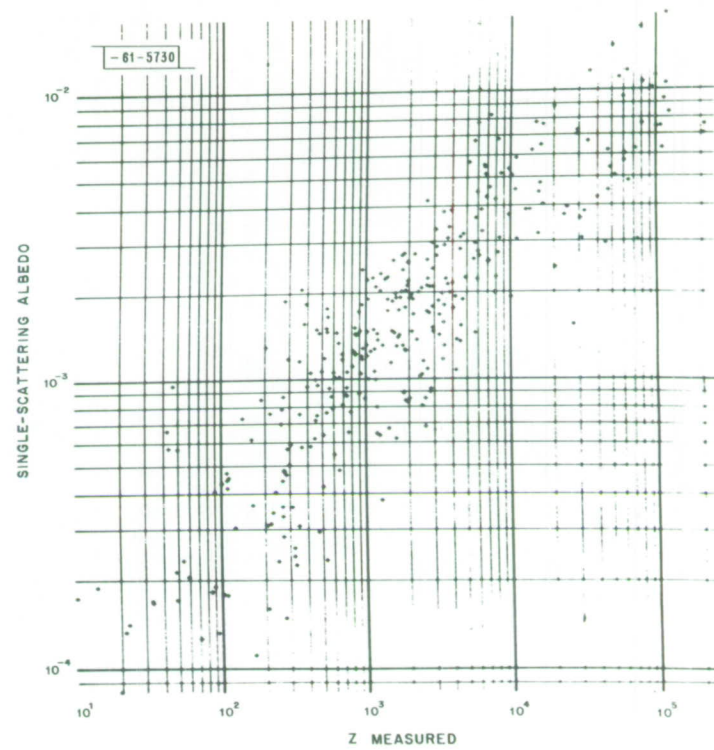


(g) Frequency: 70.0 GHz.

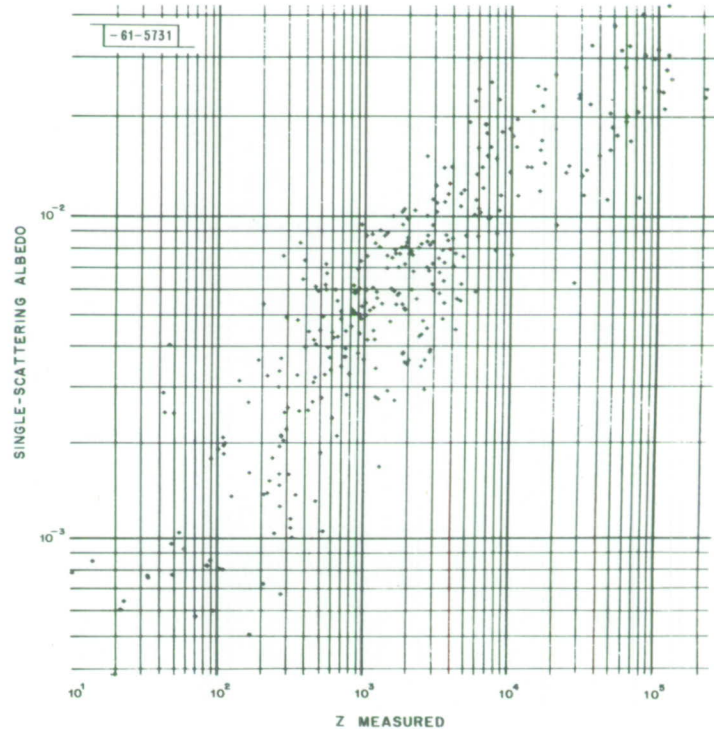


(h) Frequency: 94.0 GHz.

Fig. 13. Continued.

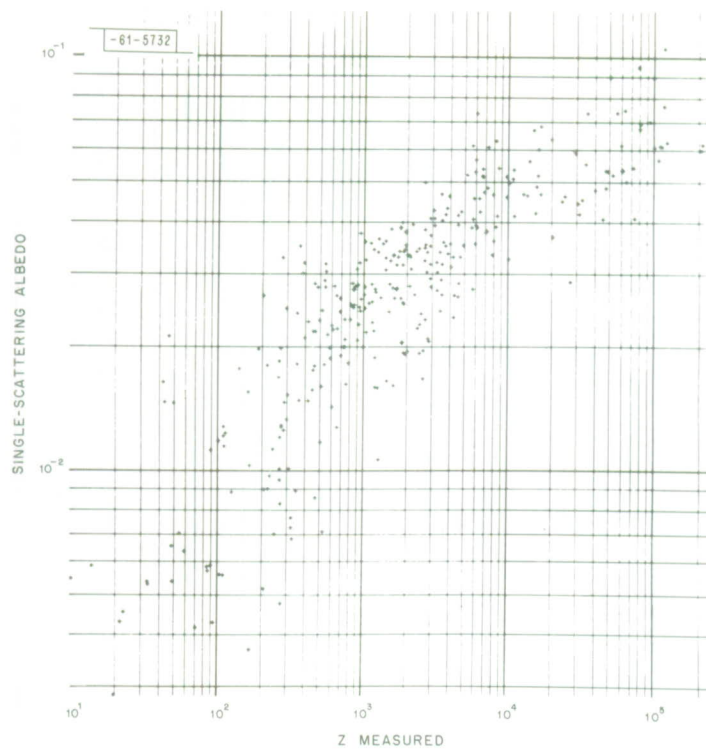


(a) Frequency: 1.29 GHz.

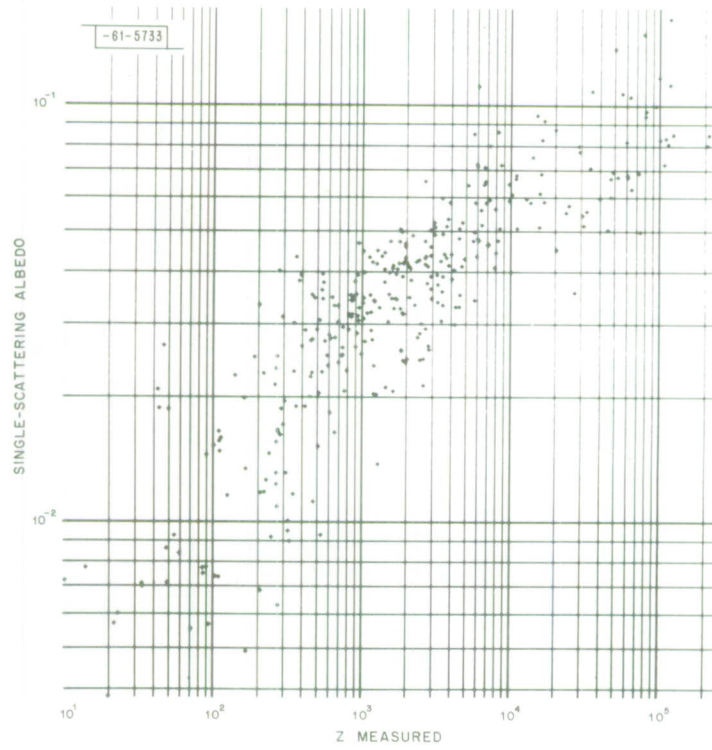


(b) Frequency: 2.80 GHz.

Fig. 14(a-h). Single-scattering albedo ω vs reflectivity factor Z . Drop temperature = 0.0°C .

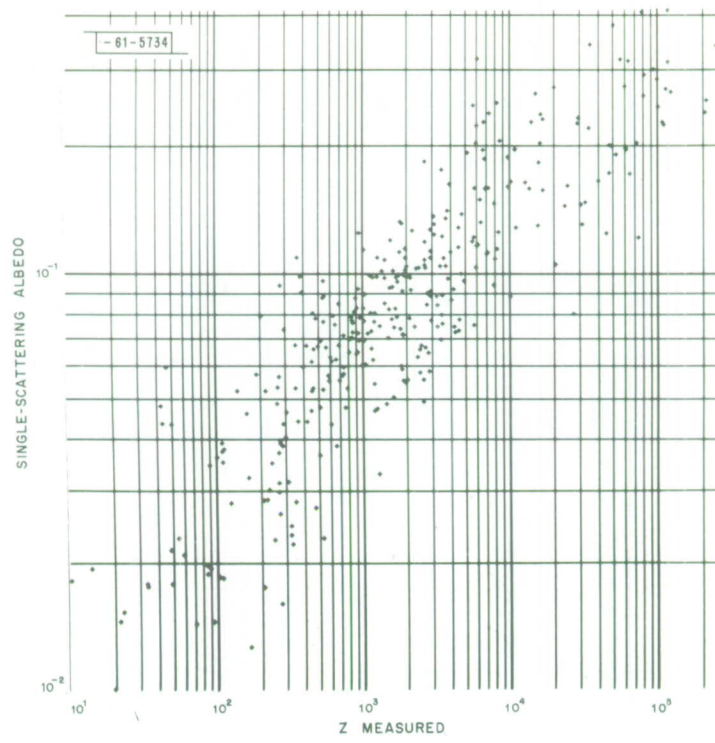


(c) Frequency: 8.0 GHz.

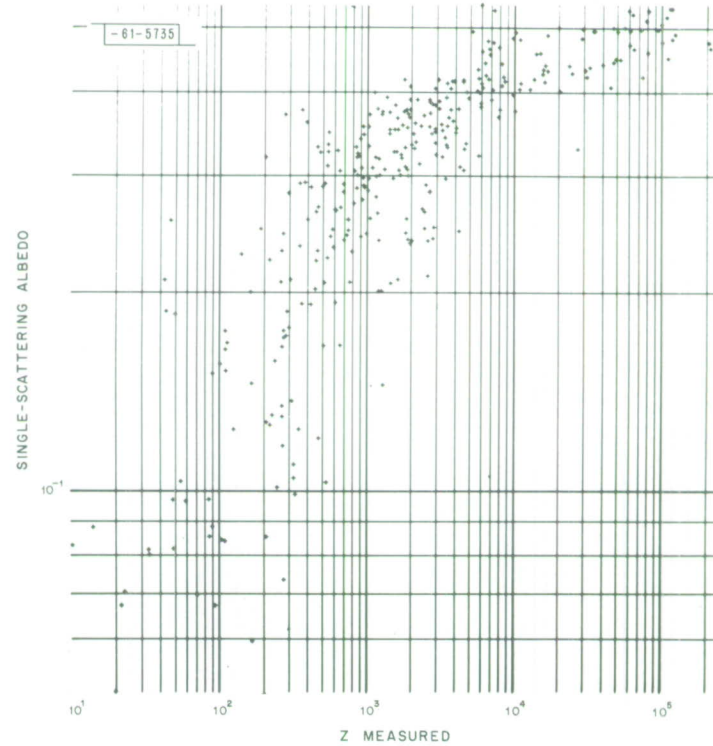


(d) Frequency: 9.35 GHz.

Fig. 14. Continued.

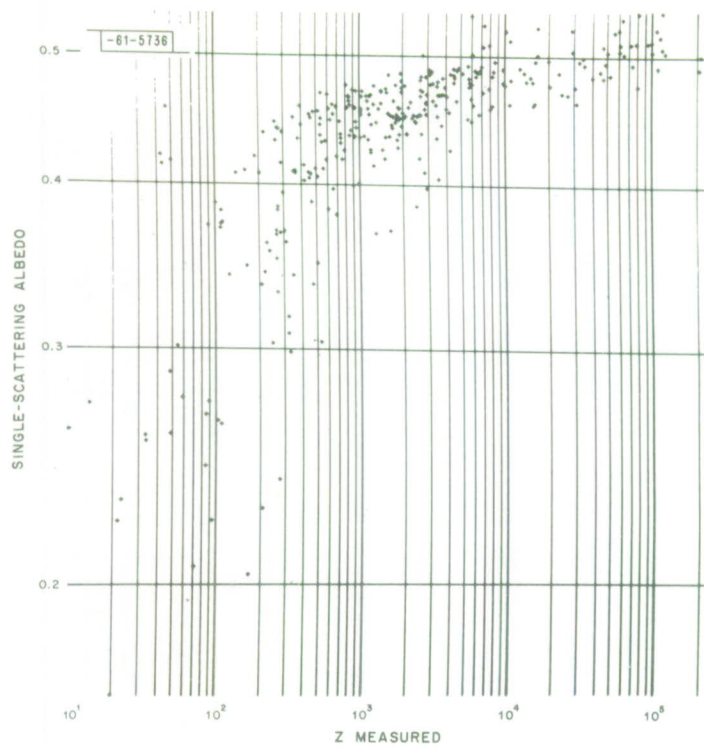


(e) Frequency: 15.5 GHz.

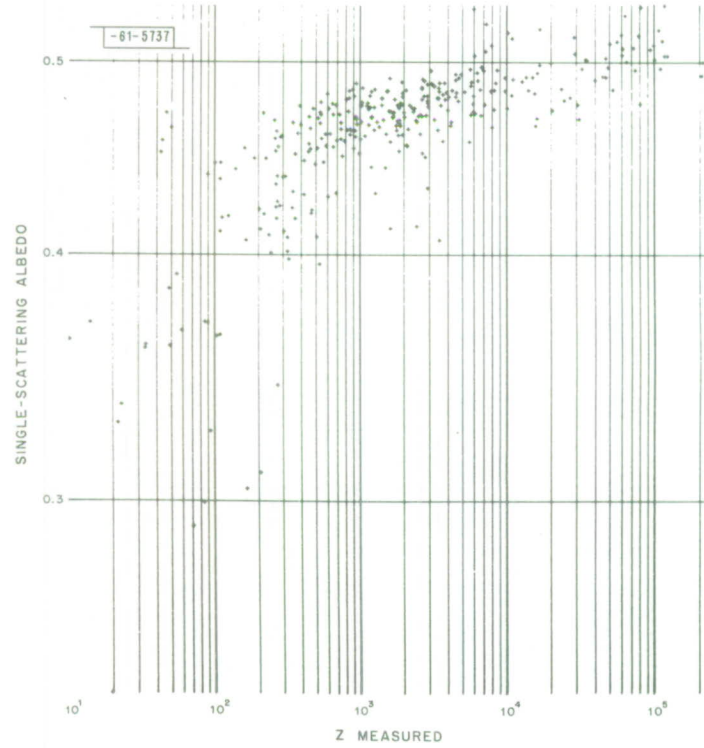


(f) Frequency: 35.0 GHz.

Fig. 14. Continued.

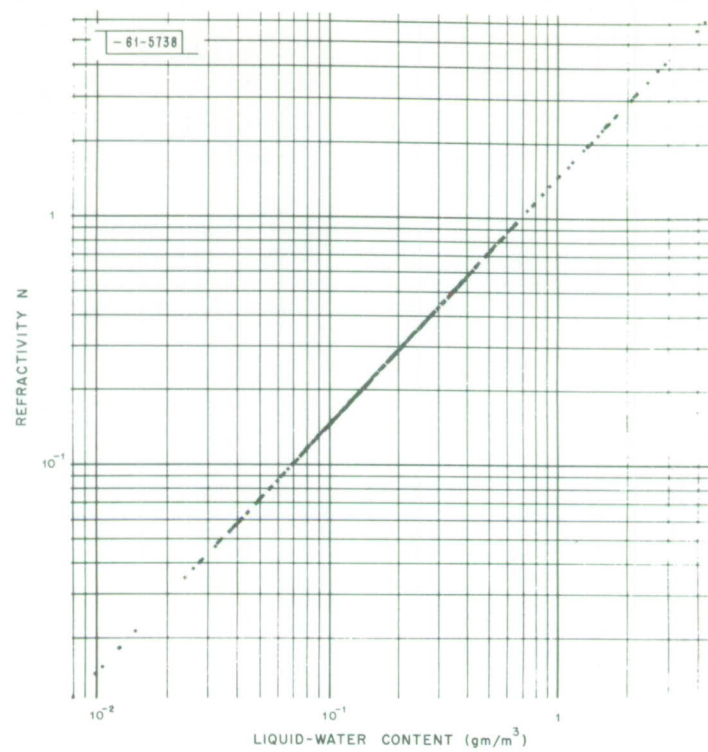


(g) Frequency: 70.0 GHz.

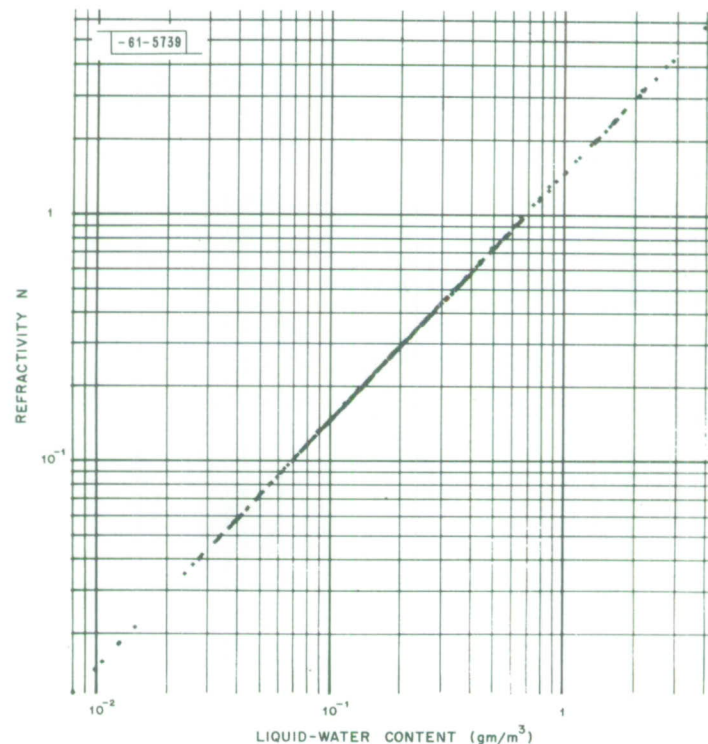


(h) Frequency: 94.0 GHz.

Fig. 14. Continued.

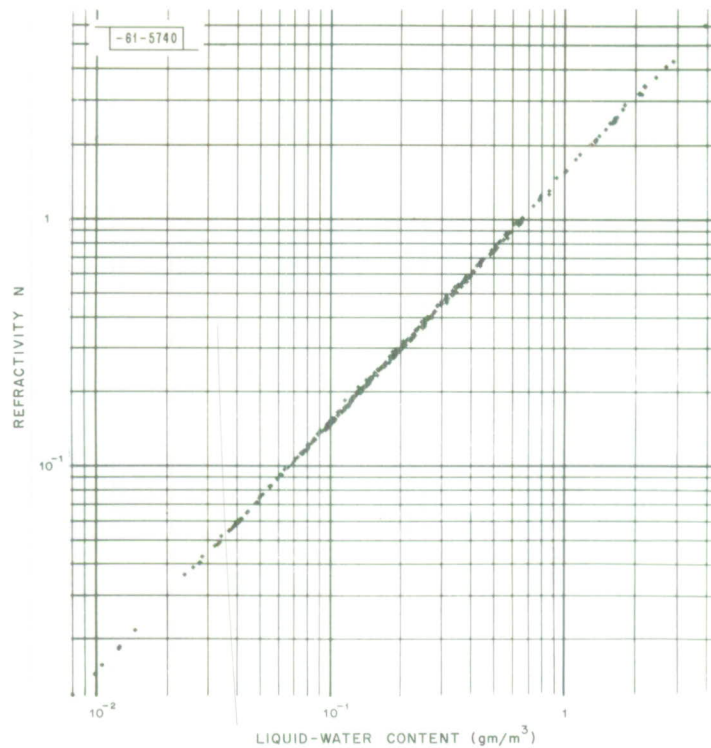


(a) Frequency: 1.29 GHz.

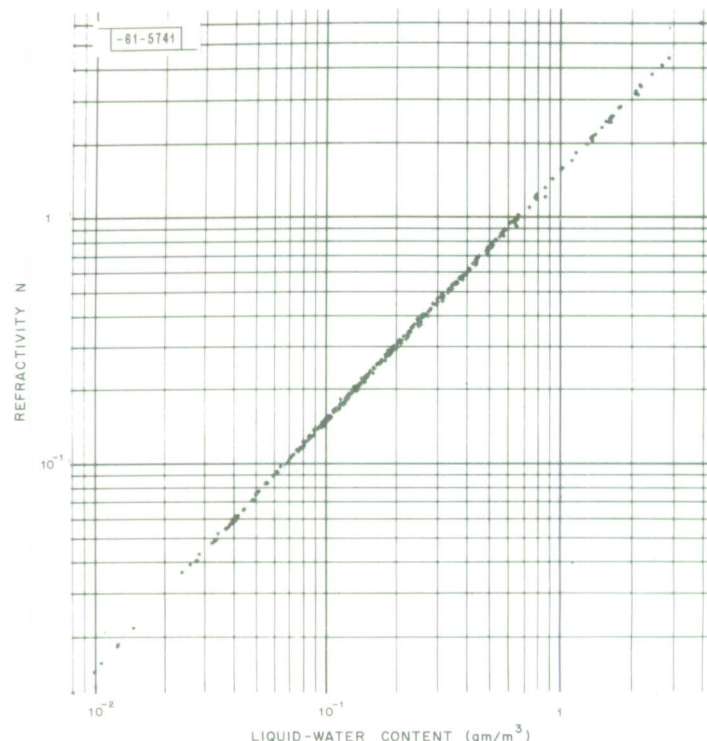


(b) Frequency: 2.80 GHz.

Fig. 15(a-h). Radio refractivity N vs liquid-water content L . Drop temperature = 0.0°C .

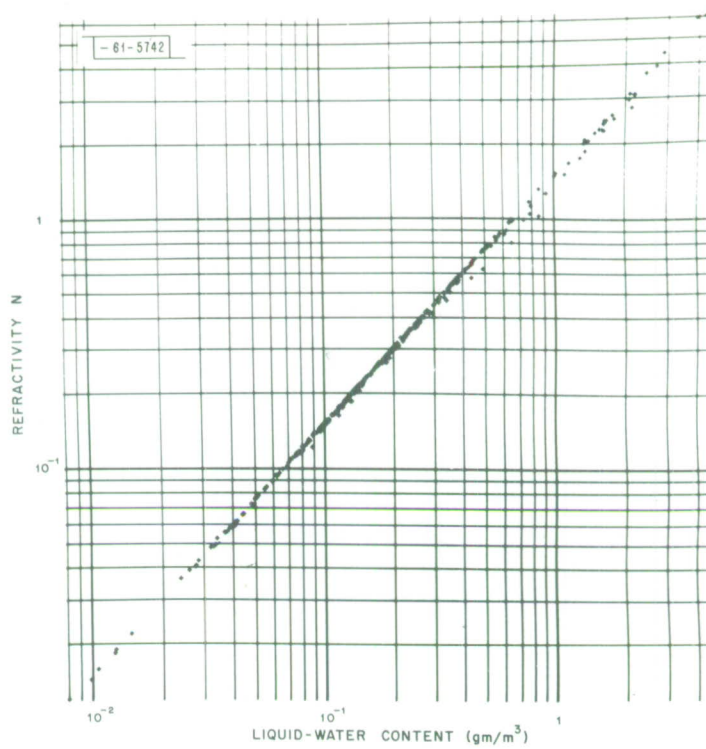


(c) Frequency: 8.0 GHz.

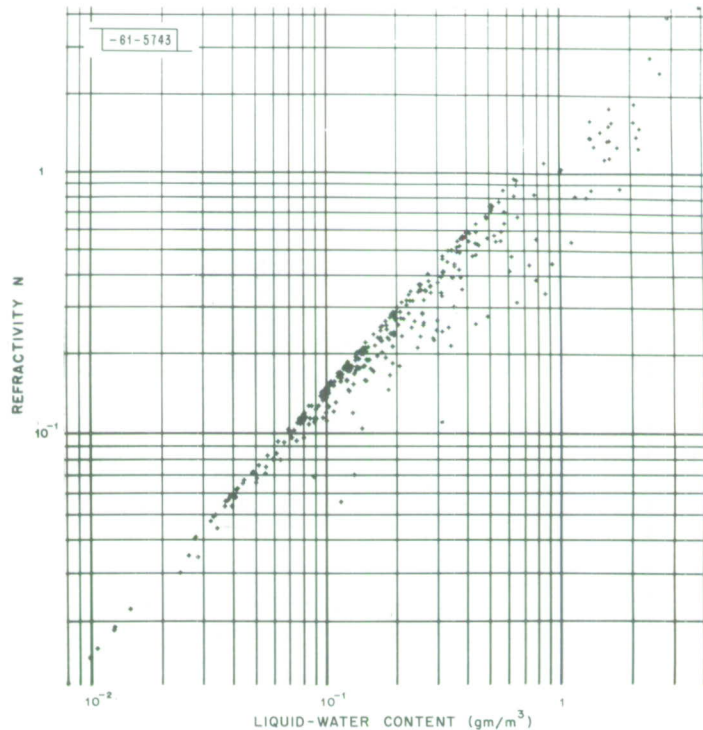


(d) Frequency: 9.35 GHz.

Fig. 15. Continued.

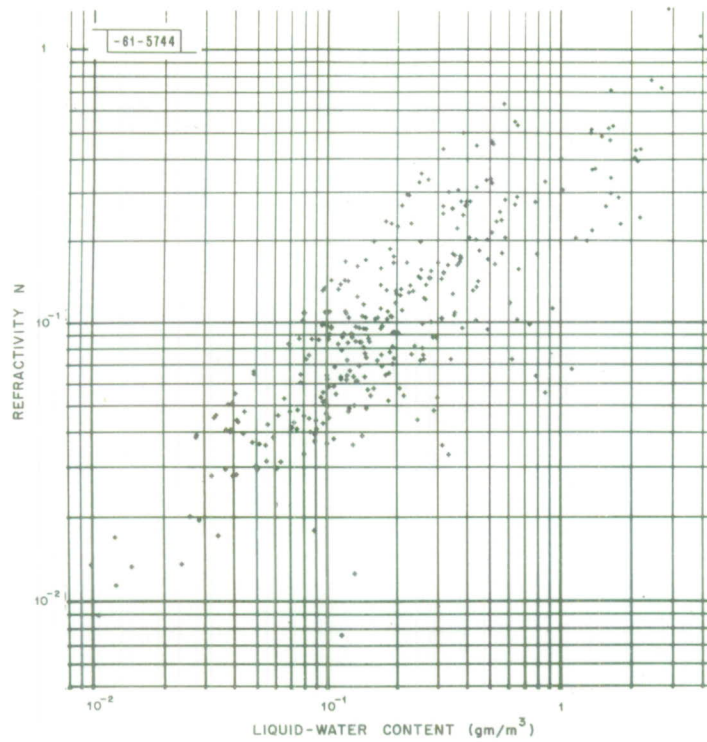


(e) Frequency: 15.5 GHz.

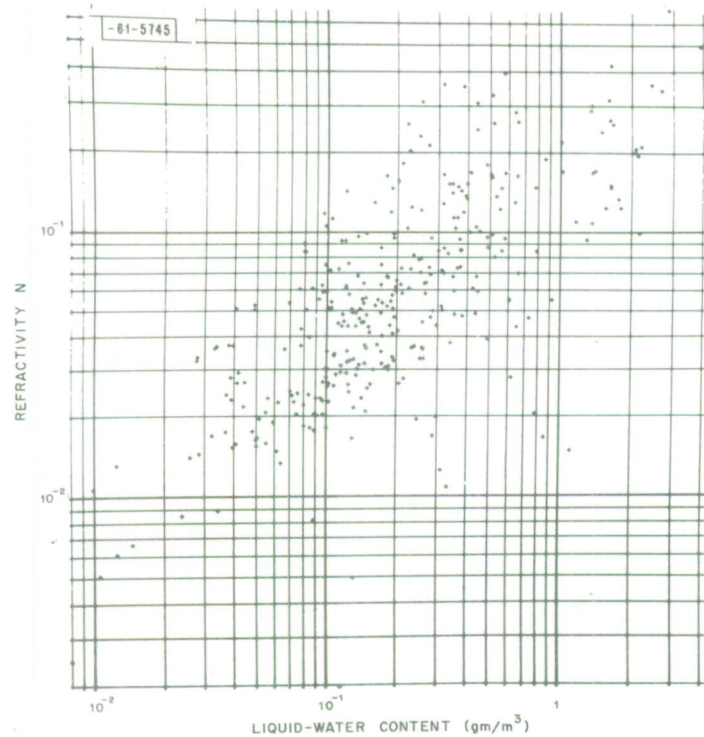


(f) Frequency: 35.0 GHz.

Fig. 15. Continued.

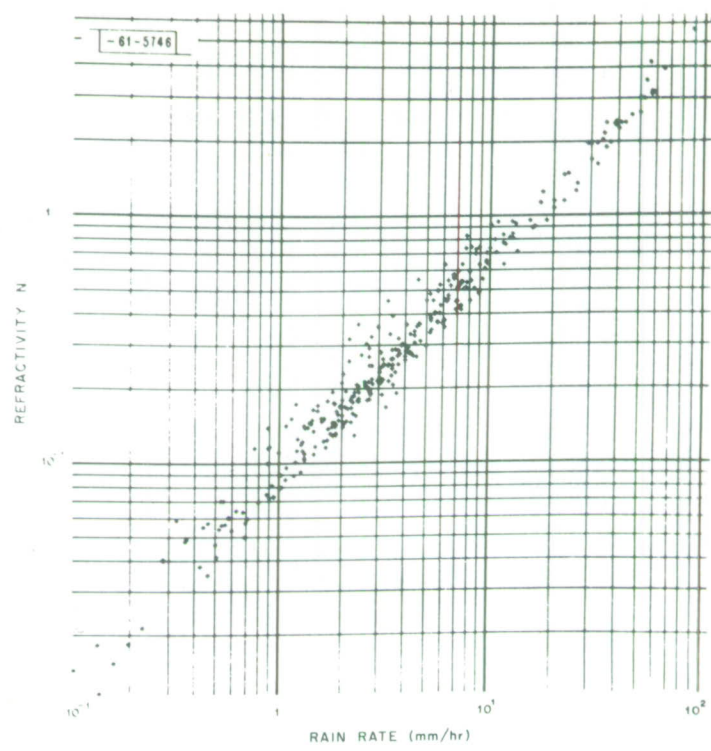


(g) Frequency: 70.0 GHz.

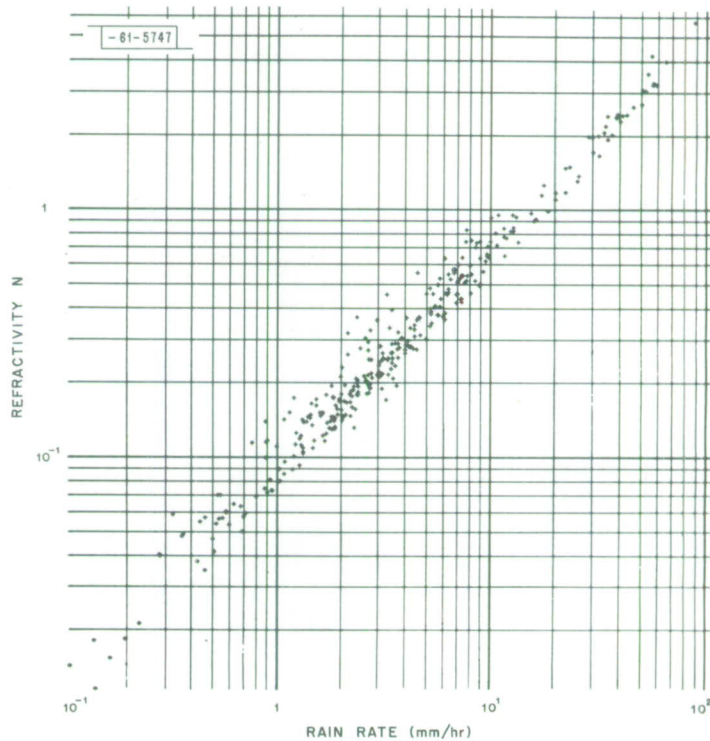


(h) Frequency: 94.0 GHz.

Fig. 15. Continued.

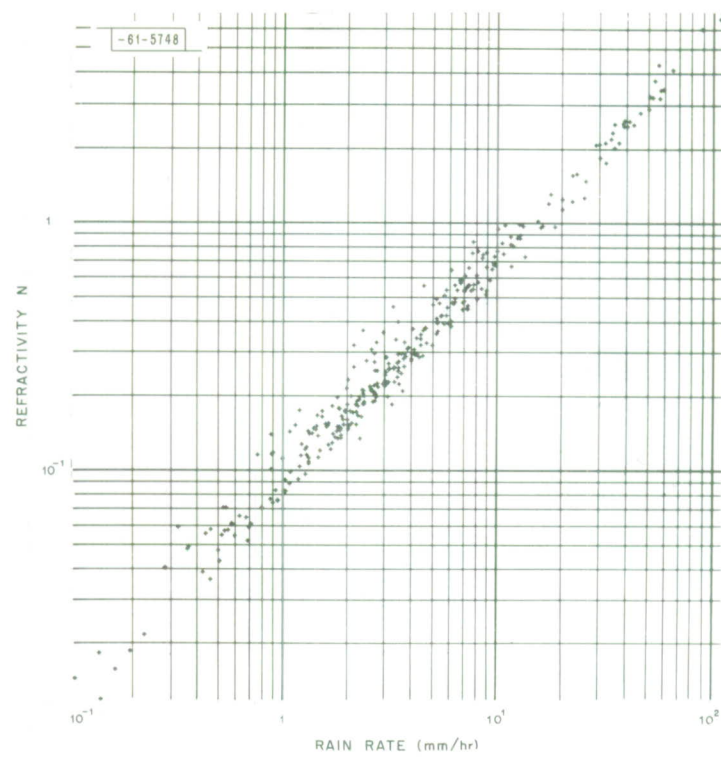


(a) Frequency: 1.29 GHz.

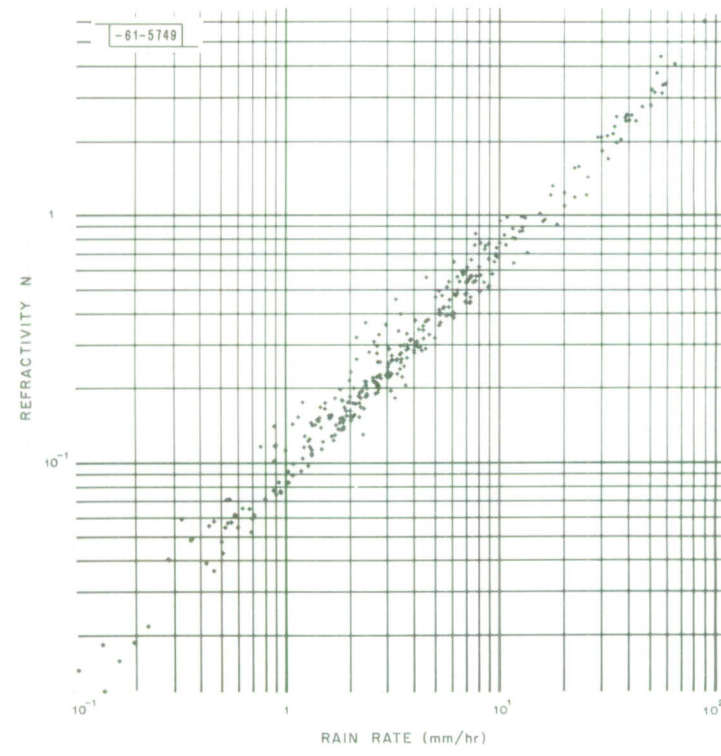


(b) Frequency: 2.80 GHz.

Fig. 16(a-h). Radio refractivity N vs rain rate R . Drop temperature = 0.0°C .

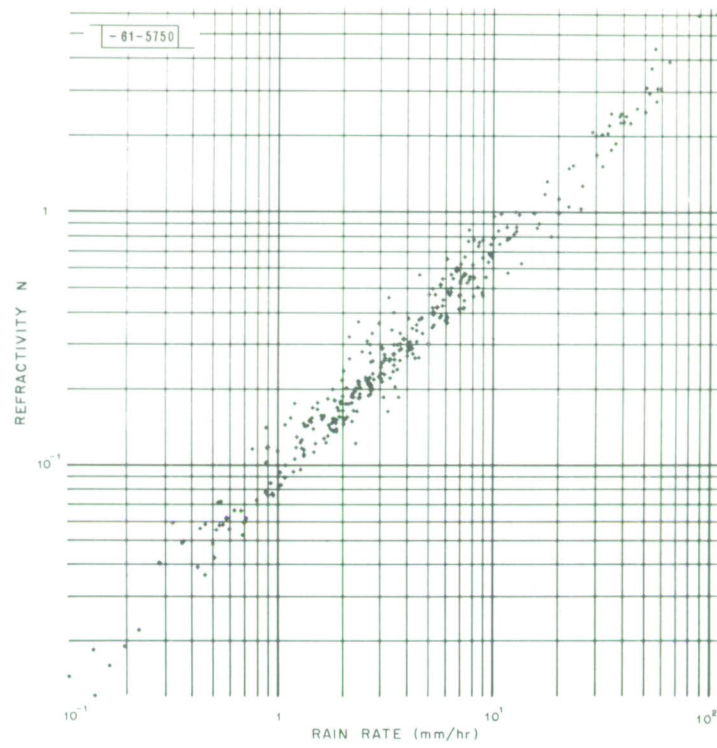


(c) Frequency: 8.0 GHz.

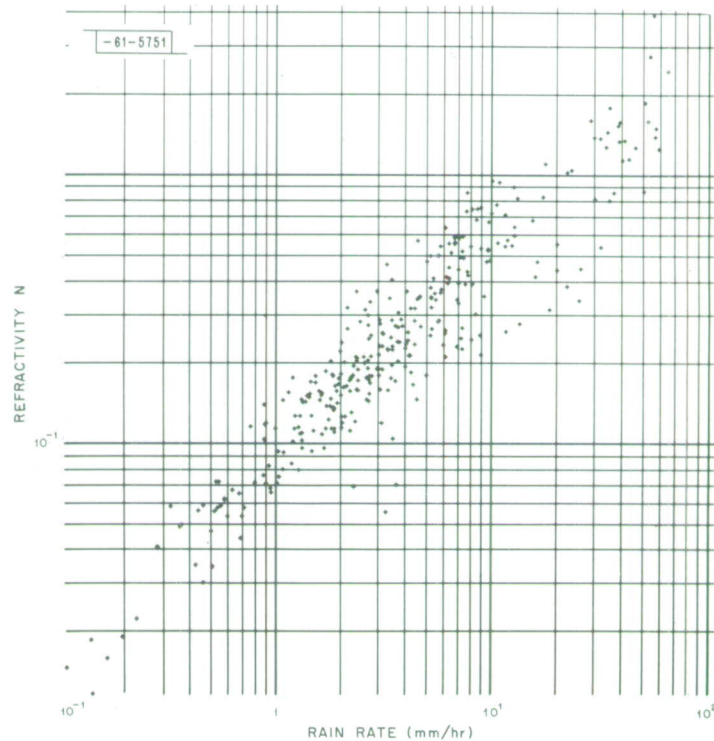


(d) Frequency: 9.35 GHz.

Fig. 16. Continued.

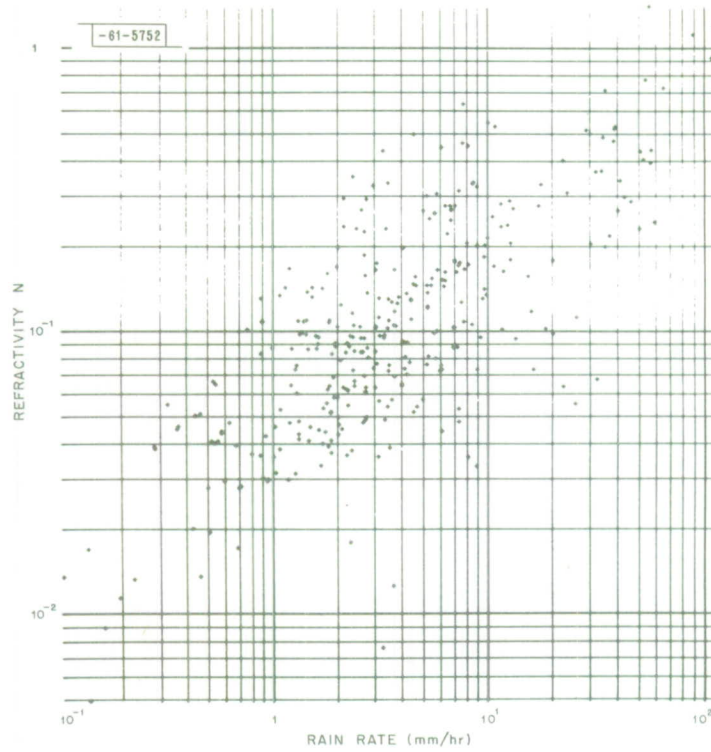


(e) Frequency: 15.5 GHz.

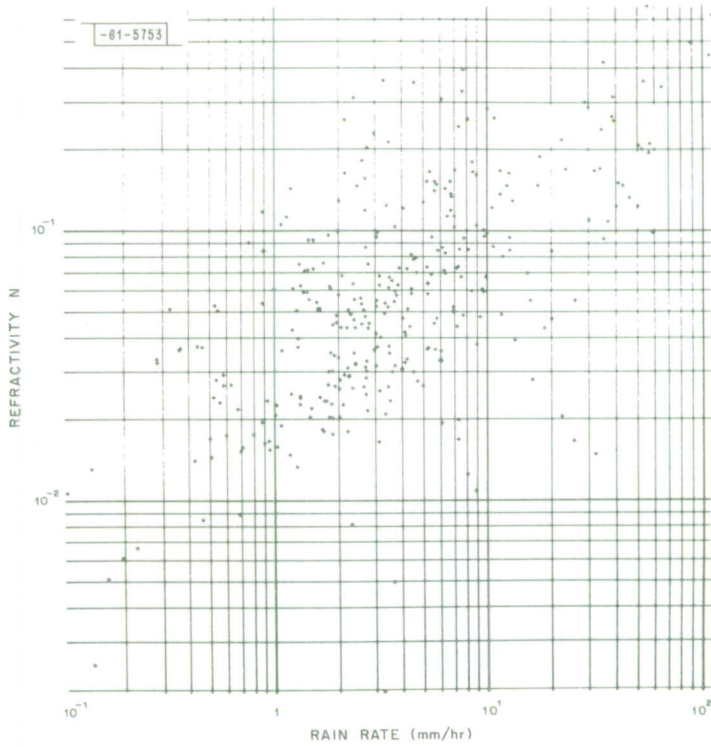


(f) Frequency: 35.0 GHz.

Fig. 16. Continued.

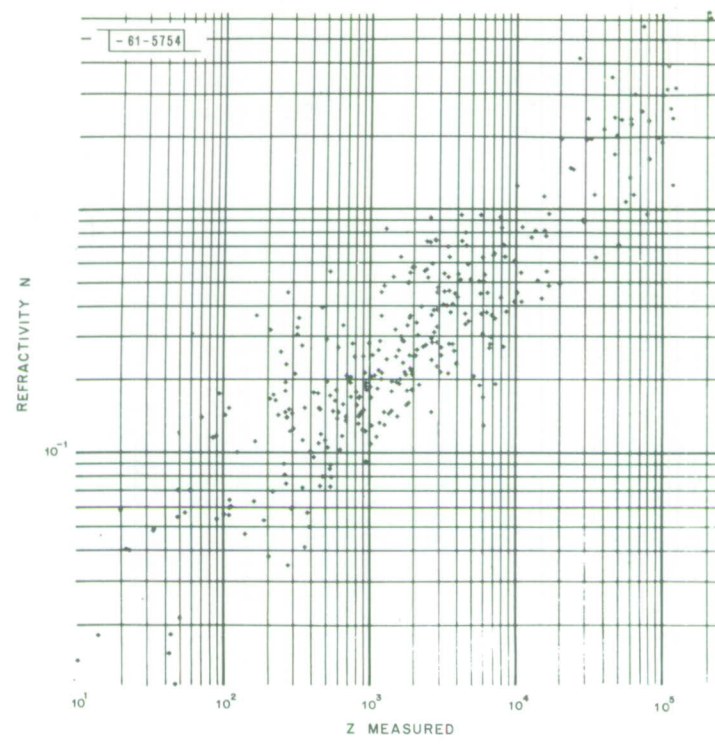


(g) Frequency: 70.0 GHz.

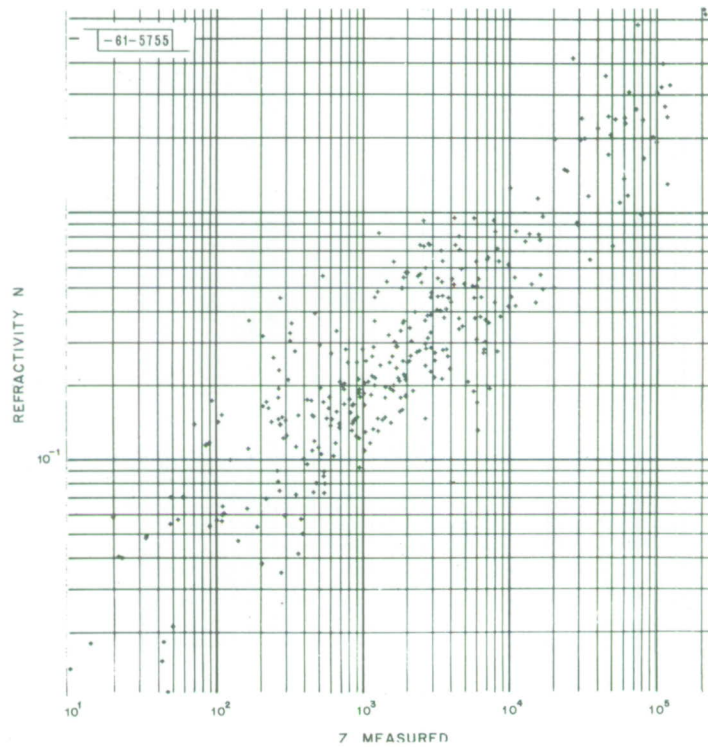


(h) Frequency: 94.0 GHz.

Fig. 16. Continued.

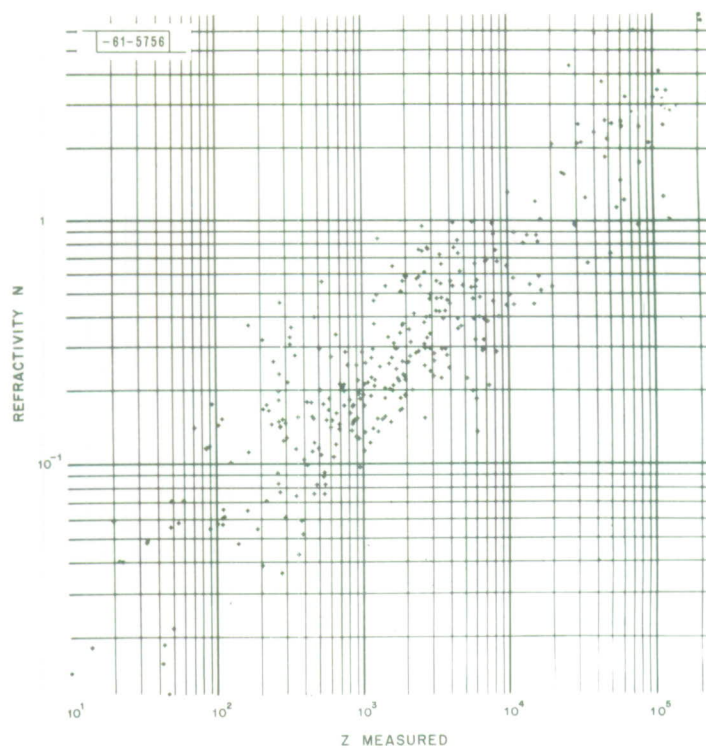


(a) Frequency: 1.29 GHz.

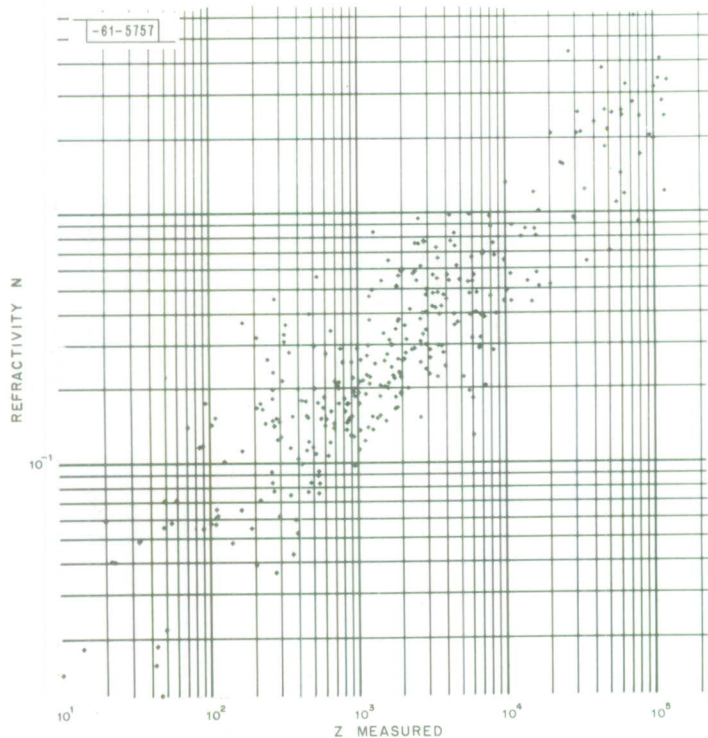


(b) Frequency: 2.80 GHz.

Fig. 17(a-h). Radic refractivity N vs reflectivity factor Z . Drop temperature = 0.0°C.

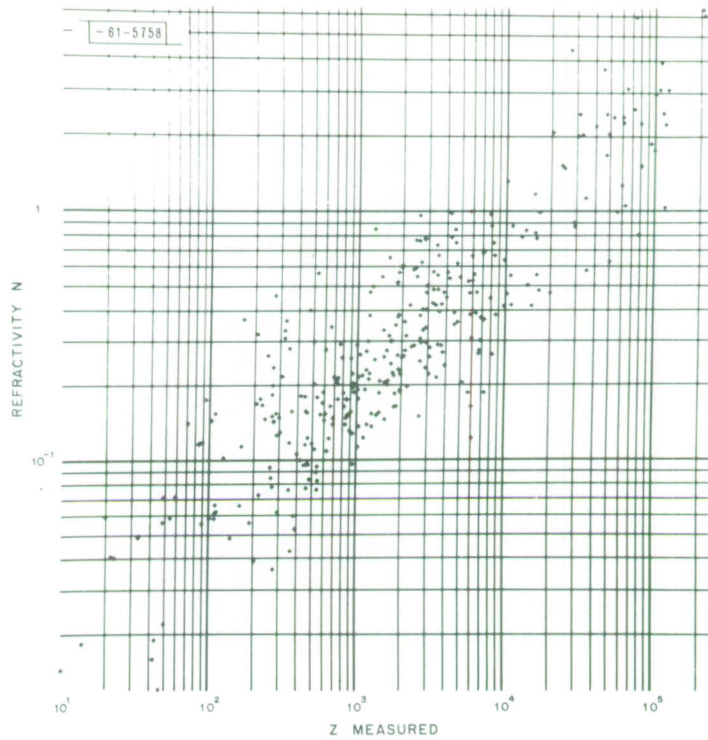


(c) Frequency: 8.0 GHz.

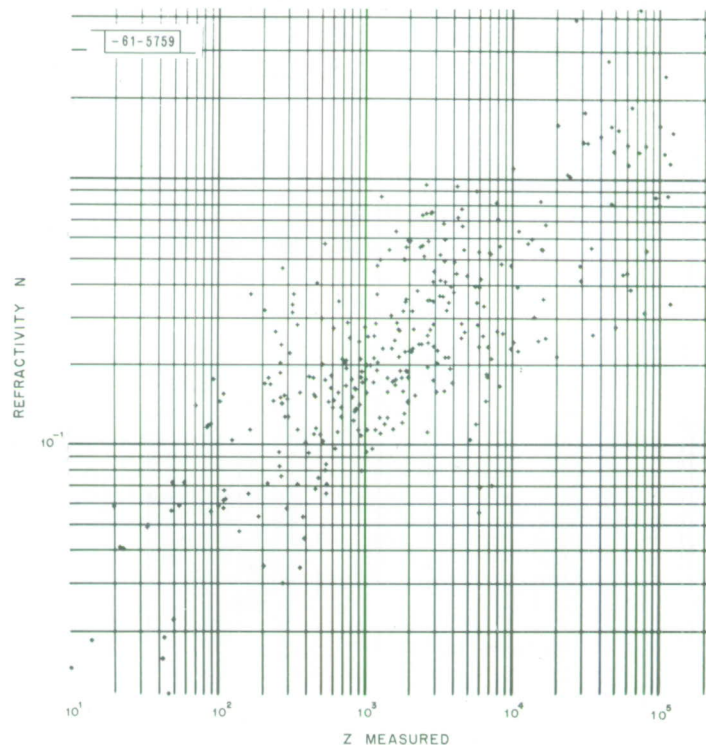


(d) Frequency: 9.35 GHz.

Fig. 17. Continued.

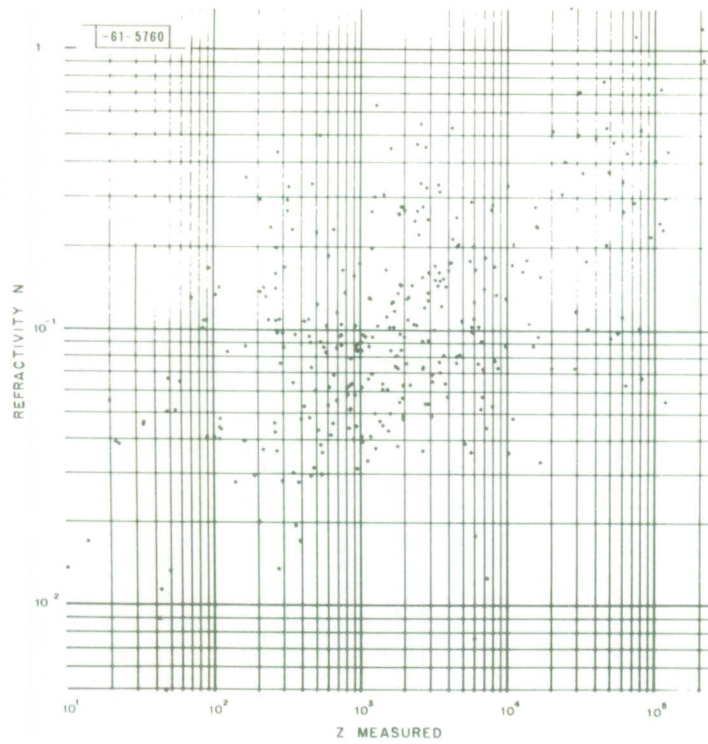


(e) Frequency: 15.5 GHz.

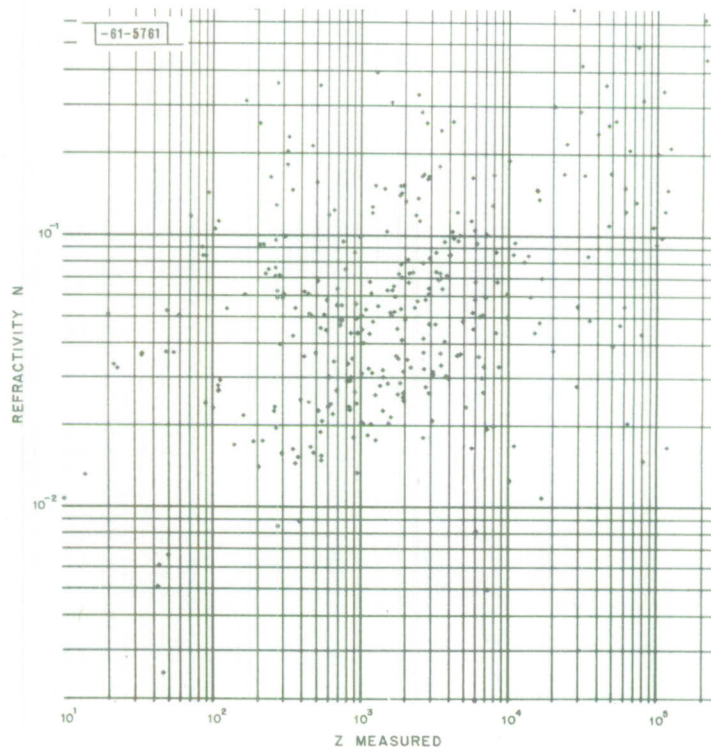


(f) Frequency: 35.0 GHz.

Fig. 17. Continued.



(g) Frequency: 70.0 GHz.



(h) Frequency: 94.0 GHz.

Fig. 17. Continued.

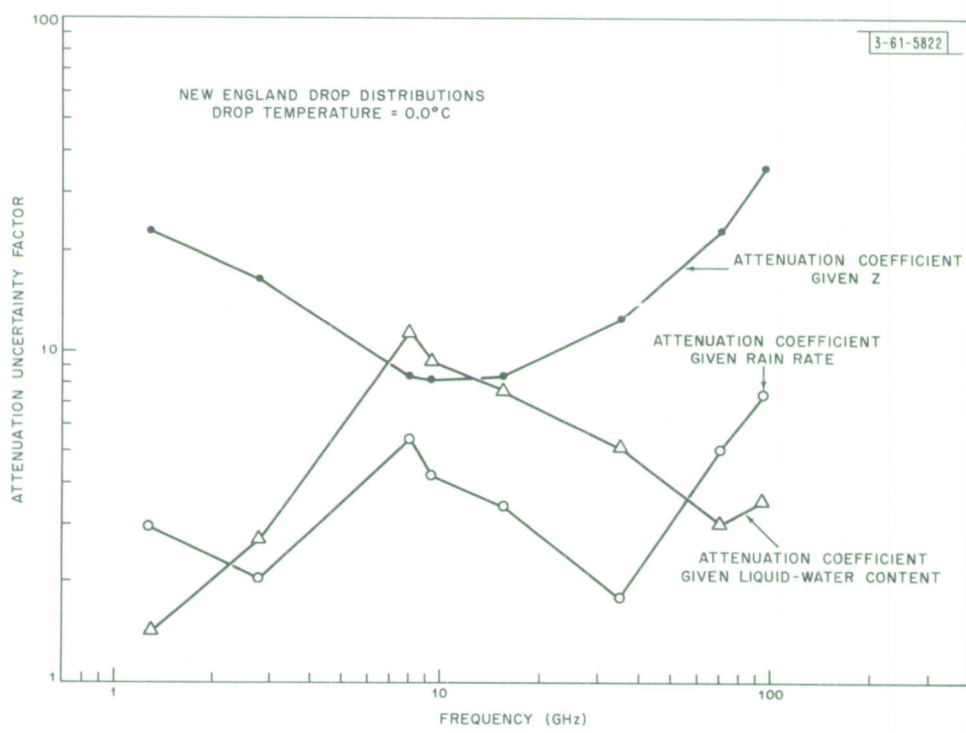


Fig. 18. Attenuation uncertainty factor calculated using Laws and Parsons model as reference.

UNCLASSIFIED

Security Classification

DOCUMENT CONTROL DATA – R&D

(Security classification of title, body of abstract and indexing annotation must be entered when the overall report is classified)